



iPLUG

Deliverable D1.2

System optimization reports and scripts

Document information

Deliverable nr	D1.2
Deliverable Name	System optimization reports and scripts
Version	01
Release date	30/06/2024
Dissemination level	Public
Status	Submitted
Authors	Paula Muñoz Peña, Montserrat Montalà-Palau Marc Cheah Mañe and Oriol Gomis-Bellmunt (UPC)



**Funded by
the European Union**

Document history:

Version	Date of issue	Content and changes	Edited by
01	22/05/2024	Original content without introduction and conclusion	UPC
02	05/06/2024	Added introduction and conclusion	UPC

Peer reviewed by:

Partner	Reviewer
IREC	
UoS	

Deliverable beneficiaries:

WP / task
WP1 / T1.3 & T1.4

Table of contents

1	Executive summary	9
2	Introduction	11
3	Multiport converter sizing and location optimisation-based methodologies	12
3.1	Introduction	12
3.2	State of the art	13
3.3	Methodology	15
3.3.1	Representative days selection	15
3.3.2	Storage sizing	16
3.3.3	Modelling of system elements	18
3.3.4	Grid-based multiport converter sizing optimisation	24
3.3.5	Energy-based multiport converter sizing optimisation	28
3.3.6	Multiport converter sizing and location	29
3.4	Case study: CIGRE	32
3.4.1	Network and profiles	32
3.4.2	Scenario building	35
3.4.3	Representative days selection	36
3.5	Case study: IEEE 33 bus system	42
3.6	Grid-based MPC sizing applied to CIGRE case study	42
3.6.1	Configuration definition	43
3.6.2	Battery sizing	43
3.6.3	Results and discussion	45
3.7	Comparison of grid-based and energy-based MPC sizing applied to CIGRE case study	63
3.8	MPC sizing and allocation applied to IEEE 33 bus case study	64
3.8.1	Configuration definitions	64
3.8.2	Results and discussion	65
3.9	Conclusions	68
4	GIS – based approach to improve the resilience of the distribution network	71
4.1	Introduction	71
4.2	Methodology	73
4.2.1	Hazards Database	73
4.2.2	Vulnerabilities Analysis	74
4.2.3	Risk assessment and Resilience analysis	77
4.3	Case Study	79
4.3.1	Hazard Database	81

4.3.2	Vulnerability analysis	84
4.3.3	Risk Assessment and Resilience Analysis	86
4.4	Conclusions	87
5	Conclusions	89
Annex I: QGIS Plugin		96
A.1	Installation	96
A.1.1	Permission access	96
A.1.2	General Requirements	96
A.1.3	Recommended additional Plugins	96
A.1.4	Specific requirement for → Impact Evaluation	96
A.1.5	Plugin Installation steps	97
A.2	Usage	97
A.3	Hazards Combination	97
A.4	Impact Evaluation	98
A.5	Risk Assesment and Resilience Index	101
Annex II: Sizing and location optimisation tool		103
B.1	Access to scripts	103
B.2	Grid-based multiport converter sizing tool	103
Glossary		106

List of Figures

1	Flowchart of the representative days selection methodology	16
2	Scheme of the storage sizing methodology	18
3	Reactive power capability of energy storage DER	22
4	Flowchart of the MPC sizing methodology considering grid constraints	25
5	General energetic scheme of a system	29
6	Flowchart of the MPC sizing and allocation methodology	30
7	Electrical scheme of CIGRE case study with multiport converter	32
8	Location of load and generation profiles	34
9	Demands during a week	34
10	Total demand (top), PV and wind power availability (bottom) on the representative days	40
11	Total demand and generation at each feeder and in total at the representative days for each scenario	41
12	Electrical scheme of 33 bus case study	42
13	Load and generation profiles of 33 bus case study	42
14	Ratio of total battery capacity required to cover 2h in island mode for scenario 2 and centralised battery option	44
15	Boxplot of $S_{n,MPC-k}$ for terminals without battery (a) and the battery terminal (b) considering all scenarios, configurations, and sensitivity parameters of Table 8	46
16	$S_{n,MPC-k}$ for terminals without battery in scenario 1 considering all configurations and sensitivity parameters of Table 8	47
17	$S_{n,MPC-k}$ for all terminals with different generation capacity	48
18	Buses voltage of scenario 2 with configurations Ref and CB-MPC3 in representative day 10 considering the base values of Table 8	49
19	Lines current of scenario 2 with configurations Ref and CB-MPC3 in representative day 10 considering the base values of Table 8	50
20	Power factor of the feeders' connection to the main grid of scenario 2 with configurations Ref and CB-MPC3 in representative day 10 considering the base values of Table 8	50
21	Multiport power exchange and battery SOC of scenario 2 with configuration CB-MPC3 in representative day 10 considering the base values of Table 8	51
22	System power flow of scenario 2 with configuration Ref in representative day 10 and hour 13 considering the base values of Table 8	52
23	System power flow of scenario 2 with configuration CB-MPC3 in representative day 10 and hour 13 considering the base values of Table 8	52
24	Annual generation (a) and Annual generation increase from Ref configuration (b) for each scenario and configuration, considering the base values of Table 8	53
25	Curtailment for each scenario and configuration, considering the base values of Table 8	54

26	Annual generation for each scenario comparing some configurations	54
27	Investment for each scenario and configuration, considering the base values of Table 8 . . .	55
28	Payback respect to Ref for each scenario and configuration, considering the base values of Table 8	55
29	Payback respect to DB for each scenario and configuration, considering the base values of Table 8	56
30	Annual generation (a) and Annual generation increase from Ref configuration (b) for each scenario and configuration, considering the base values of Table 8 and 25 % reduction of installed generation capacity	58
31	Curtailment for each scenario and configuration, considering the base values of Table 8 and 25 % reduction of installed generation capacity	58
32	Investment for each scenario and configuration, considering the base values of Table 8 and 25 % reduction of installed generation capacity	59
33	Payback respect to Ref for each scenario and configuration, considering the base values of Table 8 and 25 % reduction of installed generation capacity	59
34	Payback respect to DB for each scenario and configuration, considering the base values of Table 8 and 25 % reduction of installed generation capacity	60
35	Annual generation (a) and Annual generation increase from Ref configuration (b) for each scenario and configuration, considering the base values of Table 8 and 50 % reduction of installed generation capacity	61
36	Curtailment for each scenario and configuration, considering the base values of Table 8 and 50 % reduction of installed generation capacity	61
37	Investment for each scenario and configuration, considering the base values of Table 8 and 50 % reduction of installed generation capacity	62
38	Payback respect to Ref for each scenario and configuration, considering the base values of Table 8 and 50 % reduction of installed generation capacity	62
39	Payback respect to DB for each scenario and configuration, considering the base values of Table 8 and 50 % reduction of installed generation capacity	63
40	Energetic scheme of CIGRE case study with multiport converter	63
41	$P_{n,MPC-k}$ for all terminals with base generation capacity using energy-based optimisation	64
42	Electrical scheme of configuration 1	65
43	Electrical scheme of configuration 2	66
44	Electrical scheme of configuration 3	66
45	Electrical scheme of configuration 5	67
46	Electrical scheme of configuration 6	67
47	Total converter power for the best configurations	68
48	System losses and payback for the best configurations	68

49	Hazards Database	74
50	Risk Assessment	79
51	Case Study Definition	80
52	Case Study Definition - Zoom external grid	80
53	Wildfire Probability in day d during summer	82
54	Wind gust probability in day d during summer	82
55	Heatwave probability in day d during summer	83
56	Likelihood of being affected by the vulnerability given a hazard	84
57	Impact of each element based on maximum loads	85
58	Types of demand profiles	85
59	Impact of each element based on demand profiles	86
60	Amount of energy at risk in each element of the system because of the vulnerability and the hazards	87
61	Dialog Box of CITCEA Probability Analysis Plugin	98
62	Demand Profiles hourly adjusting factor	99
63	Dialog Box of CITCEA Probability Analysis Plugin	100
64	Dialog Box of CITCEA Resilience Index Plugin	101
65	Optimisation program structure	104
66	Flowchart of the scripts	104
67	Inputs structure of <i>Data.xlsx</i>	105

List of Tables

1	Connections and line parameters	33
2	Transformer parameters	33
3	Load distribution	35
4	Scenario definition based on generation distribution	36
5	Classification levels considered to select the representative days	37
6	Representative days selected and their weights	38
7	Representative days classification levels	39
8	Sensitivity analysis parameters	43
9	Battery sizing results	44
10	Types of power lines	81
11	Probability of having a wildfire per season	81
12	Probability of having a wildfire per season	83
13	Hazards considered in the analysis	83
14	24-hour demand profile assignment	86
15	Standard Lines. Additionally, the standard lines from pandapower can be specified by the user: pandapower_standard_lines	100

1 Executive summary

Multiport converters (MPC) are presented as a general power electronics solution for enhancing power flow operation in the distribution system and that can contribute to facilitate a massive integration of distributed renewable generation while enhancing the interconnection of multiple electrical grids and equipment. The MPC implement an integrated solution combining the advantages of energy storage and other grid support equipment.

This work develops an optimisation-based methodology to size and locate multiport converters and analyses how their introduction can improve distribution systems' performance through a techno-economical analysis. In fact, three slightly different methodologies are presented. Two case studies are also presented to validate the methodologies.

The first methodology to size multiport power converters is divided into three steps: days selection of the load and renewable resource availability profiles, storage sizing, and multiport converter sizing optimisation. The MPC sizing optimisation considers the days selected previously instead of the whole year, includes electrical constraints, and also optimises the system operation. This methodology also provides technical and economic indicators for a complete evaluation of the multiport converter integration.

This first methodology is evaluated in a case study based on a medium voltage benchmark network from CIGRE with the objective of reducing renewable generation curtailment. The multiport converter solution is compared to alternative configurations with separated batteries and a simple switch interconnection, it also considers different penetrations of renewable energy. Additionally, a sensitivity analysis of economic parameters is performed on the optimisation. Overall, the case study aims to identify the best scenarios where multiport converters can be considered as a potential solution.

The second methodology is a multiport converter sizing optimisation without grid constraints that considers the system operation in a one-year time horizon, in addition to the technical and economic indicators. This methodology is evaluated with the same CIGRE case study to analyse the impact of the electrical constraints in the multiport converter sizing.

Then, an optimisation-based methodology to size and locate multiport power converters together with a techno-economic comparison to other conventional approaches. This methodology includes AC power flow constraints and is evaluated in a case study based on IEEE 33 bus system to identify the best scenarios where multiport converters can be considered as a potential solution to avoid undervoltages and reduce losses.

On the other hand, this work also addresses the role of resilience in planning distribution networks. Efficient, reliable, and secure supply is insufficient in a context where electricity is becoming a key energy vector for economies and societies. Thus, resilience, understood as the ability to anticipate, operate, and learn from disruptive events, is becoming a crucial principle in the planning and operation of networks. This work introduces a GIS-based approach to tackle the issue of resilience in network planning. The approach includes three main stages. First, the development of a geolocated hazards database, including all those disruptive events that might affect the system but are out of the system's control. Second, the

evaluation of the vulnerabilities of the system. Third, a risk assessment and a resilience analysis. The risk assessment provides information about the amount of power or energy risked in each asset. The risk assessment allows the identification of the most critical regions and the evaluation of different mitigation actions. In addition, the resilience analysis provides information about the global power or energy risk compared to the total power or energy expected to be managed by the system. Finally, this study delves into the resilience of an MV distribution network located in a rural area in Spain and the implementation of various mitigation actions to enhance resilience through the proposed methodology.

2 Introduction

Distribution network planning and reinforcement is challenging as it can include the construction of new lines, the addition of equipment and different generation and storage elements as well as flexible loads. Moreover, to achieve a new design several studies have to be performed regarding cost, power flow, stability, and resiliency. An example of new equipment that can be considered to enhance the grid operation is the multiport converter. The iPLUG consortium aims to develop innovative methodologies to optimally size and locate multiport converters, as well as analyze the network resiliency.

This report addresses these planning and analysis methodologies separately. Section 3 presents an optimisation-based methodology to size and locate multiport converters in the distribution grid. Section 4 a GIS-based methodology to analyze and improve the distribution network's resilience. Finally, the general conclusions and corresponding future work are provided in Section 5.

Optimal design of distribution grid elements is important to avoid oversizing and obtain lower costs. Power systems planning including power electronics components, in particular Soft Open Points, has been widely studied in the literature. In that sense, proper sizing should consider both economic analysis and system operation. Multiport converters can combine several terminals, therefore their design can consider more general solutions. In this context, Section 3 proposes optimisation-based methodologies to size and locate multiport converters to reduce system losses and to reduce renewable generation curtailment. The methodology proposed is very modular and can be adapted to the case study as well as consider different algorithms in some parts. This methodology also includes technical and economic indicators to enable further system analysis.

Researchers and practitioners have widely discussed the concept of resilience in recent decades. Currently, many complex systems include a resilience perspective to anticipate, withstand, and recover from critical events. In this context, resilience is becoming a key concept in both the planning and operation of power systems. Resilience should consider all events that might affect the system, even those with low probability. In that context, Section 4 proposes a GIS-based approach to manage network resilience in the planning stage. Electrical networks are complex systems exposed to a large number of hazards that can additionally simultaneously occur. The resilience methodology proposed includes hazards and the vulnerabilities of the system. Consequently, analysts can identify the critical part of the system and evaluate mitigation actions.

3 Multiport converter sizing and location optimisation-based methodologies

3.1 Introduction

The European Union has the objective of reducing greenhouse gas emissions to be climate-neutral by 2050 [1]. To do so, the share of renewable energy and energy efficiency should increase. Precisely, the European Union is targeting 42.5 % of renewables by 2030 [2], and it is intended to continue growing. In this context, renewable generation is having a massive expansion in distribution level of the electrical grid, both at medium voltage (MV) and low voltage (LV). Additionally, due to the stochastic nature of renewable sources such as PV and wind power, it is needed a huge deployment of energy storage systems (ESS) to provide the overall system with flexibility, reliability and security [3].

The integration of renewable energy sources (RES) is transforming the conventional design and operation of the electrical grid. In particular, the high penetration of renewables is leading to a number of technical challenges related to overloads, voltage regulation, fault levels or power quality issues [4]. Solutions to increase the maximum amount of distributed energy resources (DER) that can be integrated into a distribution grid can be the construction of new lines, reinforcement of the grid with new equipment, demand management and storage systems.

In this situation, power electronics have an important role and an increasing presence in the system. In particular, voltage source converters (VSC) interconnect renewables such as wind or photovoltaic (PV) generation and battery energy storage (BESS) to the grid, but also provide active and reactive power control to reduce overloads and regulate voltages. The multiport converter (MPC) is presented as a general power electronics solution, that represents an improvement of the Soft Open Points (SOP) concept combined with several terminals and functionalities.

Multiport converters can facilitate a massive integration of distributed renewable generation while enabling the interconnection of multiple electrical grids and equipment in AC or DC and considers different voltage or frequency levels, number of phases or grounding schemes. The MPC implements an integrated solution combining the advantages of energy storage and other grid support equipment. Therefore, the overall number of power electronics can be reduced. Although the installation of multiport converters requires an additional investment in the distribution network, which must be compensated with the provided services explained before. Apart from the multiport converter, other options can be considered to increase the penetration of renewable sources such as adding regular energy storage systems, switches, new lines, and load management.

In general, the lack of optimum design usually leads to systems which are oversized or not properly planned, and therefore with higher costs. Modern distribution systems are complex and complicated, as they can involve several energy sources, energy storage, management, and power electronics. Therefore their planning and analysis is a challenge [5]. Furthermore, their design should include sizing of the assets, optimal operation, and economic analysis of the system. In that sense, the models used for

this purpose need to balance simplicity, accuracy, precision, and data granularity. Therefore, the most appropriate model will depend on the project complexity, assets considered, and data availability [6].

This work proposes two optimisation-based methodologies to size multiport power converters, with and without AC power flow, and an optimisation-based methodology to size and locate multiport power converters. Two case studies are also presented to validate the methodologies, and the obtained results are discussed.

Section 3.2 includes a literature review on electric power systems simulation and optimisation. Section 3.3 presents the methodology developed in this work. Sections 3.4 and 3.5 describe the case studies used to validate the methodology. Sections 3.6, 3.7 and 3.8 analyse the results. Finally, the main conclusions and future work are presented in Section 3.9.

3.2 State of the art

This chapter presents a literature review of the different software used for electric power systems simulation and optimisation. As one objective of this work is to develop an optimisation-based methodology, this section also explains some basic optimisation concepts.

Power systems planning tools have been widely studied in the literature [5, 6]. Several commercial software tools as well as new methodologies using mathematical models and various optimisation algorithms can be employed. These tools can have different characteristics and target users, as their applications can range from HV networks to microgrids. Therefore, a clear understanding of their features, capabilities, and limitations is needed to choose the most appropriate and apply it.

Taking a closer look at the power systems design tools, they can be mainly separated into two types. On the one hand, there are those system planning and RES design tools, which focus on renewable resources and the characteristics of other assets, for example, HOMER [7]. On the other hand, there are tools which focus on the electrical grid specifications and analysis but keep the detailed modelling of other assets out of their scope. MATPOWER, GridCal, and PyPSA are examples of these tools.

MATPOWER is a Matlab package to solve steady-state power system simulation and optimisation problems, such as power flow (PF) and extensible optimal power flow (OPF). This tool models branches, generators, loads and shunt elements such as capacitors or inductors. The generator is modelled as an active and reactive power injection at a specific bus. Loads are defined as constant values, but a dispatchable load can be modelled as a generator with negative power injection. MATPOWER includes AC and DC models to perform PF and OPF, but just for a single time period [8–10].

GridCal is an open-source power systems planning software. It is similar to MATPOWER but with a graphical user interface. GridCal performs DC PF, AC PF, DC OPF, and AC OPF with linear approximation. In contrast to MATPOWER, GridCal considers time series and simulates and optimises the whole time period. The model includes loads, shunts, generators, static generators and batteries that can be added to the buses. The connection between two buses can be modelled as a line, high-voltage direct current (HVDC), transformer, VSC, or unified power flow controller (UPFC) [11–13].

Python for Power System Analysis (PyPSA) is a Python toolbox to simulate and optimise modern electrical power and energy systems. In comparison with similar tools, PyPSA performs security-constrained linear OPF, and investment cost optimisation of the total energy system, in addition to static PF and linear OPF. Moreover, PyPSA can work with large networks and long time series. PyPSA enables to mesh AC and DC networks with converters, as well as coupling the electrical system with other energy carriers. This tool has models for standard types for lines and transformers, conventional dispatchable generators and links with unit commitment, generators with time-varying power availability, storage units with efficiency losses, and simple hydroelectricity with inflow and spillage. It also has basic components that enable to build more complicated assets such as CHP, heat pumps, resistive Power-to-Heat, Power-to-Gas, battery electric vehicles, and direct air capture [14–16]. Compared with PyPSA, the software developed in this work performs non-linear OPF and includes multiport converters.

On the other hand, reconfiguration of the distribution network or the optimal new topology is widely studied in the literature. Typically, the objective is to minimize the costs and network losses, and radial network operation is ensured. Traditionally, only lines and switches were considered. For example, [17] presents a mixed integer linear programming (MILP) that includes DC power flow. An improvement of this approach is presented in [18], where geographic information system (GIS) is applied. [19] presents a model based on the non-convex optimal power flow (OPF) with binary variables that define if each line is switched on or off. However, new methods also include power electronics. In [20], the system operation with Soft Normally-Open Points (SNOPs) is simulated in different placements, but SNOP ratings are set previously and current level constraints are not considered. Also, [21] and [22] determine the size and allocation of SOPs with a relaxed optimal power flow (OPF) with costs minimisation, using the second-order cone programming (SOCP) approach where voltage and current angles are eliminated from the power flow model to make it convex.

Regarding the optimisation, its goal is to find the values of the variables that maximise or minimise the objective, and the variables are often limited or constrained somehow. The optimisation model should balance simplicity and complexity, as too-complex models can be difficult to solve and too-simple ones may not properly represent the real system. After formulating the model, an optimisation algorithm is used to find its solution. Different algorithms can be applied according to the type of optimisation problem. Choosing an appropriate algorithm may determine the resolution speed and even finding or not a solution. A sensitivity analysis will reveal the solution sensitivity to changes in the model and data. The mathematical formulation of an optimisation can be expressed as:

$$\begin{aligned}
 & \min_{\mathbf{x} \in \mathbb{R}^n} f(\mathbf{x}) \\
 & \text{s.t.} \quad \mathbf{g}_i(\mathbf{x}) \leq 0, \quad i \in \mathcal{G} \quad \text{Inequality constraints} \\
 & \quad \quad \mathbf{h}_i(\mathbf{x}) = 0, \quad i \in \mathcal{H} \quad \text{Equality constraints}
 \end{aligned} \tag{1}$$

where \mathbf{x} is the vector of the variables, $f(\mathbf{x})$ is the scalar objective function to minimise, $\mathbf{g}(\mathbf{x})$ and $\mathbf{h}(\mathbf{x})$ are the constraints, which are scalar functions that define equations and inequalities that x must satisfy,

and \mathcal{G} and \mathcal{H} are sets of indices for the constraints.

3.3 Methodology

This section presents the methodologies proposed to size and locate multiport converters. Section 3.3.3 describes the models of the system elements used in all the methodologies. Section 3.3.3 proposes an optimisation-based methodology to size MPC considering AC power flow constraints. This general methodology includes a representative days selection step, presented in Section 3.3.1, and a storage sizing approach, presented in Section 3.3.2. Although other approaches can also be considered in these two steps. Section 3.3.5 proposes an energy-based optimisation to size the MPC. And Section 3.3.6 proposes an optimisation-based methodology to size and locate multiport power converters. Annex II includes the access and description of the tools developed.

Regarding the scope of this methodology, only steady-state analysis is performed and stability issues have been kept out of the scope. However, it is important to ensure that the power system will remain stable when increasing the renewable generation and with the introduction of the multiport converter and the battery.

This work is mainly focused on the technical aspects of introducing a multiport converter in a distribution system, although an economic analysis is also required. Due to the workload of other more significant aspects, the economic parameters are mostly based on the bibliography. A sensitivity analysis of these parameters should be performed to quantify the effect of their variability. Therefore, all economic results lead to reaching general conclusions, but their concrete values should be considered as illustrative.

Another important supposition is that the historical data of the loads and renewable sources represent a perfect forecast for the years studied. The electric loads are known to evolve with the years, and the availability of renewable sources is uncertain by nature. Not considering this variability in a planning methodology, as presented in this thesis, is a significant scope limitation.

Moreover, other simplifications have been considered in the sizing optimisation due to computational requirements. In this sense, a computer with *Windows 11 Pro* operative system of 64-bit, Intel® Core *i7* @ 3.40GHz and 16.0 G RAM is used. It was aimed that the optimisation could be solved in less than one hour.

3.3.1 Representative days selection

Ideally, a planning optimisation should consider a 1-year or more time horizon. However, sometimes this optimisation is too complex and computationally infeasible to solve with the available resources. For this reason, the methodology proposed tries to reduce the amount of data by using the idea of clusters. Therefore, considering the generation and load profiles inputs from the whole year, several representative days are selected. Then, the optimisation will consider only those specific days.

The input profiles regard annual demand and generation, which is supposed as PV and wind power.

To select the representative days all those profiles and their interactions have to be considered. Although several clustering algorithms and software can be used, this section presents a self-developed methodology shown in Figure 1.

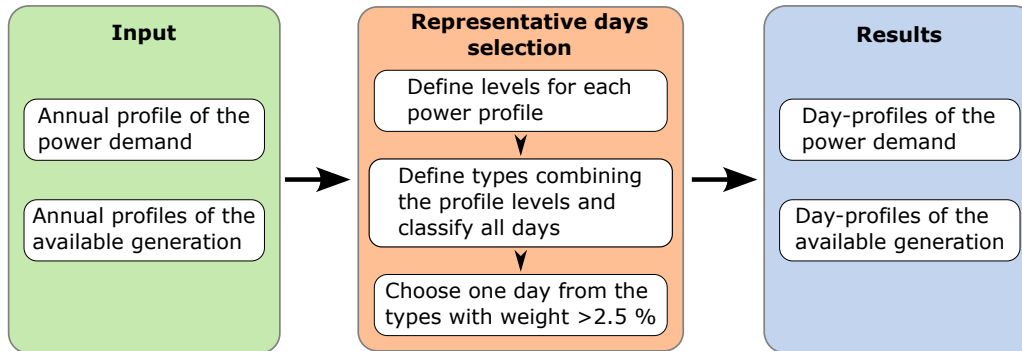


Figure 1: Flowchart of the representative days selection methodology

First, different levels of load, PV power availability and wind power availability have to be defined. To define the levels it should be analysed each profile to determine one or more representative magnitudes that describe the profile. The levels correspond to a range of values of these representative magnitudes so that there are both extremes and some middle values. The detailed definition of these levels depends on the case study, therefore it will be deeply explained in Section 3.4.3.

Then, all possible combinations between power levels of different profiles are considered. Each of those combinations can be seen as a type of day, resulting in a quite long list. Afterwards, each day of the year is classified as one of those types according to its profiles. For each type of day, a weight w can be defined as equal to the percentage of days it contains over the total amount of days considered, which is 365 for one year.

Finally, the representative day types are those with percentages w higher than 2.5 %. From each of those day types, a single day is selected. The days selected are the representative days. At this step, it should be taken into account that the selected days must have different power profiles. It should be tried as well that the selected days are from different seasons and days of the week, and that they are around the middle value of their levels.

3.3.2 Storage sizing

If energy storage is included in the system, several scenarios can occur: storage may be already in the system, it may be already sized, or storage capacity is still to be determined. If storage size is known, it must be an input in our methodology, otherwise it should be found. Moreover, the system may include different types of storage. For this work, it is assumed that batteries are used as a storage solution, but other options could be also considered.

There are several methods to size batteries, and also they can be sized based on different requirements. For example, batteries could be sized in the same optimisation as the multiport converter. But in this case, depending on the optimisation problem, it may be too complex and computationally infeasible to

solve with the available resources. For this reason, a separate methodology to size the batteries may be needed, so its capacity will later be known in the multiport converter sizing optimisation.

This section presents a self-developed methodology to size the batteries to ensure island operation. Therefore, in case the feeders are disconnected from the main grid, island operation must be ensured for a specific time period. In particular, the battery sizing is defined based on the power and energy required during the periods with a lack of generation in the system. The methodology used to size the storage is explained below, although other methodologies can also be considered.

In this step, hourly load and generation profiles for a year are employed, but grid constraints are not considered. First, the net power exchange for each h hour is defined as:

$$P_h = \sum_i P_{d-i,h} - P_{g-i,h} \quad \forall h \quad (2)$$

where $P_{d-i,h}$ and $P_{g-i,h}$ are the demand and generation powers for each node i .

Then, the net energy exchange for a period of H hours starting at hour t is defined as:

$$E_{H,t} = \sum_{h=t}^{t+H} P_h \quad (3)$$

When $E_{H,t}$ is positive the feeders require additional energy to supply the demand that must be provided by the storage. When $E_{H,t}$ is negative the feeders have a generation excess that can be used to charge the storage. In this expression, it will be needed the net power exchange of hours out of the year of data, for that reason it is supposed that the next year will have the same profile.

The battery sizing only considers periods where P_h and $E_{H,t}$ are positive. The battery power P_{bat0} and storage E_{st0} must cover all cases, and are expressed as:

$$P_{bat0} = \max(P_1, \dots, P_{N_h}) \quad (4)$$

$$E_{st0} = \max(E_{H,1}, \dots, E_{H,N_h}) \quad (5)$$

where $N_h = 8760$ is the number of hours in a year.

At this point, the battery is sized to be able to cover 100% of the cases, including the worst possible scenario. As a result, the battery could be excessively high and oversized in the majority of situations. Then, a value between 90 and 100% is considered to reduce the battery size, i.e. the battery cost. Therefore, the battery power P_{bat} and storage required E_{st} are defined such that a percentage of the total number of cases with positive $E_{H,t}$ are covered. For example, if 90 % of cases are covered, means that the 10 % of cases which need a bigger battery to be able to operate in island mode won't be considered in the sizing.

Finally, the battery capacity E_{cap} is defined as:

$$E_{cap} = \frac{E_{st}}{DoD} \quad (6)$$

where DoD is the depth of discharge.

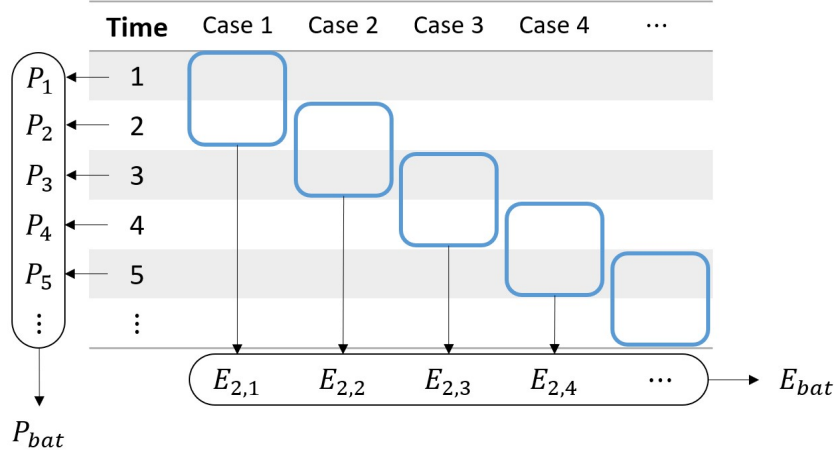


Figure 2: Scheme of the storage sizing methodology

3.3.3 Modelling of system elements

The methodology proposed aims to size and locate the multiport converters based on an optimisation that considers the system operation. For this reason, it is required to model the different assets that the system can include, which will later represent the optimisation constraints. Moreover, this methodology presents a characteristic modularity, so only some of the elements can be considered and more element models can be added easily. In this section, the models of different elements that can appear in the system are presented.

Loads

The system can include AC loads, DC loads, and electric vehicles (EV). All loads are considered to be known, although flexible loads can be added in the future. Loads parameters are the active and reactive power demand ($p_{load-i,t,d}$ and $q_{load-i,t,d}$), which are defined for each node i and for each hour t of the considered representative days d . All these variables are expressed per unit.

Main grid model

The connection of the system to the main grid consists in a simplified model characterised by the power exchange between the system and the external grid. Therefore, main grid variables are defined for each main grid MG connected to the node i for each hour t of the considered representative days d . They include active power bought and sold ($p_{buy-MG,i,t,d}$ and $p_{sell-MG,i,t,d}$), and reactive power exchanged ($q_{MG,i,t,d}$). All these variables are expressed per unit. Additionally, energy buy and sell costs can also be considered ($C_{buy-MG,i,t,d}$ and $C_{sell-MG,i,t,d}$), expressed in €.

The main grid constraints are related to:

- Maximum power exchange with the grid. The active power exchange with the grid can be limited due to technical or other factors. Then, active power exchange limits are expressed as:

$$p_{buy-MG,i,t,d} \leq p_{max-buy-MG,i,t,d} \quad \forall MG, i, t, d \quad (7)$$

$$p_{sell-MG,i,t,d} \leq p_{max-sell-MG,i,t,d} \quad \forall MG, i, t, d \quad (8)$$

where $p_{max-buy-MG,i,t,d}$ and $p_{max-sell-MG,i,t,d}$ are the maximum power bought and sold to the main grid MG connected to the node i at hour t of the day d .

- Power exchange costs. Active power bought to the main grid can represent some costs for the system, and active power sold to the main grid can imply some revenues. Then, these costs are expressed as:

$$C_{buy-MG,i,t,d} = p_{buy-MG,i,t,d} \cdot S_b \cdot \Delta t \cdot c_{buy-MG,i,t,d} \quad \forall MG, i, t, d \quad (9)$$

$$C_{sell-MG,i,t,d} = p_{sell-MG,i,t,d} \cdot S_b \cdot \Delta t \cdot c_{sell-MG,i,t,d} \quad \forall MG, i, t, d \quad (10)$$

where $c_{buy-MG,i,t,d}$ and $c_{sell-MG,i,t,d}$ are the prices for buying and selling power to the main grid MG connected to the node i at hour t of the day d , expressed in [€/kWh], S_b is the base power of the system, and Δt is the calculation period, which is 1 h.

Generator model

The generators are supposed to be from renewable sources, meaning PV and wind power, although conventional generators can also be considered. PV and wind power variables are related to their operation, including active and reactive power generated ($p_{g,i,t,d}$ and $q_{g,i,t,d}$), which are defined for each generator g connected to the node i and for each hour t of the considered representative days d . All these variables are expressed per unit.

The generator constraints are related to:

- Generation curtailment. The active power provided by each renewable generator is positive and limited by the maximum available power from the generation profiles. Then, the active power generation limits are expressed as:

$$0 \leq p_{g,i,t,d} \leq p_{max-g,i,t,d} \quad \forall g, i, t, d \quad (11)$$

where $p_{max-g,i,t,d}$ is the maximum available power from the generator g connected to the node i at hour t of the day d .

- Generator current limits. As generators are connected to the grid through VSC, they can exchange

reactive power. But the total power is limited by a maximum current, which can be expressed as:

$$p_{g,i,t,d}^2 + q_{g,i,t,d}^2 \leq (v_{i,t,d} \cdot i_{max-g,i})^2 \quad \forall g, i, t, d \quad (12)$$

$$i_{max-g,i} = \frac{s_{max-g,i}}{v_{n-i}} \quad \forall g, i \quad (13)$$

$$s_{max-g,i} = \frac{p_{n-g,i}}{PF_{g,i}} \quad \forall g, i \quad (14)$$

where v_{n-i} is the nominal voltage supposed as 1, $PF_{g,i}$ is the power factor supposed as 0.915 which corresponds to a reactive power minimum capability of ± 44 % (Figure 3) [23], and $p_{n-g,i}$ is the nominal active power of the generator.

Battery storage model

BESS variables are also related to the operation, as batteries are supposed to be sized previously to the optimisation. Therefore, BESS variables are defined for each battery b connected to the node i for each hour t of the considered representative days d . They include active charging and discharging powers ($p_{char-b,i,t,d}$ and $p_{disch-b,i,t,d}$), reactive power exchanged ($q_{b,i,t,d}$), and the state of charge ($SOC_{b,i,t,d}$). All these variables are expressed per unit. Additionally, battery cost can also be considered (C_{BESS-b}), expressed in €.

The BESS constraints are related to:

- Charging and discharging power limits, which are expressed as:

$$0 \leq p_{char-b,i,t,d} \leq p_{n-b,i} \quad \forall b, i, t, d \quad (15)$$

$$0 \leq p_{disch-b,i,t,d} \leq p_{n-b,i} \quad \forall b, i, t, d \quad (16)$$

where $p_{n-b,i}$ is the nominal active power of the battery b connected to the node i .

- SOC limits, which are expressed as:

$$SOC_{min-b,i} \leq SOC_{b,i,t,d} \leq SOC_{max-b,i} \quad \forall b, i, t, d \quad (17)$$

where $SOC_{min-b,i}$ and $SOC_{max-b,i}$ are minimum and maximum SOC values, supposed as 0.2 and 1 according to manufacturer recommendations [24].

- SOC calculation, which is expressed as:

$$SOC_{b,i,t,d} = SOC_{b,i,t-1,d} \cdot (1 - \tau_{bat}) + \left(p_{char-b,i,t,d} \cdot \eta_{char} + \frac{p_{disch-b,i,t,d}}{\eta_{disch}} \right) \cdot S_b \cdot \frac{\Delta t}{E_{cap-b,i}} \quad \forall b, i, t, d \quad (18)$$

where τ_{bat} is the energy loss ratio supposed as 0.001 [24], η_{ch} and η_{disch} are the charging and discharging efficiencies both supposed as 0.9 [24].

- Daily SOC level. The SOC must be the same at the beginning and the end of each representative day to ensure that the battery has a cycling operation. Moreover, the SOC at the beginning of the day is unknown. This can be expressed as:

$$SOC_{b,i,t=0,d} = SOC_{b,i,t=24,d} \quad \forall b, i, d \quad (19)$$

- Battery converter current limits. If the battery is directly connected to the multiport, the connection is in DC and this constraint is not applied. But if the battery is connected to the grid, a VSC is used. Therefore it can exchange reactive power with a limit of maximum current, which can be expressed as:

$$(p_{char-b,i,t,d} - p_{disch-b,i,t,d})^2 + q_{b,i,t,d}^2 \leq (v_{i,t,d} \cdot i_{max-b,i})^2 \quad \forall b, i, t, d \quad (20)$$

$$i_{max-b,i} = \frac{s_{max-b,i}}{v_{n-i}} \quad \forall b, i \quad (21)$$

$$s_{max-b,i} = \frac{p_{n-b,i}}{PF_{b,i}} \quad \forall b, i \quad (22)$$

where $PF_{b,i}$ is the power factor supposed as 0.915 which corresponds to a reactive power minimum capability of ± 44 % (Figure 3) [23].

- Battery cost. This cost can include both the storage capacity and the cost of the converter associated to the battery [24]. If the battery was connected to the MPC, then the converter cost must only be considered in the MPC cost.

$$C_{BESS-b} = C_{capexBESS-b} \cdot \frac{E_{cap-b,i}}{\eta_{char} \cdot \eta_{disch}} + P_{bat-b} \cdot C_{conv} \quad \forall b \quad (23)$$

where $C_{capexBESS-b}$ is the unitary cost of the battery storage, and C_{conv} is the unitary cost of the converter associated to the battery, expressed in [€/kW].

Multiport converter model

Multiport converter variables are related to both the operation and sizing of the converter. Operation variables are defined for each multiport converter terminal k connected to the node i for each hour t of the considered representative days d . They include the active and reactive powers exchanged by the multiport converter terminal, $p_{MPC-k,i,t,d}$ and $q_{MPC-k,i,t,d}$. On the other hand, this sizing variable is the nominal power of each multiport converter terminal connected to the node i ($s_{n,MPC-k,i}$ or $p_{n,MPC-k,i}$). This variable is expressed as the maximum apparent or active power (depending on the case) considering all hourly powers exchanged by the converter terminal. All these variables are expressed per unit.

The multiport converter constraints are related to:

- Multiport converter power balance. This must be ensured considering active powers exchanged by each converter terminal, including if a centralised battery or generator is introduced as an additional terminal of the MPC. Therefore, active power balance within a multiport converter is expressed as:

$$\sum_{k,i} p_{MPC-k,i,t,d} = 0 \quad \forall t, d \quad (24)$$

- Reactive power limits. According to IEEE Standard 1547 [23], energy storage DER should be capable of exchanging reactive power with a minimum capability of $\pm 44\%$ (Figure 3), which corresponds to a power factor of 0.915. As the multiport presented in this thesis is planned to work together with ESS, it has been limited the reactive power following the same capability curve. If this constraint was not considered, reactive power would increase a lot the multiport converter's nominal apparent power. Therefore, the reactive power limits are expressed as:

$$q_{MPC-k,i,t,d} \leq 0.44 \cdot s_{n,MPC-k,i} \quad \forall k, i, t, d \quad (25)$$

$$-q_{MPC-k,i,t,d} \leq 0.44 \cdot s_{n,MPC-k,i} \quad \forall k, i, t, d \quad (26)$$

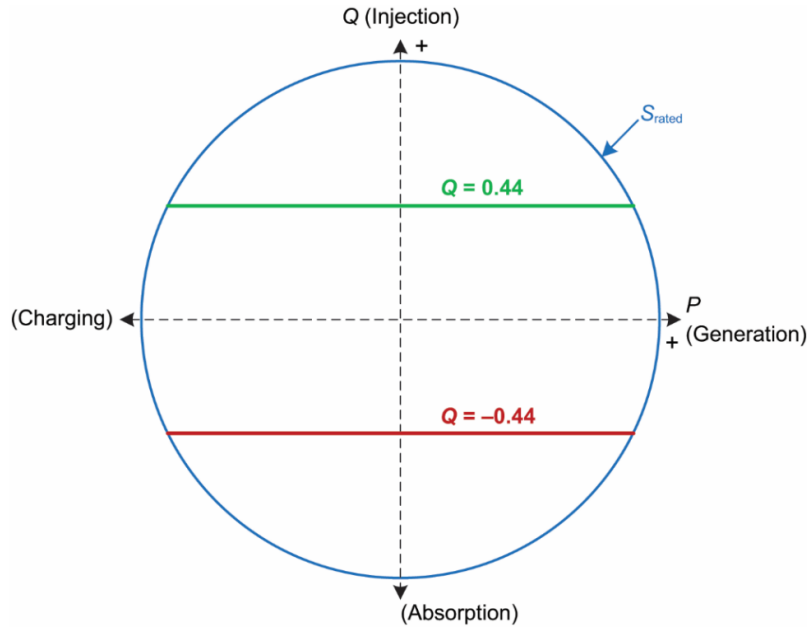


Figure 3: Reactive power capability of energy storage DER [23]

- Multiport current limits, which are expressed as:

$$p_{MPC-k,i,t,d}^2 + q_{MPC-k,i,t,d}^2 \leq (v_{i,t,d} \cdot i_{max,MPC-k,i})^2 \quad \forall k, i, t, d \quad (27)$$

$$i_{max,MPC-k,i} = \frac{s_{n,MPC-k,i}}{v_{n-i}} \quad \forall k, i \quad (28)$$

- Size of each MPC port. If the grid model is considered, then the size of each port is already determined through the current limit. Otherwise, the size of each multiport converter terminal can be defined as the maximum active power exchanged. This last case can be expressed as:

$$p_{MPC-k,i,t,d} \leq p_{n,MPC-k,i} \quad \forall k, i, t, d \quad (29)$$

$$-p_{MPC-k,i,t,d} \leq p_{n,MPC-k,i} \quad \forall k, i, t, d \quad (30)$$

- Cost of the multiport converter. Depending on the sizing variable, the cost of the MPC can be expressed as:

$$C_{MPC} = \sum_{k,i} C_{conv-k} \cdot s_{n,MPC-k,i} \cdot S_b \quad (31)$$

$$C_{MPC} = \sum_{k,i} C_{conv-k} \cdot p_{n,MPC-k,i} \cdot S_b \quad (32)$$

where C_{conv-k} is the unitary cost of the multiport converter terminal k , supposed as 150 €/kW [24].

Grid model

Grid variables are related to its operation. Therefore, they are defined for each electrical node i and for each hour t of the considered representative days d . Grid variables include active and reactive power injected ($p_{i,t,d}$ and $q_{i,t,d}$), voltage phase and magnitude ($\delta_{V_{i,t,d}}$ and $v_{i,t,d}$), and line current ($i_{i,k,t,d}$) between nodes i, k . All these variables are expressed per unit, except the phases, which are expressed in degrees.

The grid constraints are related to:

- Voltage magnitude limits:

$$v_{min,i} \leq v_{i,t,d} \leq v_{max,i} \quad (33)$$

where $v_{min,i}$ and $v_{max,i}$ are supposed as $\pm 10\%$ of the nominal value.

- The main grid is supposed to be the slack. Therefore, the voltage magnitude and angle of the main grid node are fixed at 1 p.u. and 0° respectively, for all hours t and all days d .
- AC power flow equations to ensure active and reactive power balance:

$$p_{i,t,d} = v_{i,t,d} \cdot \sum_k v_{k,t,d} \cdot \left(G_{i,k} \cdot \cos(\delta_{V_{i,t,d}} - \delta_{V_{k,t,d}}) + B_{i,k} \cdot \sin(\delta_{V_{i,t,d}} - \delta_{V_{k,t,d}}) \right) \quad \forall i, t, d \quad (34)$$

$$q_{i,t,d} = v_{i,t,d} \cdot \sum_k v_{k,t,d} \cdot \left(G_{i,k} \cdot \sin(\delta_{V_{i,t,d}} - \delta_{V_{k,t,d}}) + B_{i,k} \cdot \cos(\delta_{V_{i,t,d}} - \delta_{V_{k,t,d}}) \right) \quad \forall i, t, d \quad (35)$$

where $G_{i,k}$ and $B_{i,k}$ are the real and imaginary part of the grid admittance matrix (Y_{bus}) at nodes i, k [25] expressed per unit.

- Line current limits. The current of each line is calculated and its maximum value is limited. The current can be expressed as (37), but this expression is reformulated as (38) to avoid complex numbers.

$$\underline{v}_{i,t,d} = v_{i,t,d} \cdot (\cos \delta_{V_{i,t,d}} + j \sin \delta_{V_{i,t,d}}) \quad (36)$$

$$\underline{i}_{i,k,t,d} = (\underline{v}_{i,t,d} - \underline{v}_{k,t,d}) \cdot \frac{1}{z_{i,k}} - \underline{v}_{i,t,d} \cdot \frac{y_{i,k}}{2} \quad (37)$$

$$i_{i,k,t,d}^2 = \frac{v_{i,t,d}^2 + v_{k,t,d}^2 - 2 \cdot v_{i,t,d} \cdot v_{k,t,d} \cdot \cos \delta_{V_{k,t,d}} - \delta_{V_{i,t,d}}}{z_{i,k}^2} + \frac{y_{i,k} \cdot v_{i,t,d}^2 \cdot \cos \delta_{z_{i,k}} + \delta_{y_{i,k}}}{z_{i,k}} \quad (38)$$

$$- \frac{y_{i,k} \cdot v_{i,t,d} \cdot v_{k,t,d} \cdot \cos \delta_{y_{i,k}} + \delta_{V_{i,t,d}} + \delta_{z_{i,k}} - \delta_{V_{k,t,d}}}{z_{i,k}} + \frac{y_{i,k}^2 \cdot v_{i,t,d}^2}{4} \quad \forall i, k, t, d$$

$$i_{i,k,t,d}^2 \leq i_{max-i,k}^2 \quad \forall i, k, t, d \quad (39)$$

where $i_{max-i,k}$ is the current limit of the line between nodes i, k , $z_{i,k}$ and $y_{i,k}$ are line impedance and admittance magnitude expressed per unit, and $\delta_{z_{i,k}}$ and $\delta_{y_{i,k}}$ are their respective phases expressed in degrees.

3.3.4 Grid-based multiport converter sizing optimisation

The methodology developed in this work has the main objective of sizing a multiport converter, in this section focusing on an optimisation that includes the grid constraints. Figure 4 shows a flowchart of the general methodology, where three main steps are considered: representative days selection, storage sizing, and multiport converter sizing.

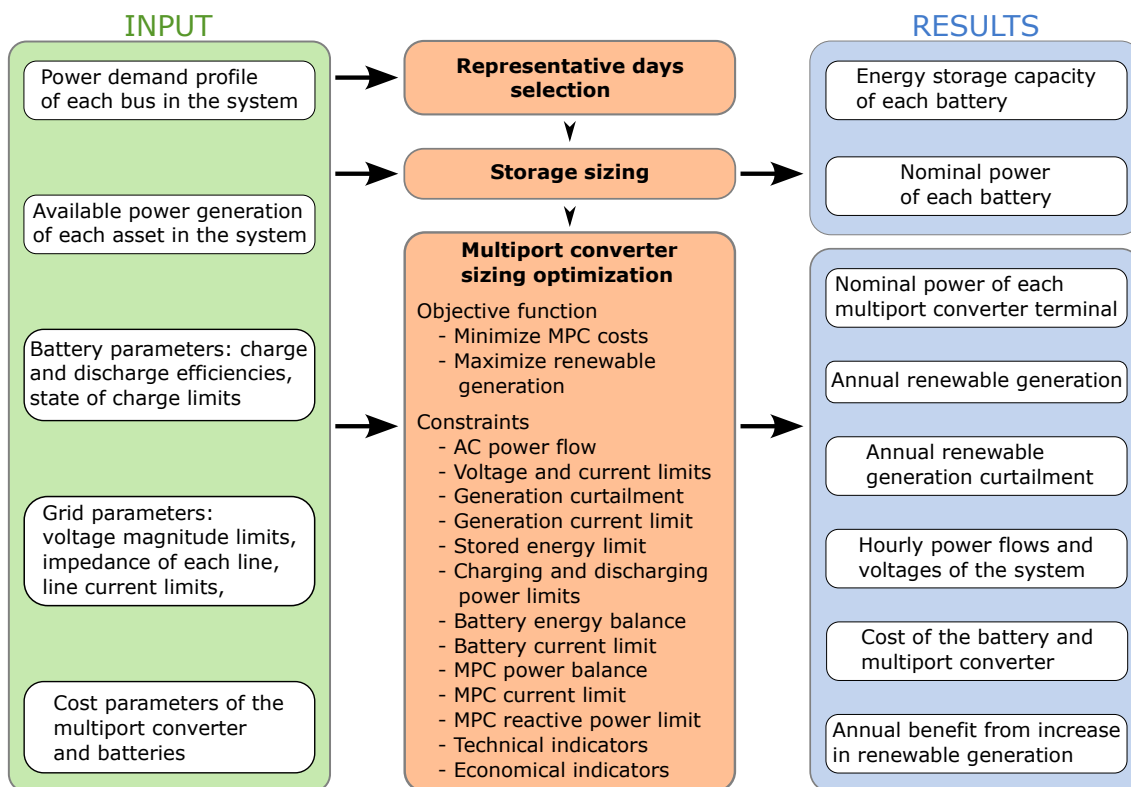


Figure 4: Flowchart of the MPC sizing methodology considering grid constraints

As inputs, generation and demand profiles for a year and with hourly resolution are provided. The technical parameters of the grid and the assets contained in the system are also needed. Moreover, cost parameters of the grid reinforcements such as storage and several interconnection options must be provided, as well as the operation costs of the connection to the external grid.

In this case, unlike Section 3.3.5, if the inputs were directly given to the optimisation problem, it would be too complex and computationally infeasible to solve with the available resources. For this reason, the optimisation is divided into three steps, simplifying the optimisation problem. The first and second steps of the methodology are representative days selection and storage sizing, as explained in Sections 3.3.1 and 3.3.2. The central part of this methodology is the multiport converter sizing, which consists of an optimisation problem that only considers the representative days selected. As mentioned before, the mathematical optimisation formulation will follow equation (1).

As a result, multiport converter size and optimal system operation are obtained. Moreover, several economical and technical indicators are provided to evaluate the advantages of installing a multiport converter. These indicators can be also employed to compare different interconnection configurations.

This methodology has been specifically developed to study a multiport converter used to interconnect MV feeders with renewable generation and energy storage. Although it can be used also on other systems including MV or LV distribution networks, microgrids, and buildings. The optimisation problem and its implementation is explained in detail below.

Optimisation problem

The nominal power of the multiport converter terminals is determined with an optimisation that considers hourly load and generation profiles and the grid constraints. As mentioned before, full-year optimisation has high computational requirements. Therefore, several representative days are considered. In that sense, the proposed optimisation considers separate submodels, one for each representative day. Each submodel will include all system components and their constraints. To combine all the submodels in the main optimisation model, some additional constraints are needed. On the one hand, the sizing variables must be common on all days. On the other hand, energetic variables and indicators that represent the whole year are estimated to be the weighted sum of the representative days selected.

Different elements can be included in the optimisation: the grid, generators, main grid, battery storage, and multiport converter. Each of those elements is modelled separately with the set of variables and constraints shown in Section 3.3.3. Therefore, equations (11) to (28), (31), (33) to (35), (38) and (39) are considered as constraints. Main grid model has been simplified to consider only its variables, but no constraints on them.

Besides the model of each component, to build the system it is needed to connect the elements. In that sense, active and reactive power balance must be done, expressed as:

$$\begin{aligned}
 P_{i,t,d} = & -P_{load-i,t,d} + \sum_{MG} (P_{buy-MG,i,t,d} - P_{sell-MG,i,t,d}) + \sum_g P_{g,i,t,d} \\
 & + \sum_b (P_{disch-b,i,t,d} + P_{char-b,i,t,d}) + \sum_k P_{MPC-k,i,t,d} \quad \forall i, t, d
 \end{aligned} \tag{40}$$

$$\begin{aligned}
 Q_{i,t,d} = & -Q_{load-i,t,d} + \sum_{MG} Q_{MG,i,t,d} + \sum_g Q_{g,i,t,d} - \sum_b Q_{b,i,t,d} + \sum_k Q_{MPC-k,i,t,d} \quad \forall i, t, d
 \end{aligned} \tag{41}$$

The multiport converter is introduced to improve feeders operation without an excessive additional cost. As the methodology aims to size the MPC, the optimisation will minimise the multiport converter cost while optimising other indicators that will depend on the case study. Moreover, some minor terms can also need to be considered in the objective function to obtain a correct optimisation performance.

This methodology can be applied to a wide range of scenarios. However, in this section, it is initially considered to be applied in scenarios with high penetration of renewable generation to explore the advantages of a multiport converter. In such scenarios, renewable generation is likely to be curtailed due to a limited line or transformer capacity. Therefore a multiport converter could be used to maximise the line and transformer capacity factor and reduce the generation curtailment. In this context, to avoid renewable energy curtailment, the income due to renewable generation is maximised for a period of 30 years, which is similar to the converter lifetime. Additionally, depending on how the variables and their constraints are formulated, other terms may be added to the objective function to obtain a correct optimisation performance.

Therefore, the optimisation will minimise the multiport converter cost and minimise generation curtailment, i.e. maximising feeders' operation income due to additional generation enabled by the multiport

converter. As a result, the objective function can be expressed as:

$$[\min] C_{MPC} - I_{ren} \cdot t_{life} + other \quad (42)$$

where C_{MPC} is the multiport converter cost, I_{ren} is the annual income from renewable generation and t_{life} is a factor to weight the two main terms supposed as 30 years, which is similar to the multiport converter lifetime, $other$ represents the additional minor term that may be needed. C_{MPC} is expressed as (31), while the expressions of I_{ren} and $other$ are presented below.

With the current optimisation, some mathematical solutions would not have physical sense. On the one hand, the battery cannot charge and discharge at the same time. These variables have been defined separately because of the efficiencies but they are opposite. On the other hand, the energy exchanged between the main grid and each feeder is also defined with two opposite variables, power bought and sold, which cannot occur at the same time. One way to solve this situation would be to relate the opposite variables with an auxiliary binary variable, but this will result in a high computational cost. Instead, it is decided to implement an equivalent in the objective function. The sum of the variable pairs is minimised to achieve that when one variable has some value, its opposite will be 0. Moreover, to relate this term with the main optimisation objective it is required to apply some coefficient, so it will not affect the overall results. This coefficient is supposed as 0.00001. Therefore, the additional objective function term can be expressed as:

$$other = 0.00001 \cdot (other_{BESS} + other_{MG}) \quad (43)$$

$$other_{BESS} = \sum_{d=1}^{N_d} w_d \cdot \sum_{b,i} \sum_{t=0}^T (p_{char-b,i,t,d} + p_{disch-b,i,t,d}) \quad (44)$$

$$other_{MG} = \sum_{d=1}^{N_d} w_d \cdot \sum_{MG,i} \sum_{t=0}^T (p_{buy-MG,i,t,d} - p_{sell-MG,i,t,d}) \quad (45)$$

where T is the amount of time steps in each day d , which has a value of 23.

Moreover, some technical and economic indicators have been defined to analyse the results and set the objective function.

The technical indicators considered are:

- Annual renewable generation (E_{ren}) which is expressed as:

$$E_{ren} = \frac{1}{\sum_{d=1}^{N_d} w_d} \cdot \sum_{d=1}^{N_d} w_d \cdot \sum_{t=0}^T \sum_{g,i} p_{g,i,t,d} \cdot S_b \cdot \Delta t \quad (46)$$

where N_d is the number of representative days, w_d is the weight of each representative day in the year.

- Renewable generation curtailment (E_{curt}). Due to grid constraints or converter power limits,

the generators may not produce as much energy as is available. The curtailment represents the percentage of renewable generation reduction with respect to the maximum available for a year. This can be expressed as:

$$E_{curt} = \frac{E_{ren-max} - E_{ren}}{E_{ren-max}} \cdot 100$$

$$E_{ren-max} = \frac{1}{\sum_{d=1}^{N_d} w_d} \cdot \sum_{d=1}^{N_d} w_d \cdot \sum_{t=0}^T \sum_{g,i} p_{max-g,i,t,d} \cdot S_b \cdot \Delta t \quad (47)$$

The economic indicators considered are:

- Investment (C_T). This represents the cost of additional equipment installed in the feeders, which mainly considers multiport converter costs (C_{MPC}). Also, costs from batteries [24] (C_{bat}) or other equipment (C_{oth}) can be included. Then, the total investment cost can be expressed as:

$$C_T = C_{MPC} + C_{bat} + C_{oth} \quad (48)$$

- Annual income from renewable generation (I_{ren}), which is expressed as:

$$I_{ren} = C_{en} \cdot E_{ren} \quad (49)$$

where C_{en} is the average annual energy price in €/kWh.

- Payback time respect an initial base configuration (PBT). This is the period to recover the initial investment based on additional income from the feeders' operation. Then, the payback time is expressed as:

$$PBT = \frac{C_T}{C_{en} \cdot (E_{ren} - E_{ren-bc})} \quad (50)$$

where E_{ren-bc} is the annual renewable generation in the base configuration. This indicator is especially useful to compare multiport converter solutions or alternative interconnection configurations.

3.3.5 Energy-based multiport converter sizing optimisation

This section presents a methodology to size multiport converters. In this case, the methodology consists in an energetic optimisation of the system, therefore, considering only active power and no grid constraints. Figure 5 shows the energy-based representation of a system with one multiport converter.

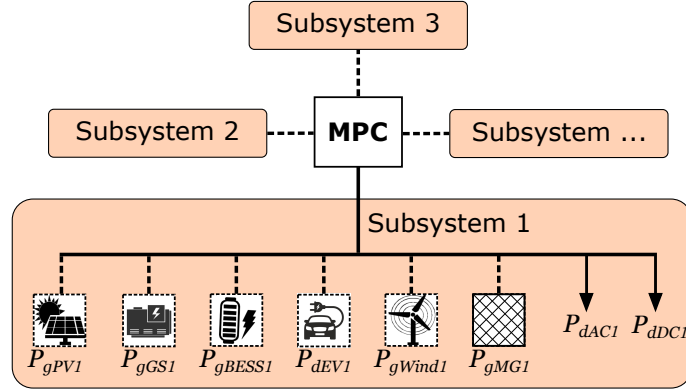


Figure 5: General energetic scheme of a system

As inputs, generation and demand profiles for a year and with hourly resolution are provided. The technical parameters of the system elements and their costs are also needed. The optimisation problem considers a one year time horizon and its formulation follows equation (1). As a result, multiport converter size, defined by the nominal power of its terminals, and optimal operation are obtained. Also other elements of the system can be sized with this methodology, for example battery storage. Several economical and technical indicators are also obtained.

This methodology has been developed as a simplification of the optimisation presented in Section 3.3.4 to analyse how grid constraints impact the multiport converter sizing. In this case, there is no need to use representative days as the optimisation is a mixed-integer linear problem (MILP) and full-year optimisation is fast enough to solve. Therefore, instead of having $t \in [0, 23]$ for each representative day $d \in [1, \dots, N_d]$, now it can be re-formulated as a single equivalent day $d \in [1]$ with $t \in [0, 8759]$.

Different elements can be included in the optimisation, each of those is modelled separately with the set of variables and constraints shown in Section 3.3.3. Therefore, equations (11), (15) to (19), (23), (24), (29), (30) and (32) are considered as constraints. Main grid model has been simplified to consider its variables, and the constraints represented by equations (7) and (8) considering the upper limit of 25 MW which represents the transformers' nominal power. Also, the power balance from equation (40) has been re-formulated as:

$$\begin{aligned}
 0 = & -p_{load-i,t,d} + \sum_{MG} (p_{buy-MG,i,t,d} - p_{sell-MG,i,t,d}) + \sum_g p_{g,i,t,d} \\
 & + \sum_b (p_{disch-b,i,t,d} + p_{char-b,i,t,d}) + \sum_k p_{MPC-k,i,t,d} \quad \forall i, t, d
 \end{aligned} \tag{51}$$

Objective function and technical and economic indicators of this methodology are the same ones presented in Section 3.3.4.

3.3.6 Multiport converter sizing and location

This section presents a methodology to size and locate multiport converters used to interconnect MV feeders.

Several representative days are considered, as full-year optimisation has high computational requirements. Multiport converter sizing is determined with an optimisation-based methodology that includes grid constraints. This optimisation would be the same as shown in Section 3.3.4, but as a different case study will be evaluated, some parts have been changed.

Several configurations are simulated to find the best location. A configuration is defined by the location of the multiport converters and switches. Then, the multiport converter sizing optimisation is performed for each configuration separately. Comparing the results of the different configurations, the configuration with lower objective function value is the optimal. Figure 6 shows a flowchart of the general methodology.

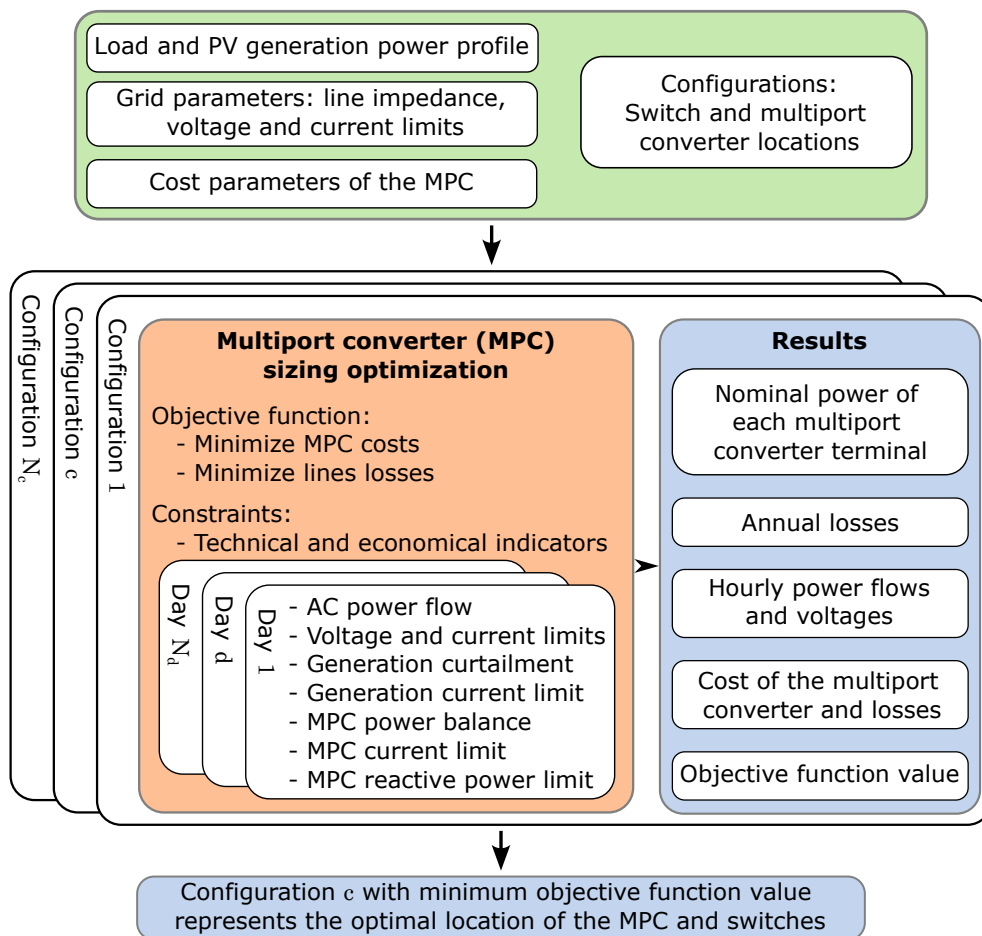


Figure 6: Flowchart of the MPC sizing and allocation methodology

Generation and demand profiles with hourly resolution are provided for different representative days. Technical parameters of the grid and assets included in the system are also needed. Moreover, cost parameters of the grid reinforcements must be provided. As a result, several economical and technical indicators are obtained to evaluate the advantages of installing a multiport converter. These indicators can be also employed to compare different interconnection configurations. In addition, multiport converter size and location, as well as system operation are obtained.

Optimisation problem

The optimisation used in this methodology is based in that presented in Section 3.3.4. The main difference is the application scenario. In this case, there are no batteries in the system, therefore equations (15) to (23) are not considered. Objective function and technical and economic indicators for this particular application scenario are presented below.

In this section, the objective of the multiport converter is initially considered to avoid undervoltages and reduce power losses in the lines. Therefore, the optimisation will minimise the losses while minimising the multiport converter cost.

As a result, the objective function can be expressed as:

$$[\min] C_{MPC} - E_{loss} \cdot C_{loss} \cdot t_{life} + other \quad (52)$$

where C_{MPC} is the multiport converter cost, E_{loss} is the annual losses, C_{loss} is the cost of the losses, supposed as 50 €/kW, and t_{life} is a factor to weight the two main terms supposed as 20 years, which is similar to the multiport converter lifetime.

The technical indicators considered are:

- Annual energy losses (E_{loss}) which is expressed as:

$$E_{loss} = \frac{1}{\sum_{d=1}^{N_d} w_d} \cdot \sum_{d=1}^{N_d} w_d \cdot \sum_{t=0}^{23} \sum_{i,k} i_{i,k,t,d}^2 \cdot r_{i,k} \cdot S_b \cdot \Delta t \quad (53)$$

where N_d is the number of representative days, w_d is the weight of each day in the year, $i_{i,k,t,d}$ and $r_{i,k}$ are the current and resistance of the line between bus i and k .

The economic indicators considered are:

- Investment (C_T). This represents the cost of additional equipment installed in the feeders, which mainly considers multiport converter costs (C_{MPC}). Also, costs from other equipment (C_{oth}) can be included, such as the cost of the VSC associated to the PV generators outside the multiport, which is supposed 150 €/kVA. Switches are considered to have zero cost. Then, the total investment cost can be expressed as:

$$C_T = C_{MPC} + C_{oth} \quad (54)$$

- Payback time respect an initial base configuration (PBT). This is the period to recover the initial investment based on additional income from the feeders' operation. Then, the payback time is expressed as:

$$PBT = \frac{\Delta C_T}{C_{loss} \cdot (E_{loss-bc} - E_{loss})} \quad (55)$$

where $E_{loss-bc}$ is the annual losses in the base configuration, and ΔC_T is the increase of total cost with respect to the base configuration. This indicator is especially useful to compare multiport converter solutions or alternative interconnection configurations.

3.4 Case study: CIGRE

This chapter presents the case study used, from where is the data obtained, and how different scenarios are built. Also, the application of the methodology first step is detailed in this chapter.

3.4.1 Network and profiles

The case study is based on the European MV distribution network from the CIGRE Task Force C6.04.02 [26]. The feeder's nominal voltage is 20 kV and the system frequency is 50 Hz. The network configuration and parameters are the same as in the CIGRE benchmark model.

This benchmark network has two feeders (indicated as A and B in Figure 7) which are optionally interconnected with switches in three locations. In the original benchmark network, switch 1 is located between buses 8-14, switch 2 is between buses 6-7, and switch 3 is between buses 4-11. In this case, only the interconnection between buses 16-17 is considered with the possibility to employ a multiport converter instead of a switch, as shown in Figure 7.

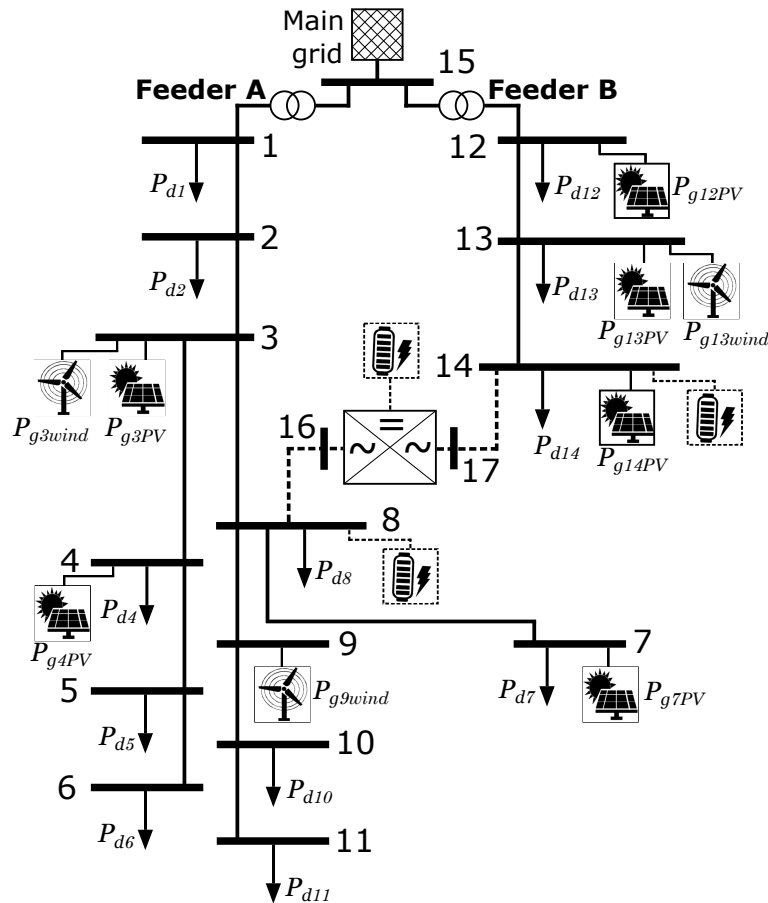


Figure 7: Electrical scheme of CIGRE case study with multiport converter

The network parameters considered for the lines and transformers are shown in Tables 1 and 2 respectively. It should be mentioned that line segment 13 will only be considered if the switch is closed. Also, line segments 14 and 15 will only be considered if there is a multiport converter. When considering

the multiport converter, buses 16 and 17 are equivalent to its AC ports, and the line segments between those buses and the feeders have in total the same length as the line segment of the original switch.

Table 1: Connections and line parameters

Line segment	Node from	Node to	$R'_{ph}[\Omega/\text{km}]$	$X'_{ph}[\Omega/\text{km}]$	$B'_{ph}[\mu S/\text{km}]$	l [km]
1	1	2	0.501	0.716	47.493	2.82
2	2	3	0.501	0.716	47.493	4.42
3	3	4	0.501	0.716	47.493	0.61
4	4	5	0.501	0.716	47.493	0.56
5	5	6	0.501	0.716	47.493	1.54
6	7	8	0.501	0.716	47.493	1.67
7	8	9	0.501	0.716	47.493	0.32
8	9	10	0.501	0.716	47.493	0.77
9	10	11	0.501	0.716	47.493	0.33
10	3	8	0.501	0.716	47.493	1.3
11	12	13	0.510	0.366	3.172	4.89
12	13	14	0.510	0.366	3.172	2.99
13	14	8	0.510	0.366	3.172	2
14	14	17	0.510	0.366	3.172	0.8
15	8	16	0.510	0.366	3.172	1.2

Table 2: Transformer parameters

Node from	Node to	Connection	V_1 [kV]	V_2 [kV]	Z_{tr} to V_2 side [Ω]	S_{rated} [MVA]
15	1	3-ph Dyn1	110	20	0.016+j1.92	25
15	12	3-ph Dyn1	110	20	0.016+j1.92	25

The CIGRE benchmark model also has loads and DER, but for our case study, these data are not used. Instead, there have been searched more detailed load and generation profiles based on real data. For that purpose, it has been searched for a location which would already have some DER units.

Load profiles are defined based on load information from six nearby towns in central Catalonia, as shown in Figure 8: Igualada, Rubió, Òdena, Castellfollit del Boix, Aguilar de Segarra, and Els Prats de Rei. It has been extracted residential hourly consumption of each city for one year, specifically for 2019, using Datadis which is a database of the Spanish electrical demand [27]. Since the load information is only for active power, reactive power demand is also included considering a power factor of 0.97.

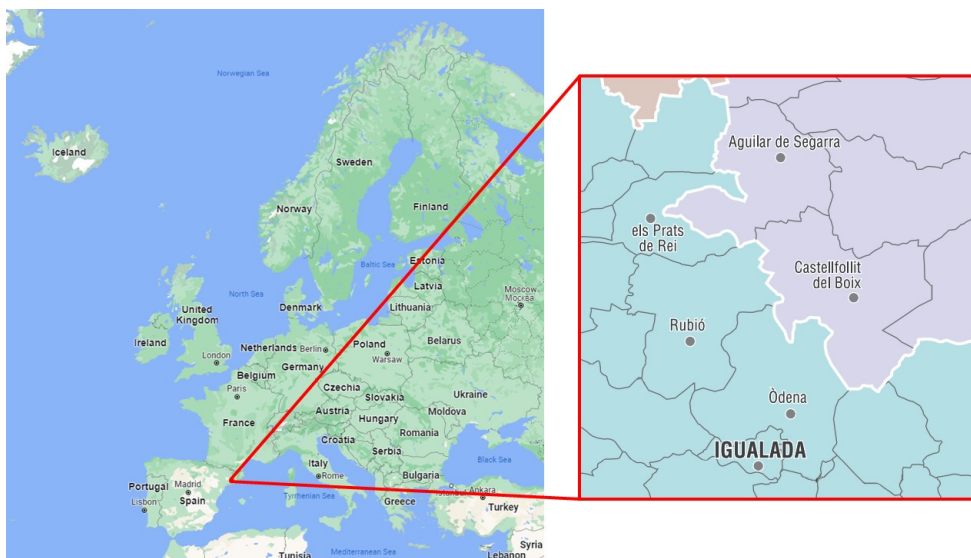


Figure 8: Location of load and generation profiles

Different loads are connected at each bus of the case study considering the load profile of the mentioned towns. In particular, the load profile of each town is considered as a base value, such that each node has a total load proportional to the base profile of a specific town. The loads of each node will be further explained in the next chapter. Figure 9 shows an example of the load profile of the towns for one week, where it can be seen that the towns have quite different profiles.

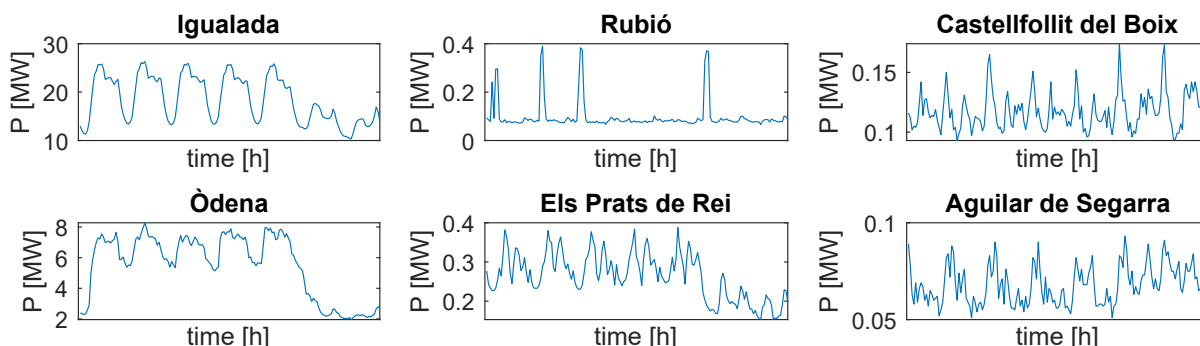


Figure 9: Demands during a week

Solar photovoltaic and wind power are considered as distributed generation of the system. Generation profiles are defined based on resource information around the area where the towns are located. The generation information is obtained for a year, specifically for 2019, from *Renewable.ninja* [28], which is a website tool to obtain PV and wind generation profiles in any location. In particular, hourly available power has been extracted for 1 kW of wind power and 1 kWp of PV power installed. It has been supposed that the power availability will be similar in the area, so a single profile of each source is obtained. Moreover, these profiles can also be considered as base values and scaled afterwards with different amounts of power installation. Therefore, the generation profiles are obtained for the installed power of each node, which will be detailed in the scenario building chapter.

Regarding the batteries, they can be distributed at each feeder or centralized as an additional multiport terminal. All batteries are sized using the methodology from Section 3.3.2. Its feeder is considered in each distributed battery, and the overall system is considered in the centralized battery.

3.4.2 Scenario building

Besides the original data, in order to put together all the previous information and make it work, it is needed to build the actual case study. This chapter focuses on how the load and generation units are distributed in the buses as shown in Figure 7.

Table 3 presents the load distribution in each node as a multiplicative factor of the towns' load profiles. This distribution is arbitrarily selected in order to have a comparable demand while ensuring that the grid structure is adequate.

Table 3: Load distribution

Node	Igualada	Rubió	Òdena	Castellfollit del Boix	Aguilar de Segarra	Els Prats de Rei
1	0	0	0	0	6	0
2	0	3	0	0	0	0
3	0	0	0	0	0	0
4	0	0	0	0	0	3
5	0	0	0	5	0	0
6	0	0	0	6	0	0
7	0	0	0.5	0	0	0
8	0	0	0.6	0	0	0
9	0	0	0	0	0	0
10	0	0	0	0	0	2
11	0	0	0	0	5	0
12	0.2	0	0	0	0	0
13	0.1	0	0	0	0	0
14	0.2	0	0	0	0	0

As this case study is focused on multiport converters to facilitate the integration of renewables into the grid, it has been found that in order to ensure that the multiport is feasible, and that there appears some curtailment, it is required that there is a really high penetration of renewable generation in the system. However, the generation distribution may have an important impact on the results. Additionally, the conclusions of this work are aimed to be as general as possible. Therefore, it has been decided to study 3 different scenarios, which represent potential situations to evaluate the advantage of interconnecting feeders:

- Scenario 1. Similar solar photovoltaic (PV) and wind capacity power are installed in Feeders A and B.
- Scenario 2. Wind generation is mainly installed in Feeder A, while PV generation is mainly located in Feeder B.
- Scenario 3. Most of the generation capacity is installed in Feeder A.

Table 4 shows the generation distribution based on the installed capacity power for each scenario. The total PV and wind generation installed in all scenarios is approximately the same to ensure a fair comparison. Furthermore, both load and generation data were distributed arbitrarily along the network so that the scenarios would have grid problems such as overvoltages, undervoltages and lines saturation.

Table 4: Scenario definition based on generation distribution

Nodes	Scenario 1		Scenario 2		Scenario 3	
	PV	Wind	PV	Wind	PV	Wind
	[MW _p]	[MW]	[MW _p]	[MW]	[MW _p]	[MW]
1	0	0	0	0	0	0
2	0	0	0	0	0	0
3	34	46	4	46	40	56
4	34	0	4	0	40	0
5	0	0	0	0	0	0
6	0	0	0	0	0	0
7	0	0	0	0	50	0
8	0	0	0	0	0	0
9	0	2	0	52	0	40
10	0	0	0	0	0	0
11	0	0	0	0	0	0
12	0	0	20	0	0	0
13	60	54	60	4	18	16
14	0	0	30	0	0	0

3.4.3 Representative days selection

Following the methodology in Section 3.3.1, the representative days have been selected.

The load profile trend is similar for different days, as during the night the load is low and there can appear some peaks during the day corresponding to dinner time and at first hour in the morning. Therefore, it has been supposed that a representative magnitude is the maximum load, which has been divided into 5 levels. For the PV power availability profile, most of the days have a similar profile

since it is not so common to have shadows. Therefore, it has been supposed that the maximum power generation is a representative magnitude, which has been divided into 4 levels. On the other hand, the wind power availability profile is quite variable. Its uncertain nature makes that, specially on days with significant wind power, the high wind power can appear for most of the day or only during a few hours. Therefore it has been taken into account both the hourly maximum power generation and the total daily generation, and have been divided into different levels. Table 5 shows the different levels considered for each magnitude.

Table 5: Classification levels considered to select the representative days

max Load [MW]	max P_{PV} $\left[\frac{\text{MW}}{\text{MWp}} \right]$	max P_{wind} $\left[\frac{\text{MW}}{\text{MW installed}} \right]$	daily E_{wind} $\left[\frac{\text{MWh}}{\text{MW installed}} \right]$
<14.5	<0.3	<0.2	<4
14.5-16.5	0.3-0.6	0.2-0.4	4-9
16.5-21.5	0.6-0.8	0.4-0.7	9-14
21.5-26.5	>0.8	>0.7	>14
>26.5			

As a result, a total of 15 representative days are selected for the multiport converter sizing. Table 6 shows the days selected and the weight of their type. Table 7 shows the detailed levels of the representative day types.

Table 6: Representative days selected and their weights

Representative day	Calendar day	Weight [%]
1	January 8	4.1
2	January 24	2.7
3	February 15	4.4
4	February 16	2.5
5	March 4	2.5
6	April 10	18.1
7	May 3	4.1
8	June 25	5.8
9	July 4	6.8
10	August 11	9.6
11	August 19	3.6
12	September 15	2.5
13	October 18	3.0
14	December 23	2.5
15	December 27	2.5

Table 7: Representative days classification levels

Representative day	max Load [MW]	max P_{PV} [$\frac{MW}{MWp}$]	max P_{wind} [$\frac{MW}{MW\ installed}$]	daily E_{wind} [$\frac{MWh}{MW\ installed}$]
1	21.5-26.5	0.6-0.8	0.4-0.7	4-9
2	21.5-26.5	0.6-0.8	0.7	14
3	21.5-26.5	0.6-0.8	0.2	4
4	16.5-21.5	0.6-0.8	0.2	4
5	16.5-21.5	0.6-0.8	0.7	9-14
6	16.5-21.5	0.6-0.8	0.2-0.4	4
7	16.5-21.5	0.3-0.6	0.2	4
8	16.5-21.5	0.6-0.8	0.4-0.7	9-14
9	21.5-26.5	0.6-0.8	0.2-0.4	4
10	14.5	0.6-0.8	0.2-0.4	4
11	14.5-16.5	0.6-0.8	0.2-0.4	4-9
12	14.5	0.6-0.8	0.4-0.7	9-14
13	16.5-21.5	0.3-0.6	0.2-0.4	4
14	14.5-16.5	0.6-0.8	0.7	9-14
15	14.5-16.5	0.6-0.8	0.2	4

Figure 10 shows the profiles of the representative days. And considering the different scenarios and feeders, Figure 11 is obtained. Where, in total, the average load is 20 MW and the average generation capacity is 45 MW.

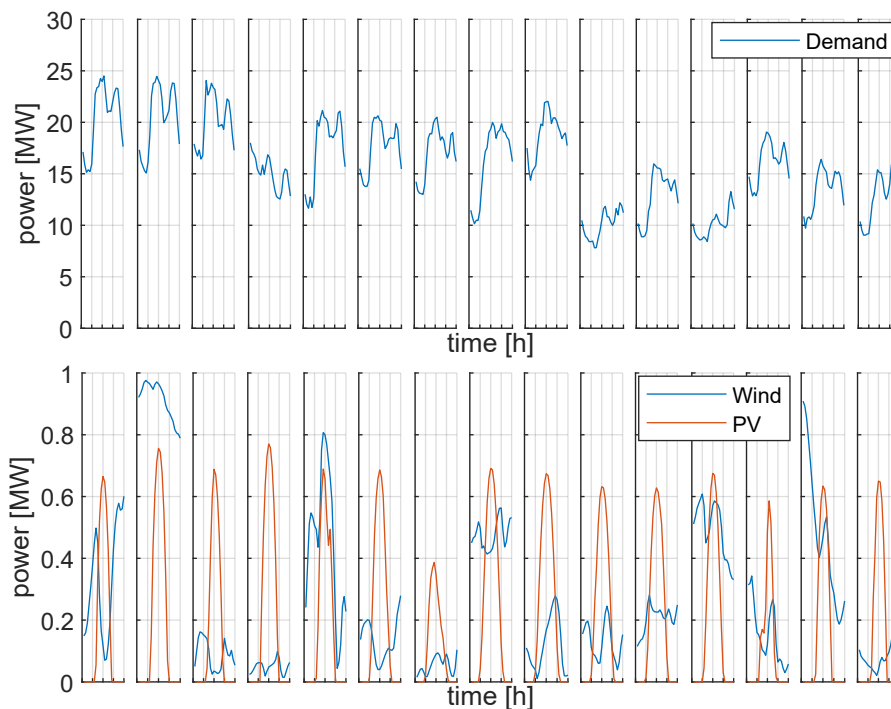


Figure 10: Total demand (top), PV and wind power availability (bottom) on the representative days

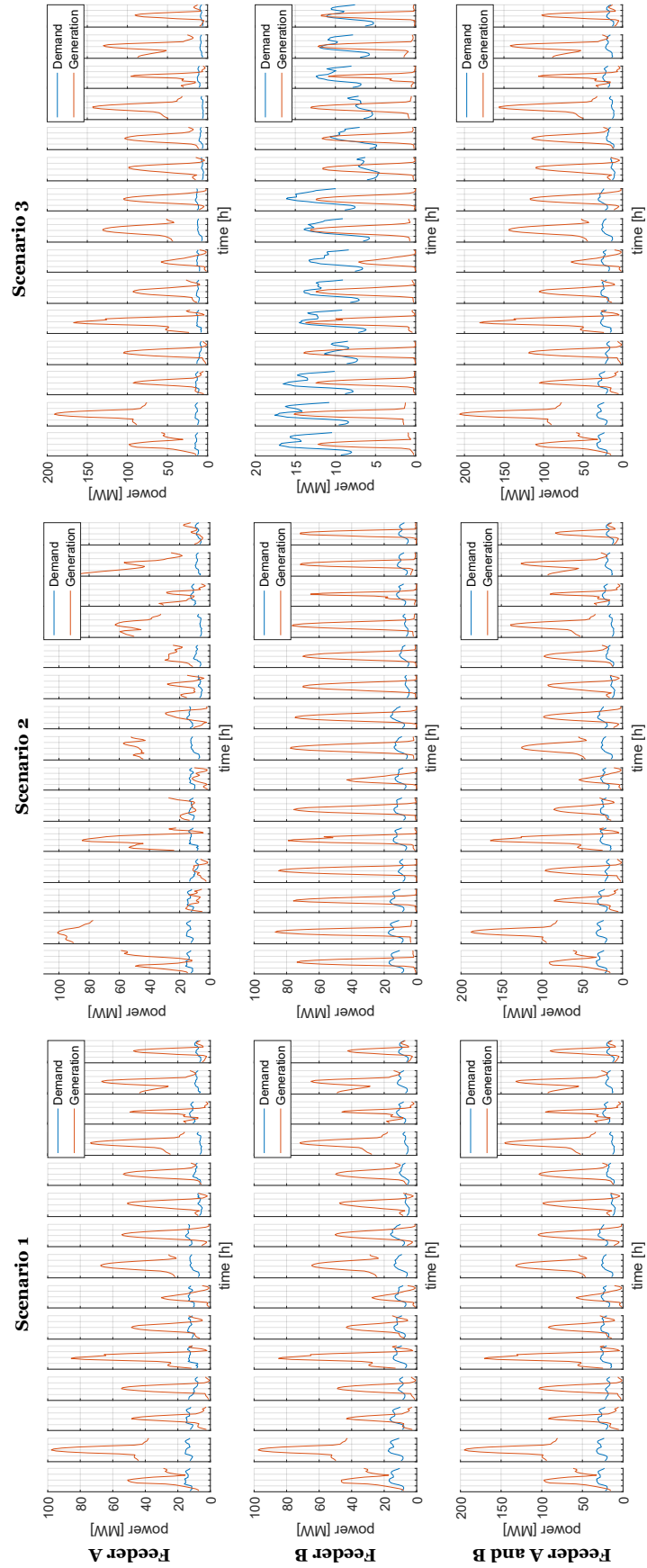


Figure 11: Total demand and generation at each feeder and in total at the representative days for each scenario

3.5 Case study: IEEE 33 bus system

The case study is based on the IEEE 33 bus system [29]. The case study is a 12.66 kV system with one feeder substation, 33 buses and switches in four locations (Fig. 12). These four interconnection options are considered as a possibility to employ a multiport converter instead of a switch.

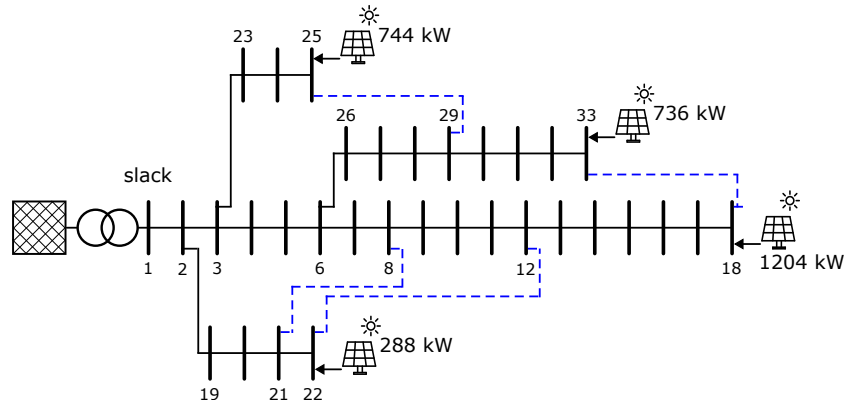


Figure 12: Electrical scheme of 33 bus case study

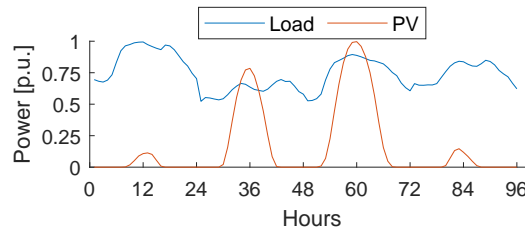


Figure 13: Load and generation profiles of 33 bus case study

The network parameters considered for the lines, hourly profiles of load and PV, and load distribution in the buses are taken from [29]. The profiles shown in Fig. 13 are adapted according to the PV power installed or maximum demand in each bus. Generation units correspond to 80 % the active power load of the branch buses. In total, the system peak load is 3715 kW.

Two generation scenarios have been considered:

- Scenario 1. The PV can only generate active power, and the nominal power of the associated VSC is the same as the nominal power of the PV.
- Scenario 2. The PV can generate both active and reactive power, and the nominal power of the associated VSC is increased to consider a power factor of 0.915 [23] in nominal conditions.

3.6 Grid-based MPC sizing applied to CIGRE case study

This section shows and analyses the results of applying the proposed methodology related to the grid-based multiport converter sizing (Section 3.3.4) to the CIGRE case study explained in Section 3.4.

3.6.1 Configuration definition

A number of configurations are defined based on MPC options, but also considering other possibilities, such as direct switch connection or different battery distributions. Three MPC options are considered: MPC without battery, MPC with converter-connected battery and MPC with direct-connected battery. This last option does not include a controllable terminal for the battery to reduce costs. The MPC configurations are compared to a base configuration without feeder interconnection and a configuration with a switch connection. Also, the introduction of distributed or centralised batteries is compared.

Then, eight configurations are defined based on the previous considerations:

- Ref: reference configuration with two separated feeders without batteries.
- DB: two separated feeders and distributed batteries, which are sized for island requirements.
- DB-S: feeders with direct switch connection and distributed batteries.
- DB-MPC: feeders with a two-terminal MPC connection and distributed batteries.
- CB-MPC3, CB-MPC3f and CB-MPC2: feeders with a three-terminal MPC connection and a centralised battery. In CB-MPC3, the battery is introduced as an additional controllable terminal of the MPC, and that third terminal is sized in the optimisation. In CB-MPC3f, the battery is introduced as an additional controllable terminal of the MPC, but the third terminal has the same size as the battery's nominal power. In CB-MPC2, the battery is introduced as an additional terminal of the MPC, but with a direct connection to the DC bus.
- MPC: feeders with a two-terminal MPC connection without batteries, where the MPC acts as a soft open point.

Finally, a sensitivity analysis with the parameters of Table 8 is performed to provide a general conclusion. Scenarios with 25 % and 50 % reduction of installed generation capacity are also analysed.

Table 8: Sensitivity analysis parameters

Parameters	Base value	Additional values
Island time for battery size	2 h	1, 3 h
Energy storage cost	750 €/kWh	650, 800 €/kWh
Converter cost	150 €/kVA	140, 160 €/kVA
Annual energy price	50 €/MWh	20, 100, 150 €/MWh

3.6.2 Battery sizing

The batteries are sized based on a requirement of island mode following the method presented in Section 3.3.2. In particular, the batteries are sized to cover a ratio of 99 % of the cases that can operate 2h in

island mode. For example, Figure 14 shows the ratio of cases for scenario 2 and a centralised battery, which results in $E_{cap} = 48.27$ kWh and represents a battery capacity reduction of around 37 % compared to a ratio of 100 % of the cases. Table 9 summarises the energy capacity and active power required for the batteries in each scenario and considering distributed or centralised options. It is clear that sharing a centralised battery between the two feeders results in lower total energy capacity and power, especially in scenarios 2 and 3. For example, in Table 9b, the energy capacity of the centralized battery is 0.5 % less than the distributed one in scenario 1, while this reduction is 8.4 % in scenario 2 and 3.1 % in scenario 3.

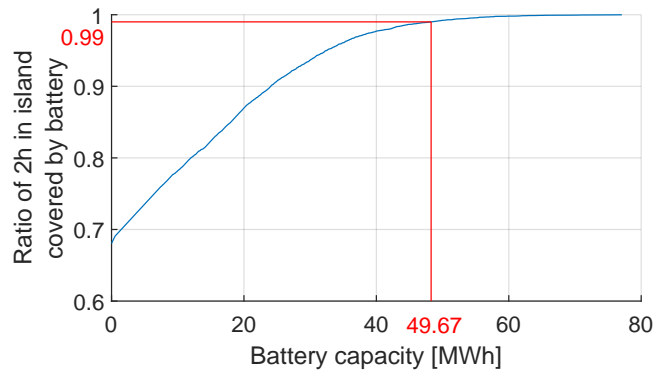


Figure 14: Ratio of total battery capacity required to cover 2h in island mode for scenario 2 and centralised battery option

Table 9: Battery sizing results

(a) Battery size for 1h island mode

	Distributed				Centralised	
	P_A [MW]	$E_{cap,A}$ [MWh]	P_B [MW]	$E_{cap,B}$ [MWh]	P_{A+B} [MW]	$E_{cap,A+B}$ [MWh]
Scenario 1	12.12	16.84	6.06	8.41	17.97	24.95
Scenario 2	11.27	15.65	8.63	12	17.97	24.95
Scenario 3	10.78	14.97	7.62	10.59	17.73	24.64

(b) Battery size for 2h island mode

	Distributed				Centralised	
	P_A [MW]	$E_{cap,A}$ [MWh]	P_B [MW]	$E_{cap,B}$ [MWh]	P_{A+B} [MW]	$E_{cap,A+B}$ [MWh]
Scenario 1	12.12	33.39	6.06	16.49	17.97	49.67
Scenario 2	11.27	30.54	8.63	23.67	17.97	49.67
Scenario 3	10.78	29.41	7.62	20.9	17.73	48.74

(c) Battery size for 3h island mode

	Distributed				Centralised	
	P_A [MW]	$E_{cap,A}$ [MWh]	P_B [MW]	$E_{cap,B}$ [MWh]	P_{A+B} [MW]	$E_{cap,A+B}$ [MWh]
Scenario 1	12.12	48.57	6.06	24.24	17.97	72.4
Scenario 2	11.27	44.65	8.63	35.12	17.97	72.4
Scenario 3	10.78	43.55	7.62	30.93	17.73	71.67

(d) Battery size for 2h island mode when installed generation is reduced 25 %

	Distributed				Centralised	
	P_A [MW]	$E_{cap,A}$ [MWh]	P_B [MW]	$E_{cap,B}$ [MWh]	P_{A+B} [MW]	$E_{cap,A+B}$ [MWh]
Scenario 1	12.61	34.58	6.51	17.65	18.96	52.55
Scenario 2	12.10	32.53	8.78	24.25	19.04	52.55
Scenario 3	11.46	31.07	7.91	21.84	18.62	51.96

(e) Battery size for 2h island mode when installed generation is reduced 50 %

	Distributed				Centralised	
	P_A [MW]	$E_{cap,A}$ [MWh]	P_B [MW]	$E_{cap,B}$ [MWh]	P_{A+B} [MW]	$E_{cap,A+B}$ [MWh]
Scenario 1	13.10	35.77	6.96	18.81	19.95	55.43
Scenario 2	12.93	34.52	8.93	24.83	20.11	55.43
Scenario 3	12.14	32.73	8.20	22.78	19.51	55.18

3.6.3 Results and discussion

This chapter shows the results related to the MPC size and analyses the performance of the system while comparing the multiport converter with other options.

It is important to mention that, as the optimisation problem is non-linear, it is most likely that the results obtained will be local optimums. Therefore there's no guarantee that no better results can be obtained applying the same optimisation problem.

Multiport converter sizing

The results related to the MPC size are analysed for all the scenarios and compared among the different configuration options. In relation to the sensitivity analysis, all the parameters in Table 8 are considered, except for the energy storage cost. This is because this cost is not included in the objective function (42), i.e. the optimisation results are not affected.

Regarding the sizing results, the rated power of the MPC terminals has low variability in scenarios 2 and 3 (Figure 15a). The terminals without battery are sized based on the optimisation presented in Section 3.3.4 and the resulting rated power is around 25 MVA, which is the nominal power of the lines

and transformers. This happens because the currents saturate the lines and transformers, which will be further explained in Section 3.6.3.

In general, the MPC appears when the revenues for energy generation are higher than the cost of the converters. In fact, adding 1 MVA in each MPC terminal would be economically feasible if the annual generation increase is at least 300 MWh. These numbers are just indicative of the ratio between the cost of the MPC and the revenues for energy in the lifetime of the converter, which can be expressed as:

$$\frac{\text{MPC price}}{\text{energy revenues}} = \frac{2 \cdot 150 \text{ €/kW}}{20 \text{ years} \cdot 50 \text{ €/MWh}} \cdot \frac{1000 \text{ kW}}{1 \text{ MW}} = \frac{300 \text{ MWh increased generation}}{1\text{MW in each MPC terminal}} \quad (56)$$

The terminal with a centralised battery can be sized based on the method in Section 3.3.2. In this case, the active power is around 18 MW, as shown in Table 9. But this terminal can also be sized in the optimisation presented in Section 3.3.4. When optimised, the size of this terminal is lower than the battery’s nominal power (Figure 15b). For example, the optimised power is in the range of 7-14 MW whereas in Table 9 the power range is 17-19 MW. This happens because there is no requirement for islanding operation in the optimisation, so the battery from Table 9 is oversized for normal operation.

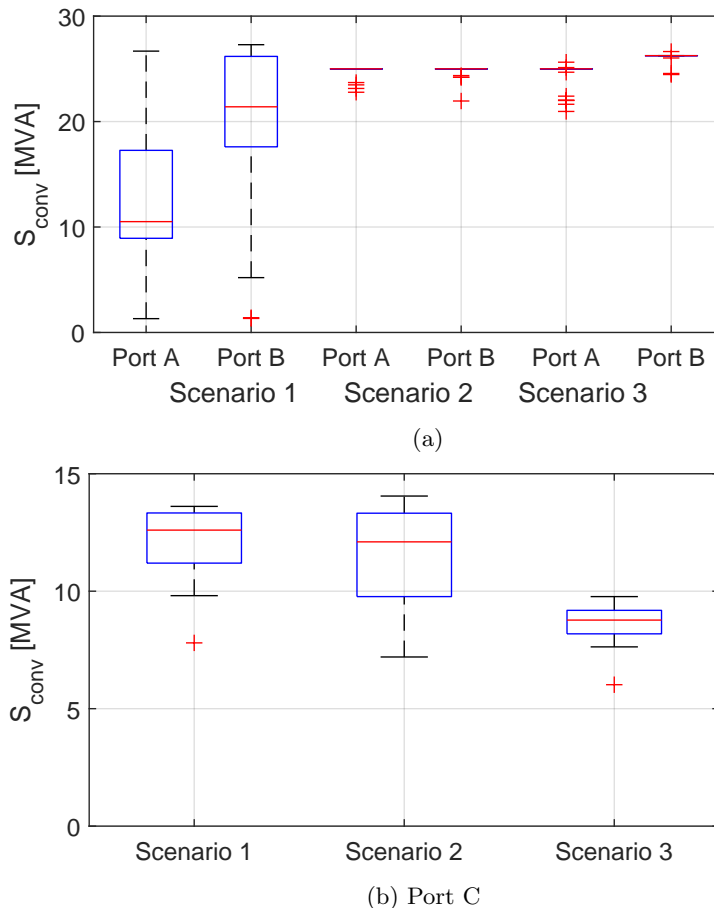


Figure 15: Boxplot of $S_{n,MPC-k}$ for terminals without battery (a) and the battery terminal (b) considering all scenarios, configurations, and sensitivity parameters of Table 8

In scenario 1, the rated power of the MPC terminals without battery has a lot of variability. Taking

a closer look (Figure 16), the energy price seems the most sensitive parameter, followed by the network configuration. The MPC size decreases when the energy price is low, and it tends to 25 MVA when the energy price increases.

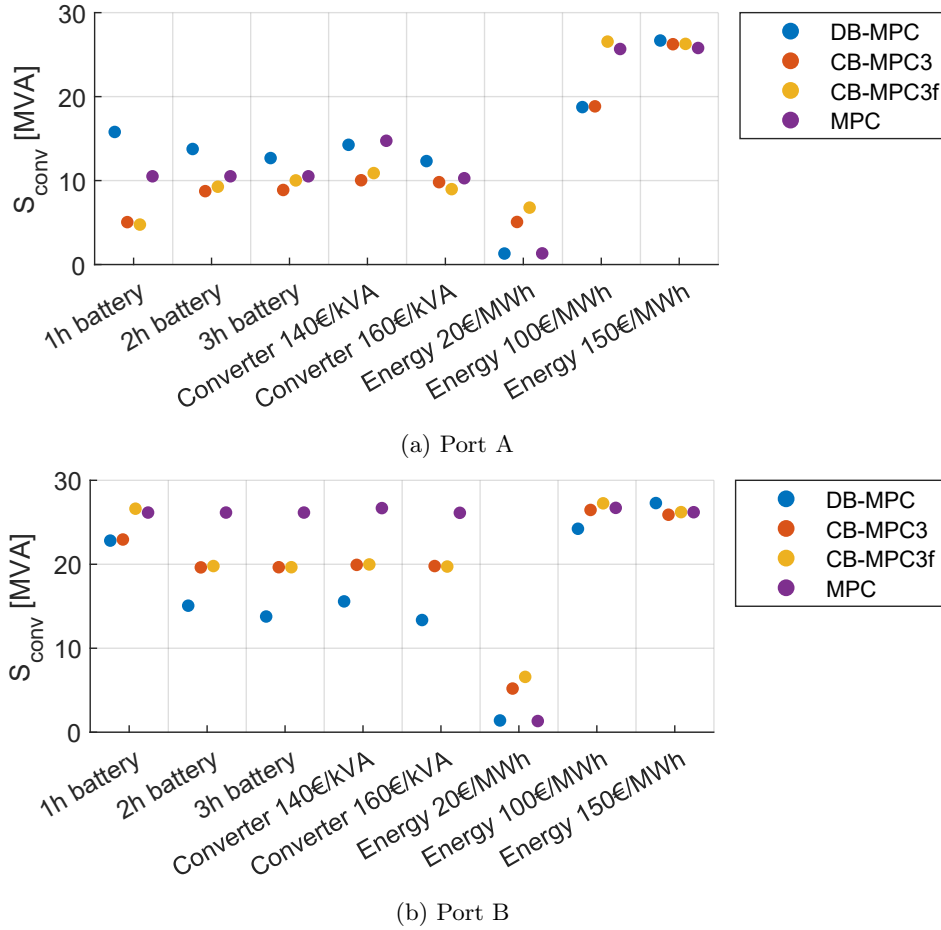


Figure 16: $S_{n,MPC-k}$ for terminals without battery in scenario 1 considering all configurations and sensitivity parameters of Table 8

However, the highest variability in MPC sizing is found when changing the generation installed capacity, which is shown in Figure 17. As a general trend, the rated power of the MPC terminals is reduced when the generation capacity is also reduced. This is very clear in scenarios 1 and 2, where the power may reach 0 making the multiport converter not a possible option to reduce renewable generation curtailment. In scenario 3, due to its generation distribution, the generation has to be reduced a lot to observe a MPC size reduction defined by the optimisation. The terminal with a centralised battery in the configuration CB-MPC3f does not follow this trend because its size is equal to the nominal power of the battery, which is higher with lower generation to be able to fulfil the islanded operation request.

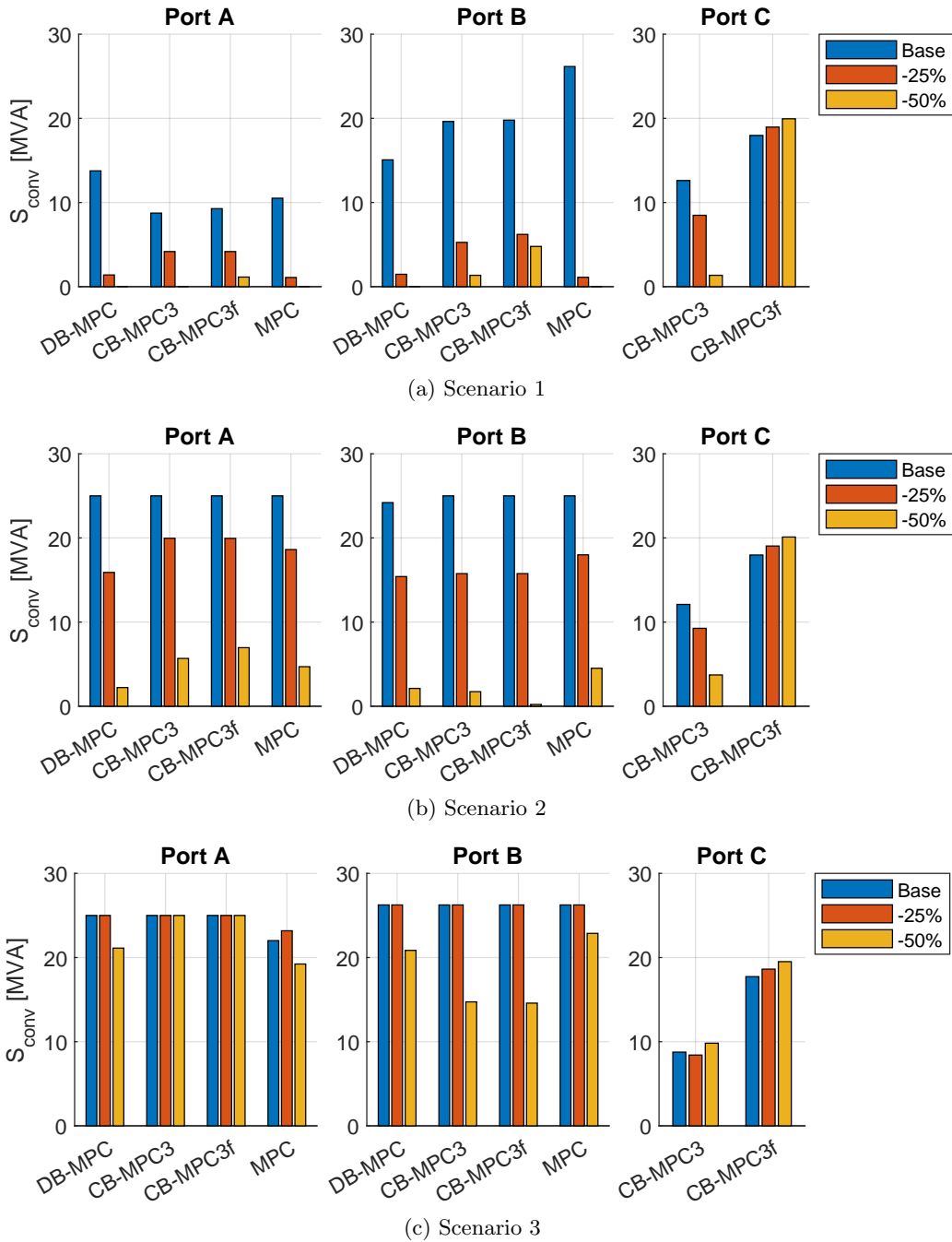


Figure 17: $S_{n,MPC-k}$ for all terminals with different generation capacity

Operation analysis

Taking a closer look at the results regarding the operation of the system, it can be seen where the problems or limitations appear and how the multiport converter contributes to improve the system performance. For this analysis, the representative day 10 of scenario 2 has been chosen and CB-MPC3 configuration has been compared with the Reference one, base values of Table 8 have been considered. This case is an example, but similar results are observed in other days and scenarios.

In the Reference configuration, the voltage throughout the day is around 1 on most of the buses,

while the currents saturate in all lines of feeder B and have a peak of around 15h in some lines of feeder A. For this reason, the multiport converter tends to be have the same nominal power as the lines and transformers in this scenario and configuration, as the MPC tries to redistribute the currents. The multiport converter has a significant impact as the voltages tend to increase in most buses especially during the mid-day. However, an off-peak in the buses of feeder B is observed around 15h, as can be seen in Figure 18. Figure 19 shows that the currents also tend to increase during the mid-day with the introduction of the MPC, where more lines get saturated including the ones connecting to the main grid. However, the power factor at the main grid connection with the feeders is similar in the reference configuration and with the multiport, as seen in Figure 20.

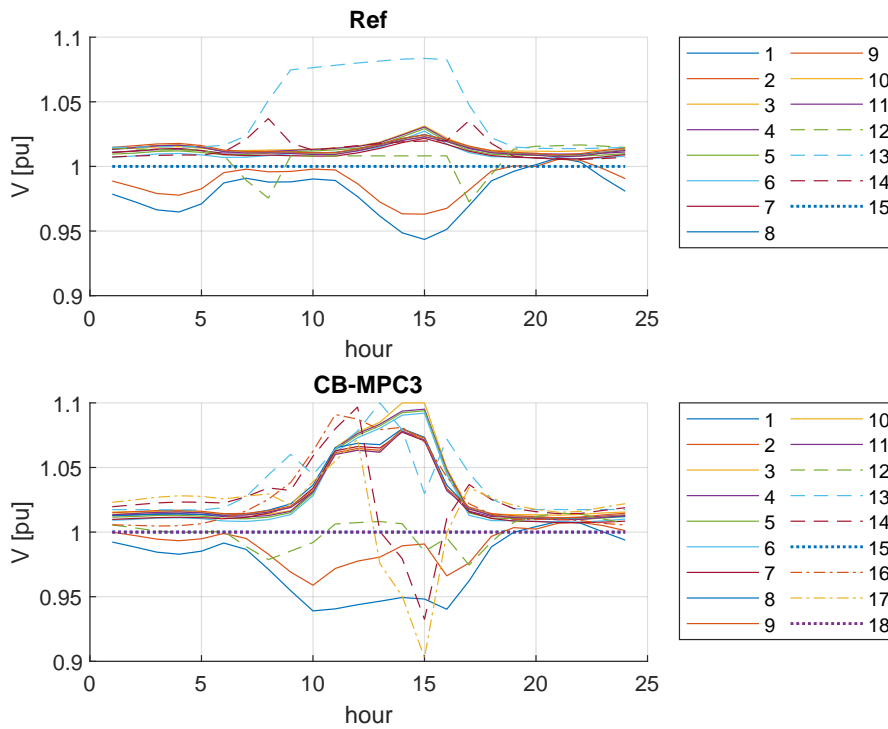


Figure 18: Buses voltage of scenario 2 with configurations Ref and CB-MPC3 in representative day 10 considering the base values of Table 8

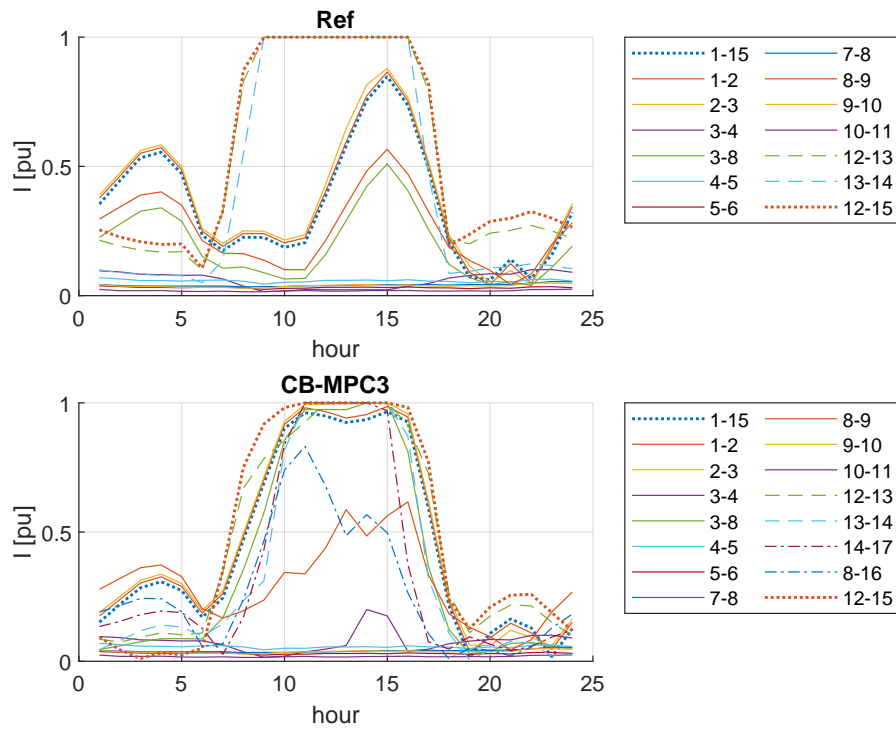


Figure 19: Lines current of scenario 2 with configurations Ref and CB-MPC3 in representative day 10 considering the base values of Table 8

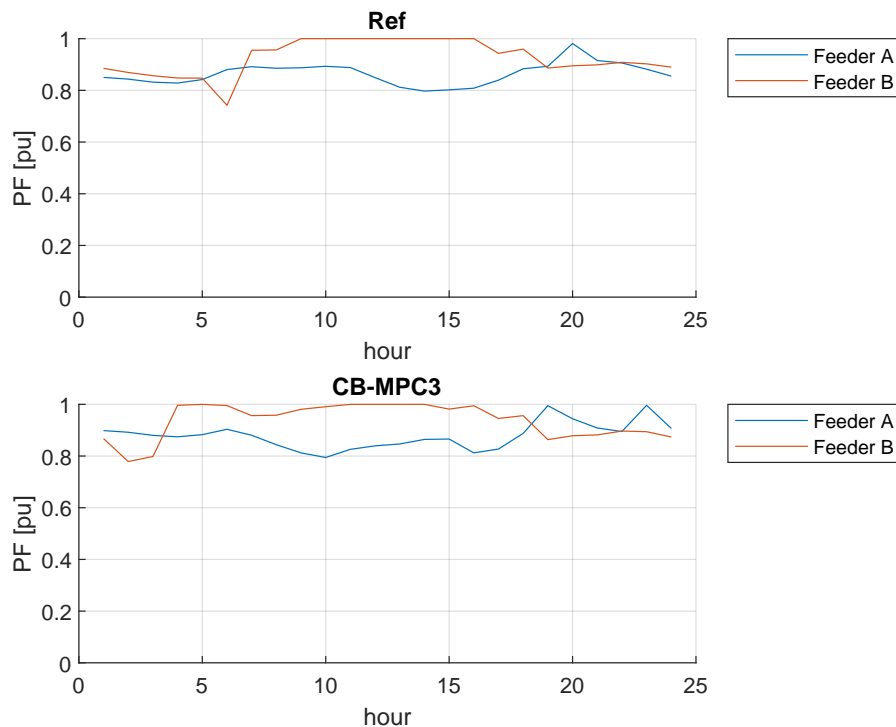


Figure 20: Power factor of the feeders' connection to the main grid of scenario 2 with configurations Ref and CB-MPC3 in representative day 10 considering the base values of Table 8

In this case, the multiport converter is mostly exchanging active power between the feeders and the

battery connected is charged during the mid-day hours. Figure 21 shows the power coming out of each MPC terminal, where it is seen that in addition to active power, the microgrid also exchanges reactive power, but in lower amounts comparatively. This figure also shows that the battery performs one full charge cycle along the day.

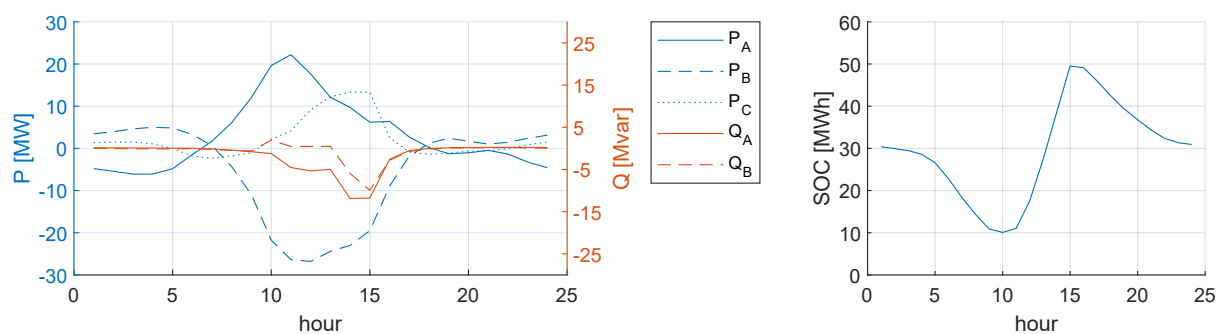


Figure 21: Multiport power exchange and battery SOC of scenario 2 with configuration CB-MPC3 in representative day 10 considering the base values of Table 8

Analysing the system at hour 13, Figures 22 and 23 clearly show that the lines of feeder B are saturated in the Reference configuration, with current equal to 1 pu highlighted in yellow, and this feeder is already injecting 25 MW to the main grid. Therefore, the renewable sources in feeder B are being curtailed, whereas in feeder A the system still has some capacity to integrate more resources. When the multiport converter is introduced, the saturations of feeder B continue and even the voltage of one bus reaches the upper limit. But in this case, feeder B is injecting 25 MW to the MPC, which also injects power to feeder A. The amount of power exchanged between the feeders is as much as possible, as in this case where the line connecting buses 2 and 3 gets saturated. As a result, feeder A increases the active power injection to the main grid by almost 8 MW. At this hour, the MPC terminal connected to feeder B is working at nominal power, while the terminal connected to feeder A is working at 49 % of the nominal power.

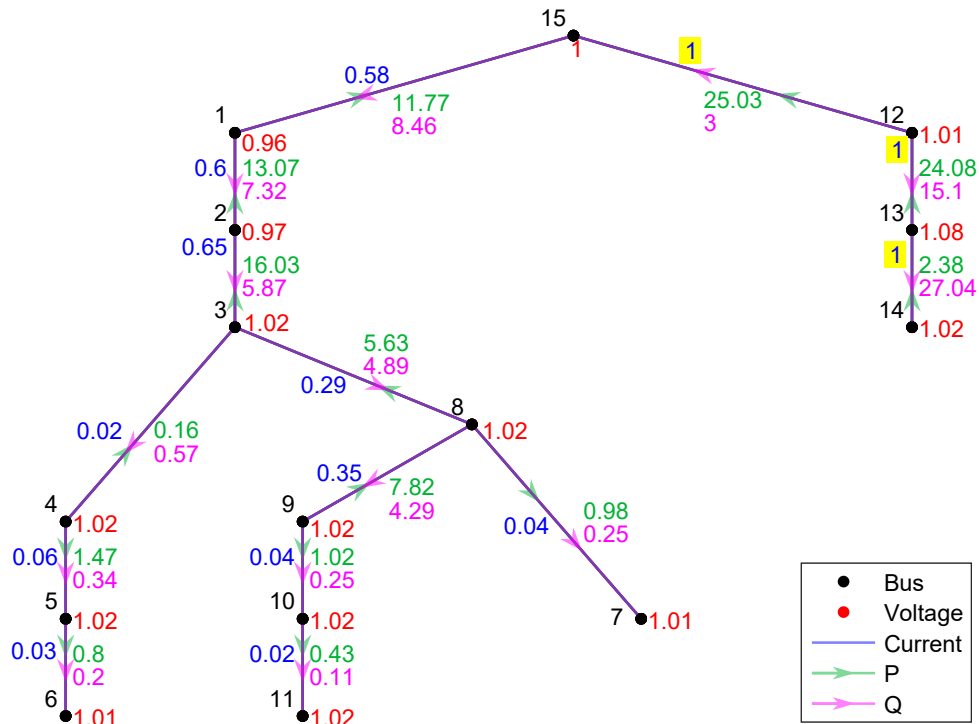


Figure 22: System power flow of scenario 2 with configuration Ref in representative day 10 and hour 13 considering the base values of Table 8

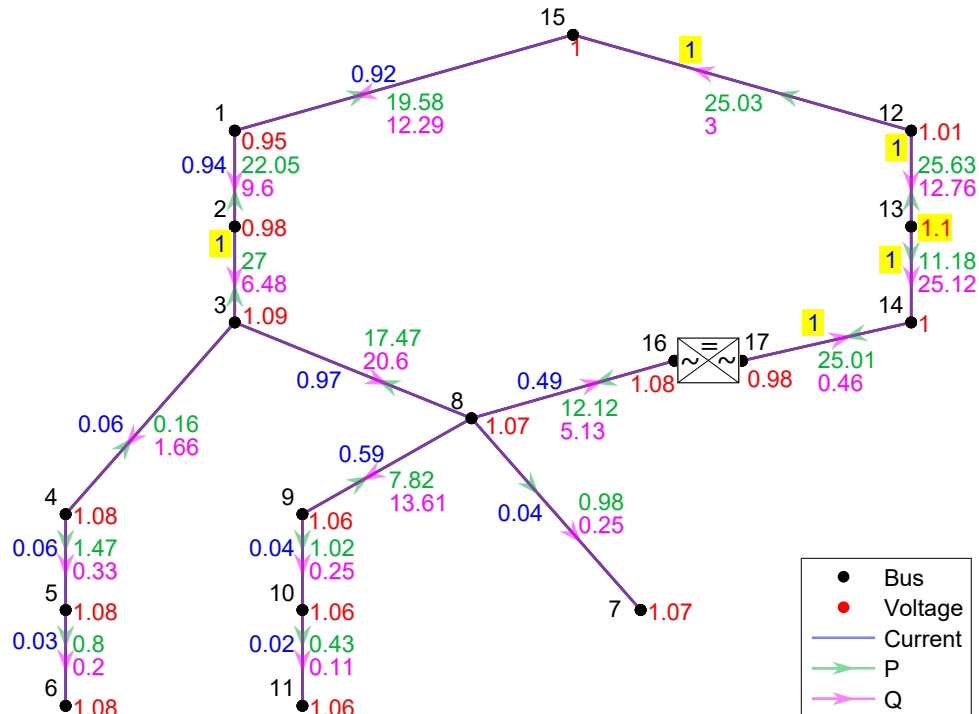


Figure 23: System power flow of scenario 2 with configuration CB-MPC3 in representative day 10 and hour 13 considering the base values of Table 8

Technical evaluation of MPC

The annual renewable generation presents significant variations depending on the scenarios, configuration options and battery size. Figure 24a shows the results considering the base values of Table 8, but equivalent results can be obtained for the additional values of the sensitivity analysis. It should be mentioned that low variability on the rated power of the MPC terminals, present in scenarios 2 and 3, will lead to limited effect of the parameter variations on the annual generation.

As expected, battery introduction improves the annual generation, with an increase of more than 5 % of DB compared to Ref, as seen in Figure 24b. Feeder interconnection with switch or MPC also contributes to the annual generation, especially in scenarios with unbalanced generation with increases of 15-20 % in scenario 2 and 25-30 % in scenario 3, as seen in Figure 24b. Annual generation increase is directly related to a curtailment reduction, as observed in Figure 25, since high penetration of renewable generation implies significant curtailment in all scenarios due to lines and transformers' saturation.

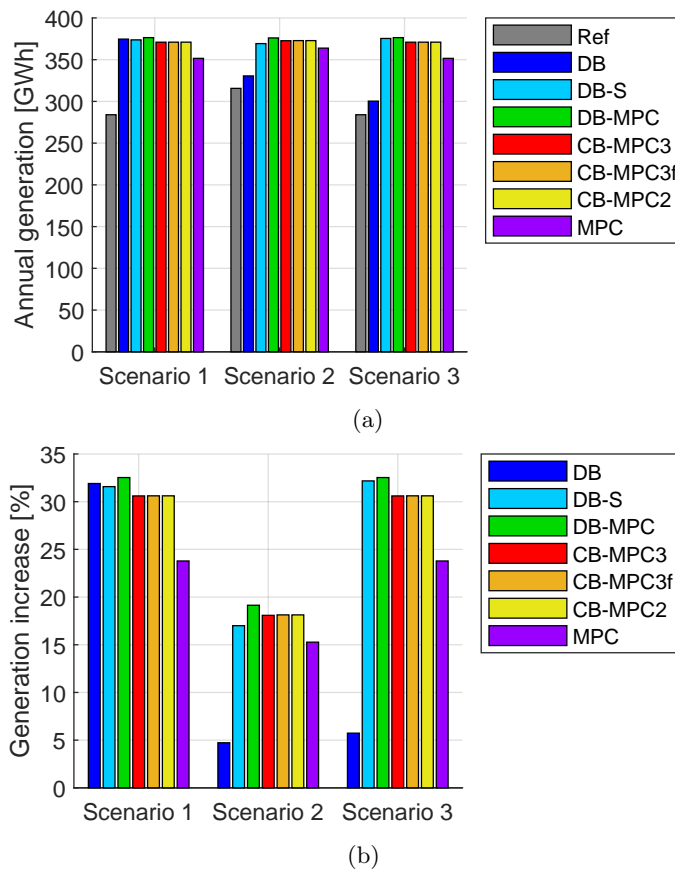


Figure 24: Annual generation (a) and Annual generation increase from Ref configuration (b) for each scenario and configuration, considering the base values of Table 8

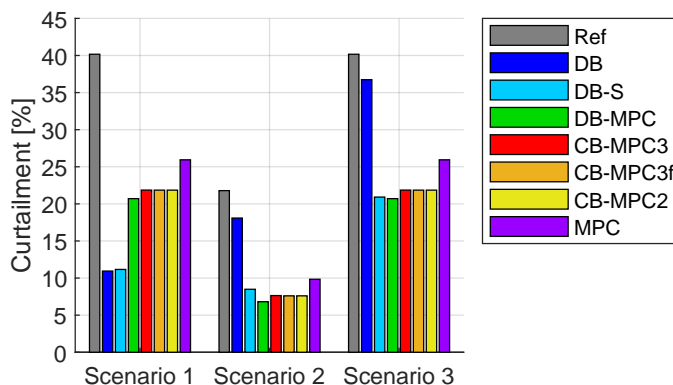


Figure 25: Curtailment for each scenario and configuration, considering the base values of Table 8

In addition, a comparison between battery and feeder interconnection options is shown in Figure 26 to understand which is the most convenient option in scenarios with high penetration of renewable generation. It is clear that when the generation is unbalanced (scenarios 2 and 3), feeder interconnection with switch or MPC (DB-S and DB-MPC options) presents a higher increase in annual generation compared to a battery capacity increase (1h and 3h island options). However, when the generation is uniformly distributed (scenario 1), increasing the battery capacity can have the same impact on annual generation as interconnections with switch or MPC. It should be also mentioned that the cost of battery capacity is significantly more expensive than the cost of interconnection equipment. Therefore, the interconnection options are preferred compared to increasing battery capacity.

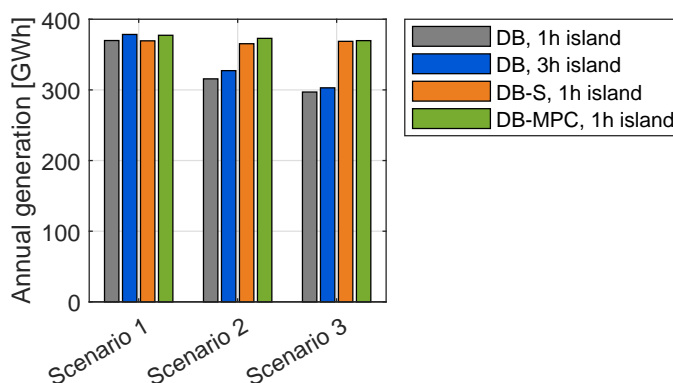


Figure 26: Annual generation for each scenario comparing some configurations

Economic evaluation of MPC

The economic analysis presents the investment C_T and payback time PBT evaluation on the case study to further compare the different configuration options and understand when the MPC is a convenient solution.

Regarding the investment, battery cost represents a significant part of the total cost, while the switch cost can be almost neglected. Figure 27 shows the results considering the base values in Table 8, where the battery cost accounts for more than 80 %. It is observed that the configurations with MPC and

centralized battery (CB-MPC3, CB-MPC3f and CB-MPC2) show slightly lower battery costs in scenarios with unbalanced generation due to a lower energy capacity, as presented in Section 3.3.2.

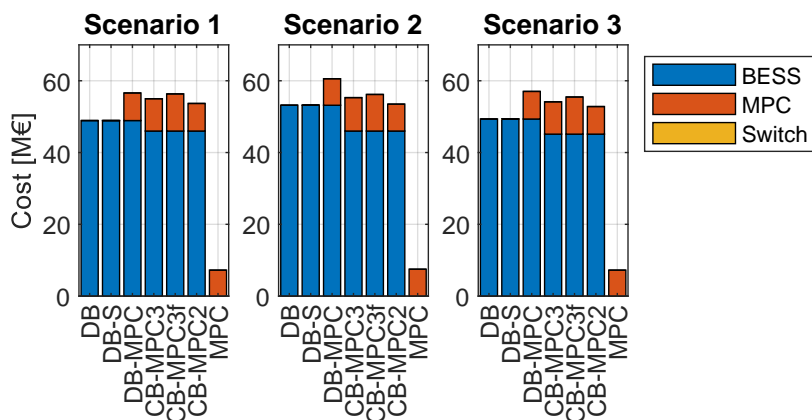


Figure 27: Investment for each scenario and configuration, considering the base values of Table 8

Although investment is significantly high, benefits from the curtailment reduction of renewable generation must be considered to provide a complete economic evaluation. The payback time is used to consider both the investment and curtailment reduction contributions. Two different payback times are considered in the economic analysis: payback respect to Ref and payback respect to DB.

The payback time results respect to the Reference configuration conclude that scenarios with feeder interconnection are the options that can mainly provide reasonable times compared with the lifetime of the components. Figure 28 shows the results considering the base values in Table 8, where the payback time is lower than 20 years for all scenarios and configurations with feeder interconnections.

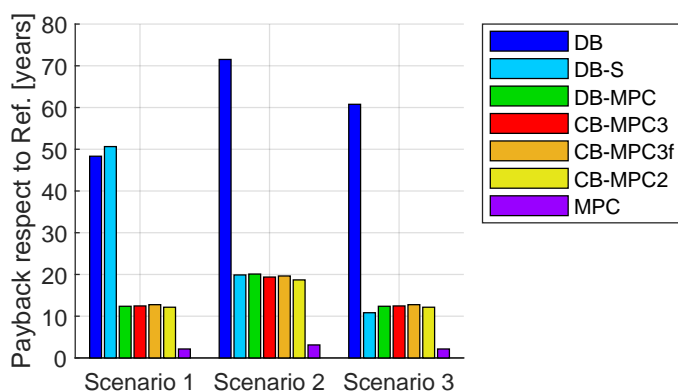


Figure 28: Payback respect to Ref for each scenario and configuration, considering the base values of Table 8

If the payback time is evaluated considering that the distributed batteries are already in place, the results are not only economically feasible but also very attractive. Figure 29 shows the results considering the base values in Table 8, where the payback time is lower than 20 years for all scenarios and in particular lower than 4 years for scenarios 2 and 3. Configurations with switch interconnection (DB-S) have a payback time almost equal to zero due to the low cost of the switch components. However,

it should be mentioned that configurations with MPC provide higher operation flexibility compared to a simple switch interconnection. Then, their payback time could be further reduced if the contribution of additional grid services were considered in the economic analysis.

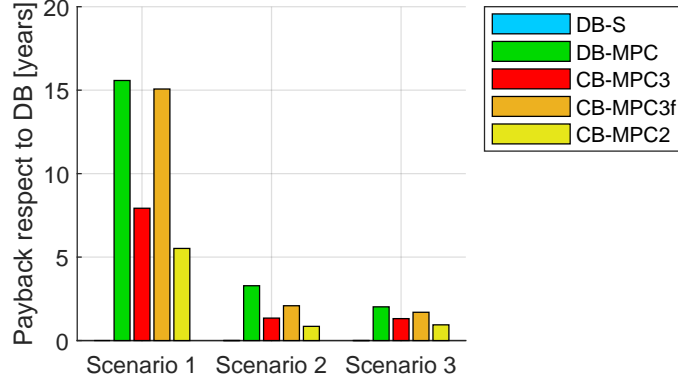


Figure 29: Payback respect to DB for each scenario and configuration, considering the base values of Table 8

Equivalent result trends are obtained considering the additional values of the sensitivity analysis parameters, but are not shown for simplicity. Even when the sizing and annual renewable generation results are approximately independent of the cost and energy prize variations considered in Table 8, as commented before, the payback time is highly affected.

Then, the payback time respect to Ref is further analysed with expressions in relation to cost parameters and energy prize. Linear regressions are derived for the expressions of the cost parameters. In particular, the regressions are obtained with a coefficient of determination R^2 close to 1.

The impact of the battery cost variation on the payback time variation is expressed as:

$$\Delta PBT = k_{bat} \cdot \Delta C_{cap} \quad (57)$$

$$k_{bat} = \begin{cases} 0.81 - 0.91 & \text{if there is MPC} \\ 0.941 & \text{otherwise} \end{cases}$$

where ΔPBT and ΔC_{cap} are the percentage variations of the payback time and battery cost. In general, battery cost variations highly affect the payback, as observed from k_{bat} , which has different values depending on the configuration.

The impact of converter cost variation (for battery and MPC) on the payback time variation is expressed as:

$$\Delta PBT = k_{conv} \cdot \Delta C_{conv} \quad (58)$$

$$k_{conv} = \begin{cases} 0.059 & \text{if there is no MPC} \\ 0.9 - 1 & \text{if there is MPC but no batteries} \\ 0.12 - 0.19 & \text{otherwise} \end{cases}$$

where ΔC_{conv} is the percentage variation of the converter cost. In this case, the converter cost has a low influence on the payback time, as observed from k_{conv} , except when the only element considered is the multiport.

When there is no MPC or its sizing is not affected by the annual energy price, then the total system cost remains invariable. In this case, annual energy price impact has been analysed based on an expression that can be directly derived from equation (50):

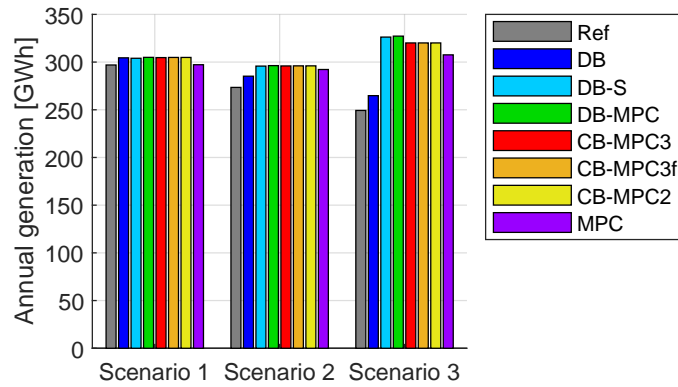
$$\Delta PBT = \frac{1}{1 + \Delta C_{en}} - 1 \quad (59)$$

where ΔC_{en} is the percentage variation of the annual energy price. Configurations with MPC of scenarios 2 and 3 have low sizing variability, therefore the energy price impact on them can be explained with small deviations from equation (50). On the other hand, configurations with MPC of scenario 1 have significant variability as explained in Section 3.6.3, therefore the energy price impact is significantly higher than shown in equation (59), especially when the energy price is reduced. Overall, it is clear that this price has a significant impact on the payback time.

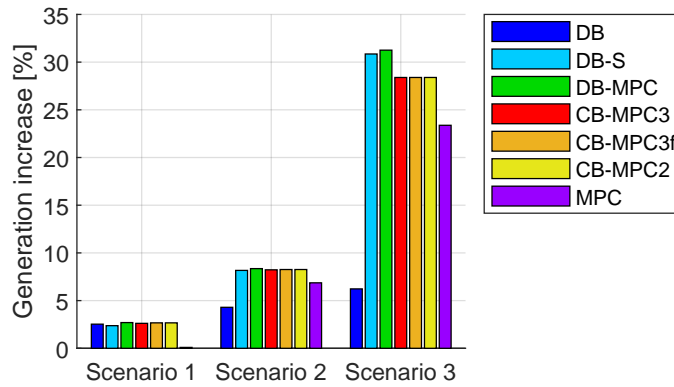
Scenario with 25 % generation reduction

The initial scenario considers a significantly high penetration of renewable generation. A 25 % reduction of generation installed capacity is considered in this chapter in order to analyse the effect on the MPC sizing and performance results.

In this case, a larger battery is needed due to the islanding requirement of the battery sizing method, and the MPC size is already discussed in Section 3.6.3. As a consequence, the investment increases increase due to the larger battery cost (Figure 32). Annual generation and curtailment are reduced, as seen in Figures 30 and 31. Moreover, the curtailment is significantly lower than in the initial scenario, therefore differences in the annual generation between the configurations are less evident.



(a)



(b)

Figure 30: Annual generation (a) and Annual generation increase from Ref configuration (b) for each scenario and configuration, considering the base values of Table 8 and 25 % reduction of installed generation capacity

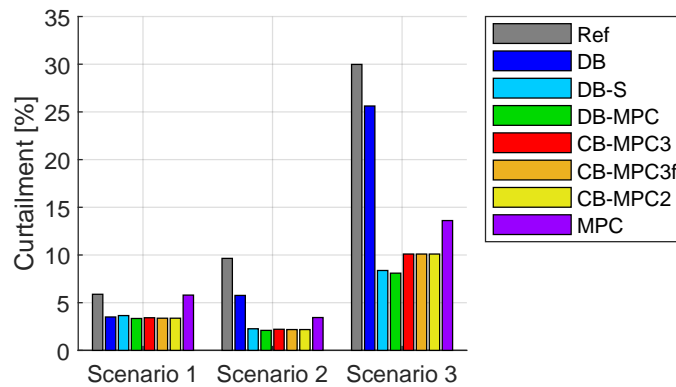


Figure 31: Curtailment for each scenario and configuration, considering the base values of Table 8 and 25 % reduction of installed generation capacity

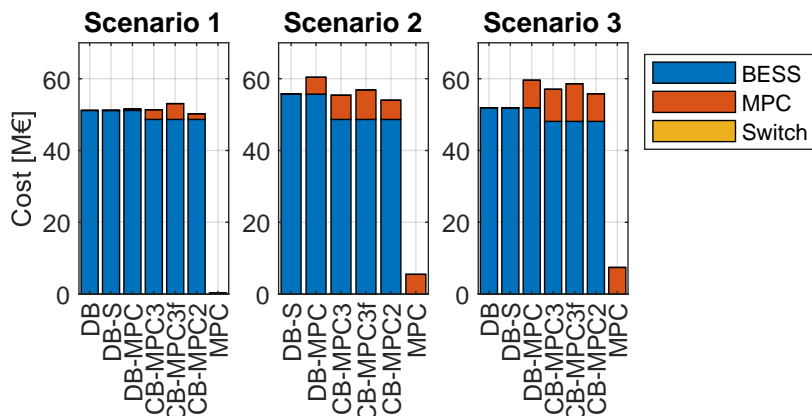


Figure 32: Investment for each scenario and configuration, considering the base values of Table 8 and 25 % reduction of installed generation capacity

The payback time presents a significant increase due to the reduction of income from the sold renewable energy and the increase in battery costs, as seen in Figure 33. In this case, only scenario 3 would be feasible in all interconnection configurations. While in scenarios 1 and 2, only the multiport acting as a soft open point without batteries in the system would have a payback time respect to Ref lower or similar to the lifetime of the converter. If the batteries were already in the system, the multiport would be economically feasible in almost all configurations, as shown in Figure 34. Sometimes, even reaching higher benefits with lower costs, because the centralized battery is smaller than the distributed one. In Figure 34, the configurations whose payback is not clearly seen is because it is almost 0 years.

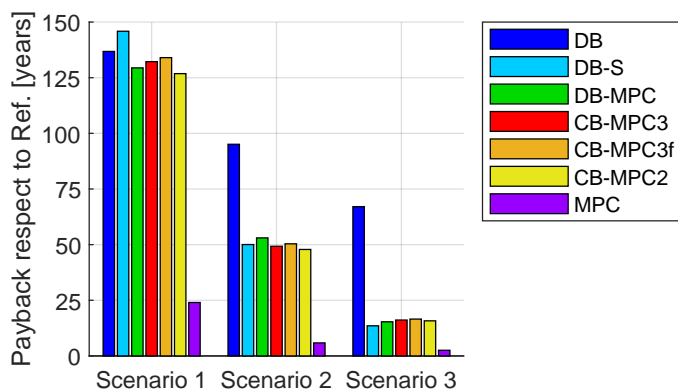


Figure 33: Payback respect to Ref for each scenario and configuration, considering the base values of Table 8 and 25 % reduction of installed generation capacity

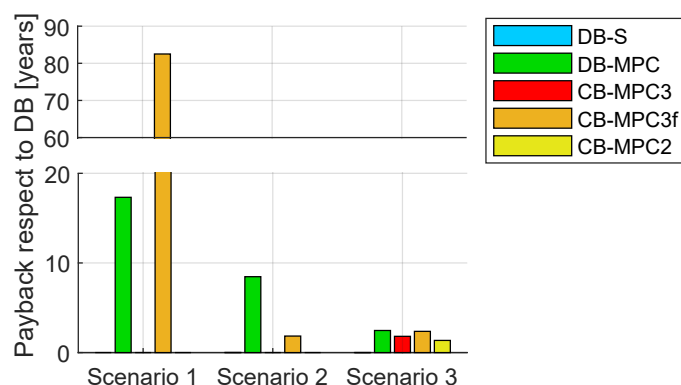
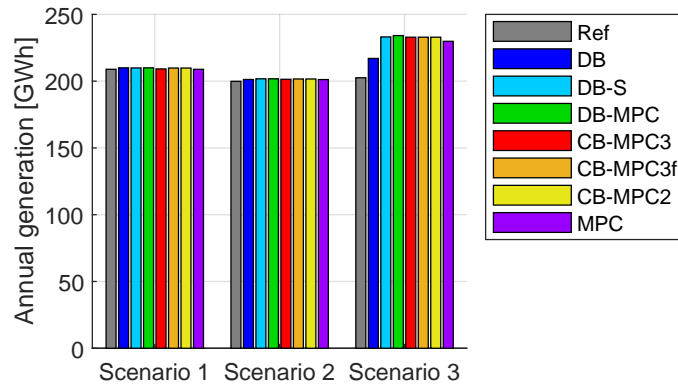


Figure 34: Payback respect to DB for each scenario and configuration, considering the base values of Table 8 and 25 % reduction of installed generation capacity

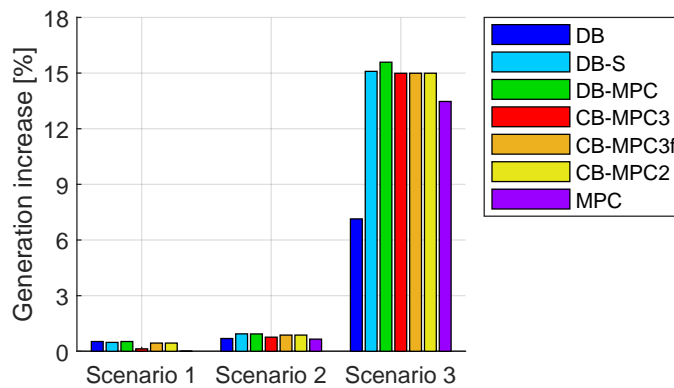
Scenario with 50 % generation reduction

The previous scenario still has significant penetration of renewable generation. A 50 % reduction of generation installed capacity is considered in this chapter in order to further analyse the effect on the MPC sizing and performance results.

This case follows the same trends explained in Section 3.6.3, but with more extreme values. The battery is even larger, and the investment is also higher (Figure 37). Although, the multiport converter tends to disappear in some scenarios and configurations. This is due to the almost nonexistent curtailment from the Ref configuration in scenarios 1 and 2 (Figure 36). In those cases, the annual generation has almost no variation between configurations (Figure 35), which leads to extremely high paybacks respect to Ref (Figure 38). On the other hand, scenario 3 shows some increases in annual generation when introducing batteries and/or interconnecting the feeders (Figure 35), but they are not enough to make the paybacks respect to Ref feasible (Figure 38).



(a)



(b)

Figure 35: Annual generation (a) and Annual generation increase from Ref configuration (b) for each scenario and configuration, considering the base values of Table 8 and 50 % reduction of installed generation capacity

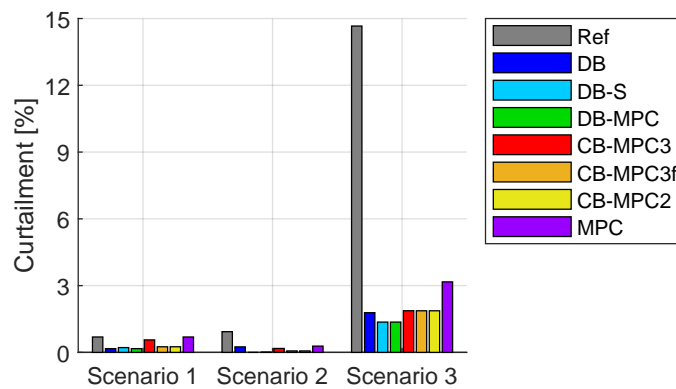


Figure 36: Curtailment for each scenario and configuration, considering the base values of Table 8 and 50 % reduction of installed generation capacity

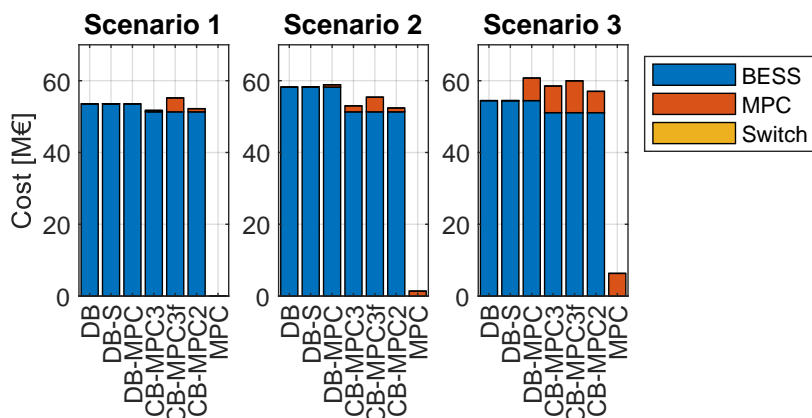


Figure 37: Investment for each scenario and configuration, considering the base values of Table 8 and 50 % reduction of installed generation capacity

In fact, the payback respect to the Reference configuration only approaches the feasibility region with the MPC configuration without any battery (Figure 38). Scenario 1 does not have a multiport converter without battery, as its size would be zero, scenario 3 would have a payback of around 5 years, and the payback of scenario 2 is 21 years, similar to the lifetime of the converter (20-25 years).

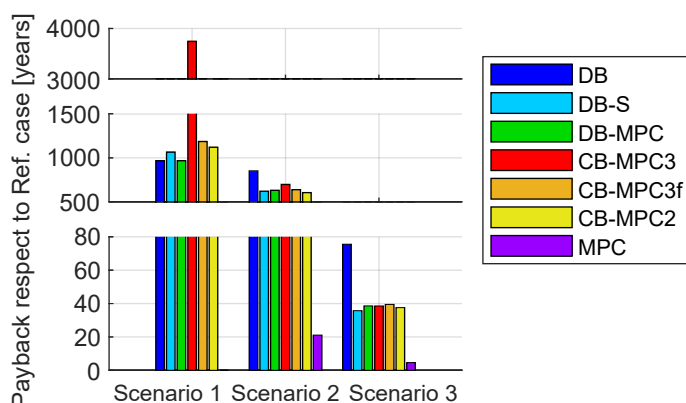


Figure 38: Payback respect to Ref for each scenario and configuration, considering the base values of Table 8 and 50 % reduction of installed generation capacity

The payback respect to DB configuration is a bit harder to interpret. Figure 39 shows that scenario 1 would only be feasible with distributed batteries and some interconnection. Configuration CB-MPC3f is not shown for scenario 1 because the generation is lower than with distributed batteries and the cost is higher, so payback would be infinite. In scenario 3 all configurations are feasible, and in scenario 2 the only unfeasible configuration is the multiport converter with distributed batteries.

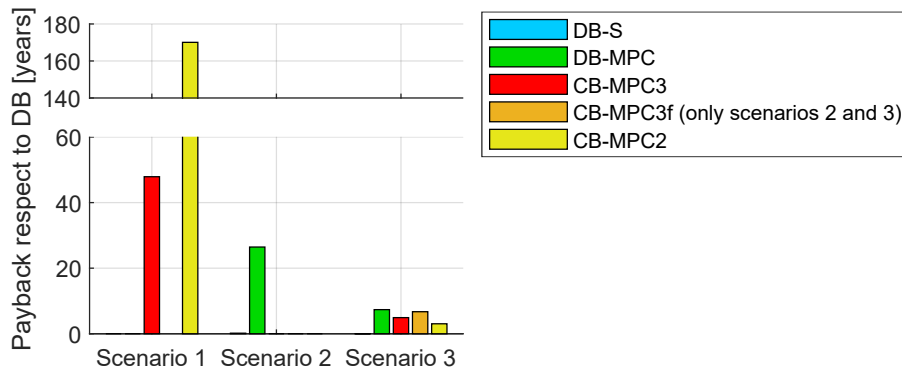


Figure 39: Payback respect to DB for each scenario and configuration, considering the base values of Table 8 and 50 % reduction of installed generation capacity

To conclude, the MPC application in this case study is only feasible for scenarios with high generation or if the generation is unbalanced between feeders and the batteries are assumed to be initially installed in the system.

3.7 Comparison of grid-based and energy-based MPC sizing applied to CIGRE case study

This section shows a brief comparison between the grid-based and the energy-based optimisation to size the multiport converter in the CIGRE case study. This case study is represented in Figure 7, but for the energy-based optimisation it can be simplified as:

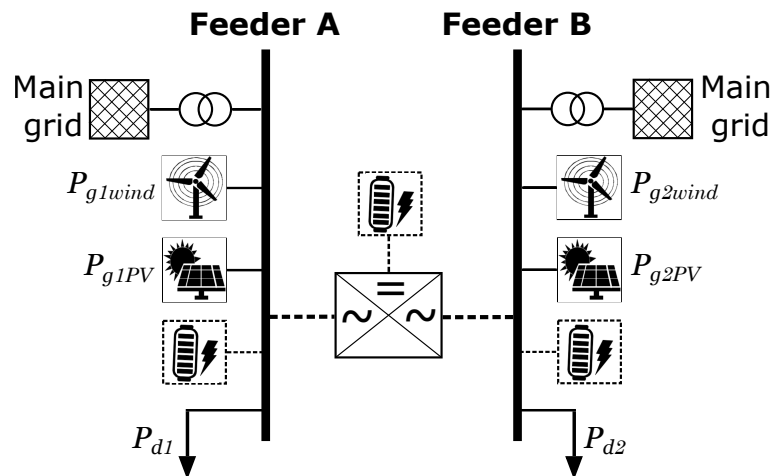


Figure 40: Energetic scheme of CIGRE case study with multiport converter

There are several results that can be analysed in this methodologies comparison, but the most significant one is the multiport converter sizing. The nominal power of all converter terminals with base generation capacity is shown in Figure 17 for the grid-based, and in Figure 41 for the energy-based.

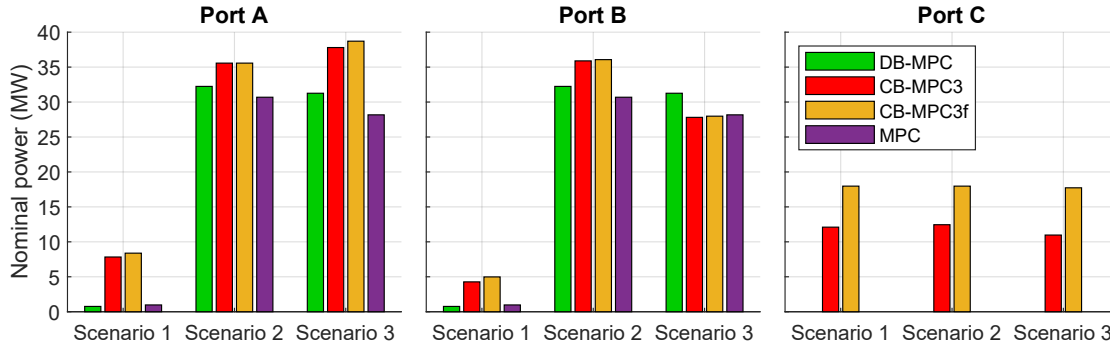


Figure 41: $P_{n,MPC-k}$ for all terminals with base generation capacity using energy-based optimisation

The energy-based optimisation results in higher MPC powers when the generation is unbalanced. This is because the grid-based optimisation is limiting the converter power to 25 MVA, which corresponds to the maximum allowed current on the lines and transformers. On the other hand, in balanced distribution scenarios, the energy-based results in lower MPC powers. This is because, as lines saturation is not considered, the generators can inject as much energy to the main grid as desired until saturating the transformer.

As a general conclusion, considering the AC-OPF or at least some power flow limits is proven to be an important factor in the multiport converter sizing of this case study.

3.8 MPC sizing and allocation applied to IEEE 33 bus case study

Multiport converter configurations are analysed based on the methodology presented in the Section 3.3.6 and considering the 33 bus case study with different scenarios (Section 3.5). The results aim to provide a general conclusion about the application and contribution of multiport converters for voltage support and loss reduction in feeders with distributed generation and high load penetrations.

3.8.1 Configuration definitions

Several configurations are defined based on interconnection locations and MPC options, but also considering direct switch connection.

Two MPC options are considered:

- Two-terminal MPC, similar to a SOP, considering the PV generation is connected to the buses as shown in Fig. 12.
- Three-terminal MPC, considering that the PV generation is connected to the third terminal instead of the buses to which the MPC is connected. Therefore, the MPC between buses 8 and 21 or between 12 and 22 will include the PV of bus 22; the MPC between buses 25 and 29 includes the PV of bus 25; and the MPC between buses 18 and 33 includes the PV of buses 18 and 33.

Moreover, all possible configurations combining MPC and switches are considered for the different

locations. Therefore, options from 1 to 4 MPCs will be considered for all locations assuming that remaining locations will have switches, which can be open or closed.

When comparing the different configurations, the increase of total cost refers to the increase of power electronics in the system with respect to the same scenario without multiport converters but considering that the switches of the same interconnections are closed. The annual losses in the base configuration also refer to the losses in the scenario without multiport converters but considering that the switches of the same interconnections are closed. For example, the configuration of a multiport converter between buses 12 and 22 is compared with the configuration of having a closed switch between buses 12 and 22.

3.8.2 Results and discussion

The results related to the MPC size and location are analysed and compared among the different configurations and scenarios.

Before adding any multiport converter, not all configurations fulfil the requirement of having a minimum voltage of 0.95 p.u. In scenario 1, buses 18 and 33 can reach a minimum voltage of 0.91 p.u., making it is necessary to close the switches connecting buses 8-21, 12-22 and 25-29 to stay within the voltage limits. Alternatively, if the PV can generate reactive power, as in scenario 2, all switches can remain open without compromising the voltage limit of 0.95 p.u.

In scenario 1 and considering two-terminal MPC, the results show that the best configuration is to mesh the system using most of the available locations. Compared with the switches, the multiport converter can provide reactive power support to increase the voltages and reduce lines' losses. And even if all switches are open, having a single MPC is enough to keep the voltages higher than 0.95 p.u. The best configuration results in a multiport converter interconnecting buses 18 and 33, with switches between buses 8-21, 12-22 and 25-29 (conf. 1). As buses 18 and 33 are the most critical to have undervoltages, the MPC enables to increase their voltage. The size of the MPC in this configuration is 40 kVA for the terminal connecting to bus 18, and 41 kVA for the terminal connecting to bus 33. The second-best configuration consists in an MPC between buses 18-33 and switches between buses 12-22 and 25-29 (conf. 2), where the size of the multiport terminals is 56 and 58 kVA respectively.

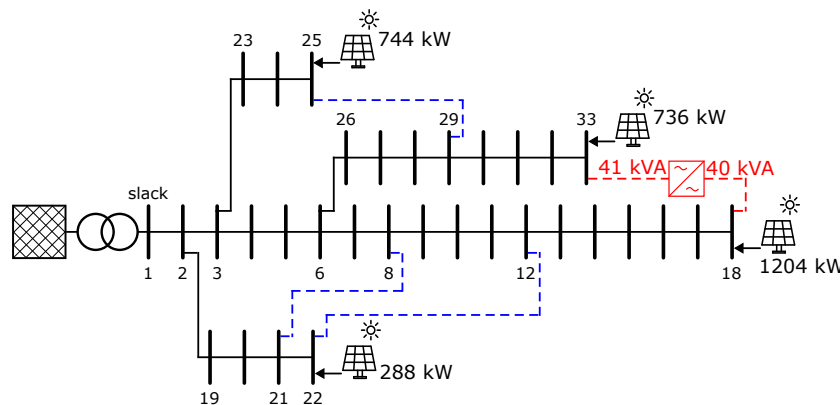


Figure 42: Electrical scheme of configuration 1

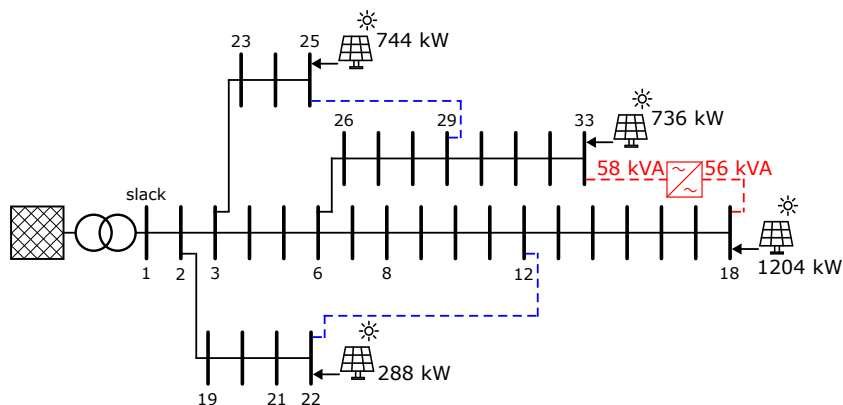


Figure 43: Electrical scheme of configuration 2

Although investment is high, benefits from reduction of system losses must be considered to provide a complete economic evaluation. The payback time is used to consider both investment and losses reduction. For scenario 1 and two-terminal MPC, the paybacks obtained in the best configurations are very high compared with the lifetime of the converter (20-25 years). Therefore, in this case it is not economically feasible to consider multiport converters unless voltage requirements or if the switches can only be closed in emergency situations.

In scenario 2 and considering two-terminal MPC, the optimal configuration includes multiport converters only when all switches remain open. It is preferable to close the switches, if possible, than to have a multiport converter. The best configuration in scenario 2 consists in a multiport converter that interconnects buses 12 and 22 (conf. 3), where each terminal connecting has a nominal power of 278 and 253 kVA, respectively. And the second-best configuration includes a multiport converter between buses 12-22 and 8-21 (conf. 4). In this case, the paybacks obtained from the MPC cost and losses reduction are lower than 20 years (Fig. 48).

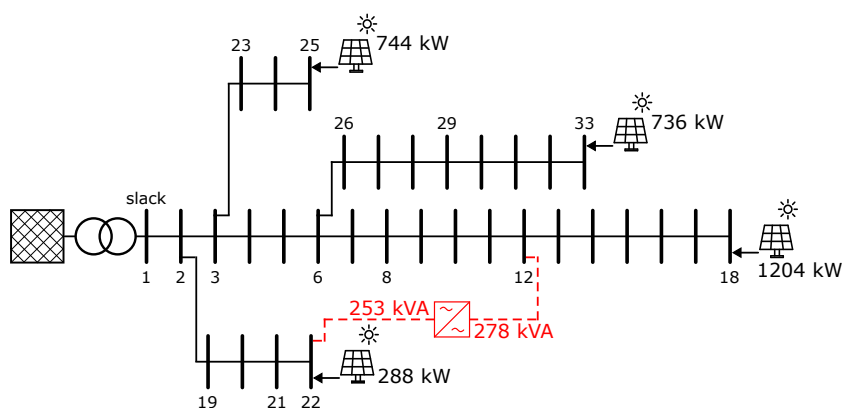


Figure 44: Electrical scheme of configuration 3

In scenario 1 and considering a three-terminal MPC, the optimal configuration results in all PV generators connected to the multiport converters (Fig 47). The best configuration for this case consists in an MPC that connects buses 12-22 with 446 and 390 kVA and a third port for the PV with 46 kW, an

MPC between buses 25-29 with 275 and 308 kVA and a third port for the PV with 159 kW, and an MPC that connects buses 18-33 with 229 and 828 kVA and a third port for the PV with 946 kW (conf. 5). This configuration is economically feasible, as the losses reduction compensates the multiport converter costs, resulting in a payback of 12 years. The second-best configuration for this scenario consists in an MPC that connects buses 8-21 with 155 and 139 kVA and a third port for the PV with 288 kW, an MPC between buses 25-29 with 283 and 532 kVA and a third port for the PV with 744 kW, an MPC that connects buses 18-33 with 103 and 332 kVA and a third port for the PV with 385 kW, and a closed switch between buses 12-22 (conf. 6). This configuration represents a reduction of power electronics from the base case.

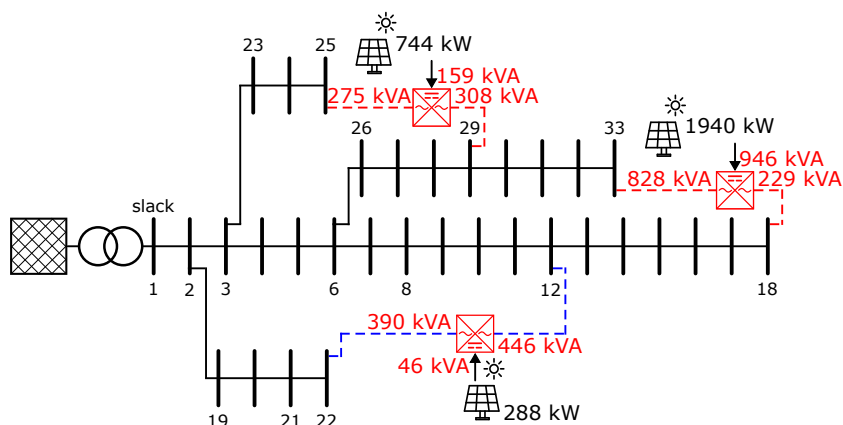


Figure 45: Electrical scheme of configuration 5

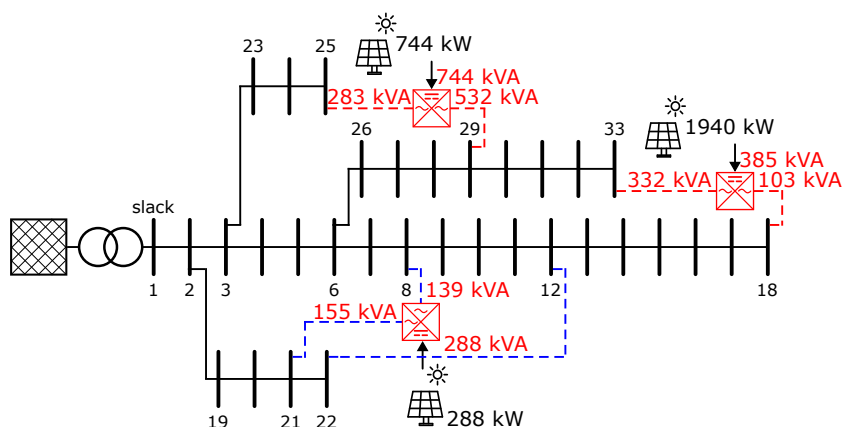


Figure 46: Electrical scheme of configuration 6

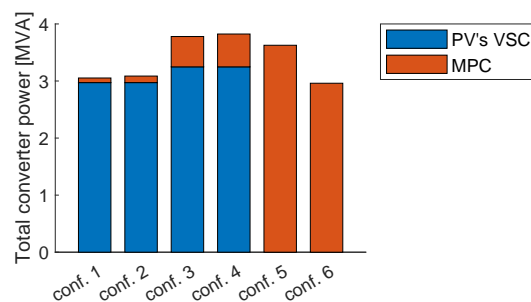


Figure 47: Total converter power for the best configurations

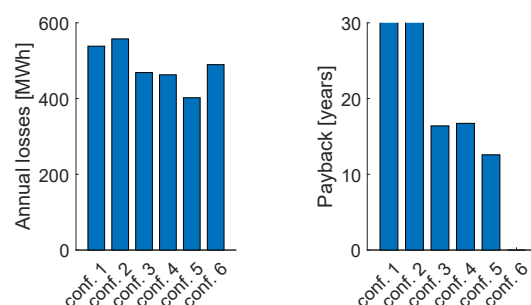


Figure 48: System losses and payback for the best configurations

3.9 Conclusions

This work analysed the multiport converter as a potential solution to reduce generation curtailment in distribution grids with a high penetration of renewables. A general methodology was presented to size the required multiport converter based on an optimisation problem with electrical constraints. This methodology also provides technical and economic indicators for a complete evaluation of the multiport converter integration.

A case study inspired by the medium voltage CIGRE benchmark network was considered, where the general methodology was validated to size a three-terminal multiport converter with and without battery terminals. The results concluded that in scenarios with unbalanced distributed generation in the feeders, the rated power of the multiport converter terminals used to exchange power between different feeders was sized with a relatively constant value similar to the nominal power of the system. Whereas in scenarios with balanced distributed generation in the feeders, the size of the rated power of the multiport converter terminals was more dependent on the interconnection configuration and economic parameters.

This case study was also used to compare the multiport converter solution to alternative configurations with separated batteries and a simple switch interconnection. As a general conclusion, the results showed that the multiport converter provides clear advantages and is economically viable. In particular, the multiport converter can reduce power curtailment in equivalent terms or even better than battery solutions, especially in scenarios with unbalanced distributed generation in the feeders. From an economical point of view, all scenarios are feasible to install a multiport converter as long as the penetration

of renewables is high. Different renewable penetrations were also compared. If renewable generation capacity is reduced, scenarios with unbalanced generation are the most economically feasible. However, scenarios with balanced generation are complicated to be considered unless batteries are initially installed in the feeders.

In general, for all scenarios, a multiport converter with a centralised battery is the best option. Configuration with a switch interconnection could provide similar economical results compared to the multiport converter options. However, the multiport converter has improvement margin since additional grid support services can be provided and are not evaluated in this work.

Moreover, an equivalent methodology to size the multiport converter without electrical constraints was also presented. In this case, a simplified version of the same case study was used to validate the methodology. The results show that the electrical constraints may have a significant impact in the optimisation results.

This work also analysed the multiport converter as a potential solution to reduce losses in the system lines and avoid undervoltages. A general methodology was presented to size and locate the required multiport converter based on an optimisation problem with electrical constraints. This methodology also provides technical and economic indicators for a complete evaluation of the multiport converter integration.

This last methodology was validated in a case study based on the IEEE 33 bus system. The results conclude that the multiport converter provides clear advantages and can be economically viable in some cases. In scenarios where the renewable generators can only inject active power, the multiport converter acting as a SOP is located between the buses that would have undervoltages if there was no MPC, although this case is not economically viable. Alternatively, all the generation can be directly connected to multiport converters, resulting in a higher reduction of losses and even reducing the amount of power electronics in the system. In scenarios where the generators can inject both active and reactive power, the multiport acting as a SOP is only recommended to provide additional loss reduction when all switches remain open.

Future work

This work had a limited time and scope, but there are things to improve and the project will continue for some years. Further work on this topic can include:

- Consider other battery sizing methodologies.
- Planning methodologies usually consider one or several years. This work proposes a methodology to consider a few days instead, but other clustering algorithms or simplification methodologies can be considered to reduce the amount of data and speed up the optimisation.
- The optimisation of battery and MPC location.
- Consider other functionalities and economical benefits of the multiport converter.

- Consider multiplexed multiport converter
- Improvement of the software regarding solver time and finding global solutions. As due to the solver used and the problem being non-linear, the results shown in this thesis are probably local optimums.
- Consider battery degradation and ageing in the methodology.
- Consider forecast uncertainties of the loads and resource availability in the optimisation.

4 GIS – based approach to improve the resilience of the distribution network

4.1 Introduction

In the last decades, the concept of resilience has been gaining importance. C.S. Holling introduced the concept of resilience in [30] in 1973 and applied it to ecological systems. The word comes from the Latin verb *"resilio"* which means *"spring back"*, [31]. Holling defined resilience as *"a measure of the persistence of systems and of the ability to absorb change and still maintain the same relationships between state variables"*. Since then, the concept of resilience has been extended to various intricate systems, including organizational or social-economical ones, [32]. As a result, new definitions have arisen regarding the concept of resilience, rendering it a term shrouded in ambiguity.

Recently, resilience has become a fundamental concept in power systems. In 2012, the IPCC published a Special Report to manage the risks that might arise due to extreme weather conditions, [33]. Resilience is defined as *"the ability of a system and its component parts to anticipate, absorb, accommodate, or recover from the effects of a hazardous event in a timely and efficient manner, including through the preservation, restoration, or improvement of its essential basic structures and functions"*. The report also recognizes the vulnerabilities of the power systems and how this might impact keeping the supply to all consumers.

In that context, in 2015, the European Joint Research Center (JRC) published the report *"Building a Resilient Europe in a Globalised World"*, [34]. The report addresses the necessity of an interdisciplinary approach to building a resilient European Union (EU). Based on the publication, in 2020 the *"2020 Strategic Foresight Report"* was published, [35], introducing resilience as a new concept for EU policies. One year later, Regulation (EU) 2021/241 established the Recovery and Resilience Facility to address the European recovery after the COVID-19 crisis, [36]. The regulation identified the energy transition as a key contributor due to its capacity to achieve *"climate targets, fostering sustainable growth, creating jobs and preserving energy security"*. In 2023, Regulation (EU) 2023/435, [37], after the impact of Russia's war against Ukraine, introduced additional measures in the recovery strategy. In this regulation, the resilience of the transmission and distribution networks is identified as a crucial element to guarantee system flexibility, minimize congestion, and ensure supply chains, among others.

In the US, the Department of Energy is focused on the modernization and expansion of the electricity grid to integrate renewable energies while increasing resilience, [38]. In this line, the US Department of Energy's National Renewable Energy Laboratory defines resilience as *"The ability to anticipate, prepare for, and adapt to changing conditions and withstand, respond to, and recover rapidly from disruptions through adaptable and holistic planning and technical solutions"*, [39]. Besides, the research center developed different methodologies to address the resilience issue from evaluation to decision support, [40–44].

Considering the importance of resilience in power systems, [45] proposes a specific definition and quantification methods of resilience in power systems. The authors distinguish between two time horizons.

First, the focus lies on operational or short-term considerations. Within this timeframe, resilience is oriented to optimize the operation of the assets efficiently during disruptive events. Second, the emphasis is placed on infrastructural or long-term considerations. In this time horizon, resilience is focused on planning the system to manage future disruptive events. Besides, the authors noted, as others such as [32,46], that resilience cannot be confused with reliability. Contrary to reliability, resilience includes all hazards and events, as those with very low probability, consider the transition times and the effects on customers, grid operators, and infrastructure. As a result, resilience is linked to risk-based approaches to evaluate both the potential disruptive events and the weaknesses of the infrastructure.

By the two predefined temporal scopes, various works oriented the resilience analysis in planning, such as [40,47,48], and operating the system, as for [49–51]. Due to the ambiguity of the resilience concept, a large number of works address the topic from different perspectives, as a detailed review of the current state-of-the-art is out of this scope of work, [52,53] are suggested for further information. Regarding the disruptive events considered in resilience studies, [40] identifies three types: natural, technological, and adversarial. In literature, natural disruptive events are the most explored in resilience analysis as described in [54]. Notwithstanding, human-caused disruptive events have been gaining interest in recent years, in particular, cyberattacks. [55].

This work proposes a GIS-based approach to assess the resilience of planning power systems. The proposed methodology relies on the framework developed by NREL [40], which stems from a comprehensive risk assessment. Thus, this work discerns between hazards and vulnerabilities. Disruptive events that may impact the infrastructure without being controllable define hazards. In turn, weaknesses relate to vulnerabilities and are determined by their likelihood of occurrence when a hazard is present and the potential impact they may cause. This work expands the typical risk assessment studies in two main points. First, the integration of geospatial data into a Geographic Information System (GIS). Recently, GIS has gained interest in different fields of study, from the medical sector to transportation planning, [56,57]. Thus, the authors identified GIS as a promising system for managing the information related to networks. In a GIS system, the topology of the network is mapped along with the potential disruptive events that might affect it to orient decision-making about mitigation actions. Second, some works such as [40] qualitatively evaluate the impact of each element on the whole system, this work quantitatively quantifies the impact through an Optimal Power Flow (OPF) analysis.

Finally, a specific case study, which consists of a network located in a rural area in Spain, is analyzed through the proposed GIS-based approach to validate the methodology proposed.

Section 4.2 details the proposed method to assess the resilience of a network in three stages: hazard database development, vulnerability analysis and resilience analysis. Section 4.3 presents a simple case study to validate the proposed methodology. Finally, Section 4.4 includes the main conclusions of this work and further work.

4.2 Methodology

This section describes the GIS-based methodology proposed to evaluate the network's resilience. First, Section 4.2.1 contains the procedure for building the hazard database, including simple and combined events. Second, in Section 4.2.2, the authors define the method for evaluating a system's vulnerabilities based on its likelihood and impact. Third, Section 4.2.3 outlines the risk assessment and resilience analysis methodology.

This work implemented this methodology in PyQGIS, resulting in three interrelated Plug-ins. Annex I includes a detailed description of the developed plug-ins.

4.2.1 Hazards Database

This section describes the procedure for building the hazard database. \mathbf{H} symbolizes the hazard database. H is a vector defined as $\mathbf{H} = [h_1, h_2, \dots, h_h, \dots, h_N]$ where h_h represents each hazard included in the database and N the total number of hazards. Each h_h is a geospatial layer composed of polygons. Each polygon defines the probability of occurrence in each region. Thus, each geometry included in h_h includes:

- Geolocation.
- Probability of having the hazard inside the region during summer months, June-August.
- Probability of having the hazard inside the region during winter months, December-February.
- Probability of having the hazard inside the region during spring months, March-May.
- Probability of having the hazard inside the region during autumn months, September-November.

As previously mentioned, a resilience analysis should consider all events that might affect the system, even the ones with very low probability. As a result, the hazard database, \mathbf{H} , might include many datasets of hazards. Many authors mention that diverse hazards might impact power systems and classify them into natural, technological and adversarial categories, [40, 54]. Besides, various simple events may coincide, leading to increased damage to the system. Hence, it is necessary to evaluate the potential combination of simple hazards. The relationship between two events (A and A') can be categorized as follows:

1. **Mutually exclusive events.** In this case, two events cannot occur concurrently, i.e. $P(A \cap A') = \emptyset$.
2. **Dependent events.** In this case, the probability of the second event (A') changes once the first event (A) occurs, that is $P(A \cap A') = P(A'|A) \cdot P(A)$.
3. **Independent events.** In this case, the probability of the second event (A') is not dependent on the occurrence of the first event (A), that is $P(A \cap A') = P(A) \cdot P(A')$.

Each combination produces a new layer, h_h . The dataset contains the same information as the input hazards. However, the probabilities are updated based on the type of relation between the hazards. Further combinations of events can consider a dataset obtained from a previous combination.

Thus, the \mathbf{H} finally contains simple and combined events in GIS-data, Figure 49.

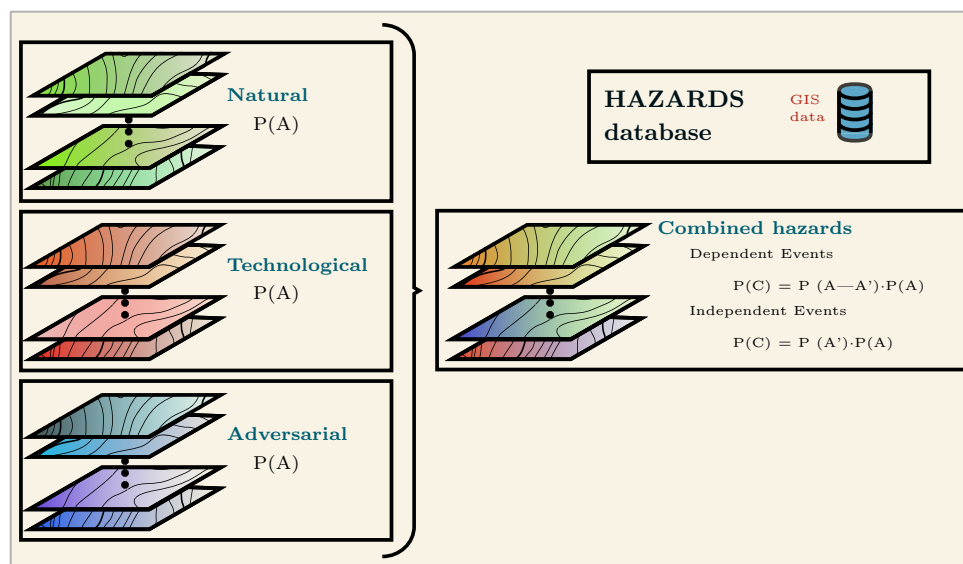


Figure 49: Hazards Database

4.2.2 Vulnerabilities Analysis

This work defines vulnerabilities as the weaknesses of a system. Thus, the vulnerability analysis focuses on a specific electrical network, \mathbf{N} , composed of buses and power lines. \mathbf{N} is a vector defined as $\mathbf{N} = [f, w]$, where f and w are geospatial layers that provide information related to buses and power lines, respectively. Each layer consists of vector data. However, f includes points (one per bus) and w lines (one per power line). Besides, each geometry included in each layer contains the following numerical information:

Layer f :

- Geolocation
- Name of the bus
- Nominal voltage magnitude of the node in kV.
- Available power from the generators connected to a node.
- Expected power to the loads connected to a node.
- Connection to the external grid, 1 if the connection exists, 0 otherwise.

Layer w :

- Geolocation
- Line Name
- Line resistance in ohm per km.
- Line reactance in ohm per km
- Line capacitance in nanoFarad per km.

The vulnerabilities can be characterized once the system, N , is defined. The vulnerability analysis involves three main steps: vulnerability identification, likelihood characterization, and impact calculations.

Regarding vulnerability identification, the process might involve the different stakeholders of the systems, consumers, Distribution System Operators (DSOs), Transmission System Operators (TSOs), utilities, public administration, and so on. This process results in a list of V vulnerabilities for each system's element.

Notwithstanding, the presence of a vulnerability does not necessarily mean that the system will be compromised. Thus, the likelihood of being affected by a vulnerability varies depending on the hazard. Consequently, a specific vulnerability likelihood is determined for each event included in the hazard database and for each vulnerability identified, $\mathbf{L}_{\mathbf{v},\mathbf{h}}$. $\mathbf{L}_{\mathbf{v},\mathbf{h}}$ includes likelihood for each element of the system, that is $\mathbf{L}_{\mathbf{v},\mathbf{h}} = [l_{-f}, l_{-w}]$. l_{-f} and l_{-w} are the likelihoods of the vulnerability v when hazard h_h occurs in each bus, f , and power line, w , respectively. $\mathbf{L}_{\mathbf{v},\mathbf{h}}$ only includes tabular data, that is, no geospatial information is included.

According to [58], the impact can be quantified from a technological, economic, or social perspective, such as in terms of energy not supplied by the system, the cost of the energy unsupplied, or the number of vulnerable customers unsupplied. As the main aim of an electrical network is to supply the demand, this work quantifies the impact considering the amount of energy not supplied. The difference between the active energy supplied when all elements are operating and the active energy supplied when an element is not under operation determines the consequence of that element. Thus, $\mathbf{I} = [l_{-f}, l_{-w}]$ where l_{-f} and l_{-w} include the impact that each bus and power line, respectively, might have on the system.

To determine the power supplied to the loads, the authors propose an OPF analysis. AC and DC OPF can provide valid solutions. Nevertheless, it is necessary to carefully consider the advantages and limitations of each analysis in every individual case. The AC OPF includes reactive power and loss constraints. Consequently, this approach yields more accurate results though demanding higher computational time. Conversely, the DC OPF notably simplifies the mathematical formulation. This approach leads to a significant reduction in computational time while resulting in less accurate outcomes.

The impact evaluation is based on the methodology detailed in Section 3.3.4. The mathematical model requires technical parameters about buses and power lines obtained from the numerical data provided by the \mathbf{N} layers. Thus, the following aspects should be noted:

1. The tabular data included in the vectorial data f provides the buses' technical information.
2. Each geometry of f , defined as a point, provides the technical information of a bus i .
3. The tabular data included in the vectorial data w provides the power lines' technical information.
4. Power lines are defined by subindex i and k . i corresponds to the initial bus and k to the end bus.
5. The initial and end buses, i and k , are determined from the geospatial data of w .
6. Each geometry of w , defined as a line, provides the technical information of a power line defined by an i, k combination.
7. The length of each power line, i, k , is determined from the geospatial data of w .

As a consequence, the impact of each bus and power line, ι_{-f} and ι_{-w} can be expressed as:

$$\iota_{-f} = \sum_i \sum_t \sum_d p_{load-i,t,d}^N - \sum_i \sum_t \sum_d p_{load-i,t,d}^{N-f} \quad (60)$$

$$\iota_{-w} = \sum_i \sum_t \sum_d p_{load-i,t,d}^N - \sum_i \sum_t \sum_d p_{load-i,t,d}^{N-k} \quad (61)$$

Where $p_{load-i,t,d}^N$ is the total active power load supplied when all buses and power lines are in operation and $p_{load-i,t,d}^{N-f}$ is the total active power supplied to loads when bus f is not connected and $p_{load-i,t,d}^{N-k}$ is the total active power supplied to loads when power line k is not connected.

The objective function of the methodology described in Section 3.3.4 minimizes the multiport converter cost and the generation curtailment. In this section, as resilience is oriented to the maximization of the demand supplied, the objective function is redefined as follows:

$$[max] \sum_i \sum_t \sum_d p_{load-i,t,d} \quad (62)$$

In the AC OPF, the objective function is subject to (11) to (14) and (33) to (39).

Besides, as this methodology does not consider the introduction of specific technologies (40) and (41) can be simplified as:

$$p_{i,t,d} = -p_{load-i,t,d} + \sum_g p_{g-i,t,d} + \sum_{MG} (p_{buy-MG,i,t,d} - p_{sell-MG,i,t,d}) \quad \forall i, t, d \quad (63)$$

$$q_{i,t,d} = -q_{load-i,t,d} + \sum_g q_{g-i,t,d} + \sum_{MG} (q_{buy-MG,i,t,d} - q_{sell-MG,i,t,d}) \quad \forall i, t, d \quad (64)$$

Finally, this methodology introduces an additional constraint to limit the maximum power delivered to the load to its maximum instantaneous demand.

$$0 \leq p_{load-i,t,d} \leq p_{max-load-i,t,d} \quad \forall load, i, t, d \quad (65)$$

In the DC OPF, three main simplifications are introduced:

1. Line resistances are considered negligible. Thus, $G_{i,k} = 0$ and $B_{i,k} = \frac{-1}{x_{i,k}}$.
2. The voltage magnitude equals the base voltage in all nodes. Thus, $v_{i,t,d} = v_0$ and $v_{k,t,d} = v_0$. Assuming a voltage magnitude = 1, then, $v_0 = 1$.
3. The difference between voltage phases is considered greatly small. Thus $\cos(\delta_{V_{i,t,d}} - \delta_{V_{k,t,d}}) \approx 1$ and $\sin(\delta_{V_{i,t,d}} - \delta_{V_{k,t,d}}) \approx \delta_{V_{i,t,d}} - \delta_{V_{k,t,d}}$

Considering all previous assumptions, in a DC OPF, (34) and (35) are expressed as:

$$p_{i,t,d} = \sum_k \left(\frac{-1}{x_{i,k}} \cdot (\delta_{V_{i,t,d}} - \delta_{V_{k,t,d}}) \right) \quad \forall i, t, d \quad (66)$$

$$q_{i,t,d} = \sum_k \left(\frac{-1}{x_{i,k}} \right) \quad \forall i, t, d \quad (67)$$

A DC OPF neglects (67) as reactive power flow is not considered.

Initially, the methodology executes the OPF, AC or DC, for all interconnected elements. Subsequently, it proceeds with the optimization until determining the impact of each component, **I**. Thus, the maximum number of simulations is $(f + w + 1)$. The results obtained from the OPF, **I**, are tabular data. However, this data could be geolocated considering the geospatial data of **N**.

4.2.3 Risk assessment and Resilience analysis

After developing the hazard database, H , for a specific region and evaluating the vulnerabilities, $L_{v,h}$ and I , of a system, N , a risk assessment methodology provides information about the system's resilience. As shown in Figure 50, the risk assessment considers four main stages.

First, the power lines of the networks are segmented, if required, to provide more detailed information. In this way, the network defined as $N = [f, w]$ turns into $N = [f, w_q]$ where q expresses the number of segments of each power line.

Second, the extension of the hazard database is adjusted to the system's regions, optimizing the computational time required.

Third, the intersections between the geospatial data of the system, N , and the hazard database, H , are evaluated for a certain season of the year. As a result, a new system's vector is created, $\mathbf{P}_h = [\rho-f_h, \rho-w-q_h]$. Thus, $\rho - f_h$ is a vector data of points that includes, for each bus, the probability of being affected by each hazard, h_h , of the database **H** in the considered season. In turn, $\rho - w_h$ is a vector data of lines that includes, for each power line, the probability of being affected by each hazard, h_h , of the database **H** in the considered season.

Fourth, considering the vulnerability analysis, the power or energy at risk R , in each system element is determined as follows:

$$\mathbf{R} = \sum_h \sum_v \mathbf{P}_h \cdot \mathbf{L}_{v,h} \cdot \mathbf{I} \quad (68)$$

As $L_{v,h}$ has been defined as the likelihood of being affected by the vulnerability once a hazard occurs, the $(P_h \cdot L_{v,h})$ factor provides the combined probability of having both simultaneously. Thus, the hazard's probability and the vulnerability's likelihood are combined as dependent events. \mathbf{R} is a vector defined as $\mathbf{R} = [r_f, r_w]$. r_f and r_w are vectorial data. The geospatial data of \mathbf{R} is taken from \mathbf{P}_h which, in turn, was taken from \mathbf{N} . Thus, r_f is point vector data where each point is a system's bus. Accordingly, r_w is a line vector data where each line is a system's power line. The tabular data associated with each vector data contains the total amount of energy at risk in each element because of the hazards and vulnerabilities that might affect it.

Finally, a resilience index, \mathcal{R} , for the whole system is determined based on the total energy risked by each element as follows:

$$\mathcal{R} = \frac{R_T}{I_T} \quad (69)$$

Where R_T is the total energy at risk in the system, the value is obtained from the tabular data of \mathbf{R} . R_T is obtained by summing the amount of energy at risk in each element obtained from (69) and saved in \mathbf{R} . In turn, I_T is the sum of the partial impacts identified in the system. The value is obtained by summing the partial impacts saved in \mathbf{I} . As a result, \mathcal{R} is a numerical index that provides information about the global resilience of the system. Consequently, the variable enables the comparison of different systems.

This methodology allows the analysis of an electrical network from a resilience perspective. Besides, this methodology can evaluate the impact of various mitigation actions.

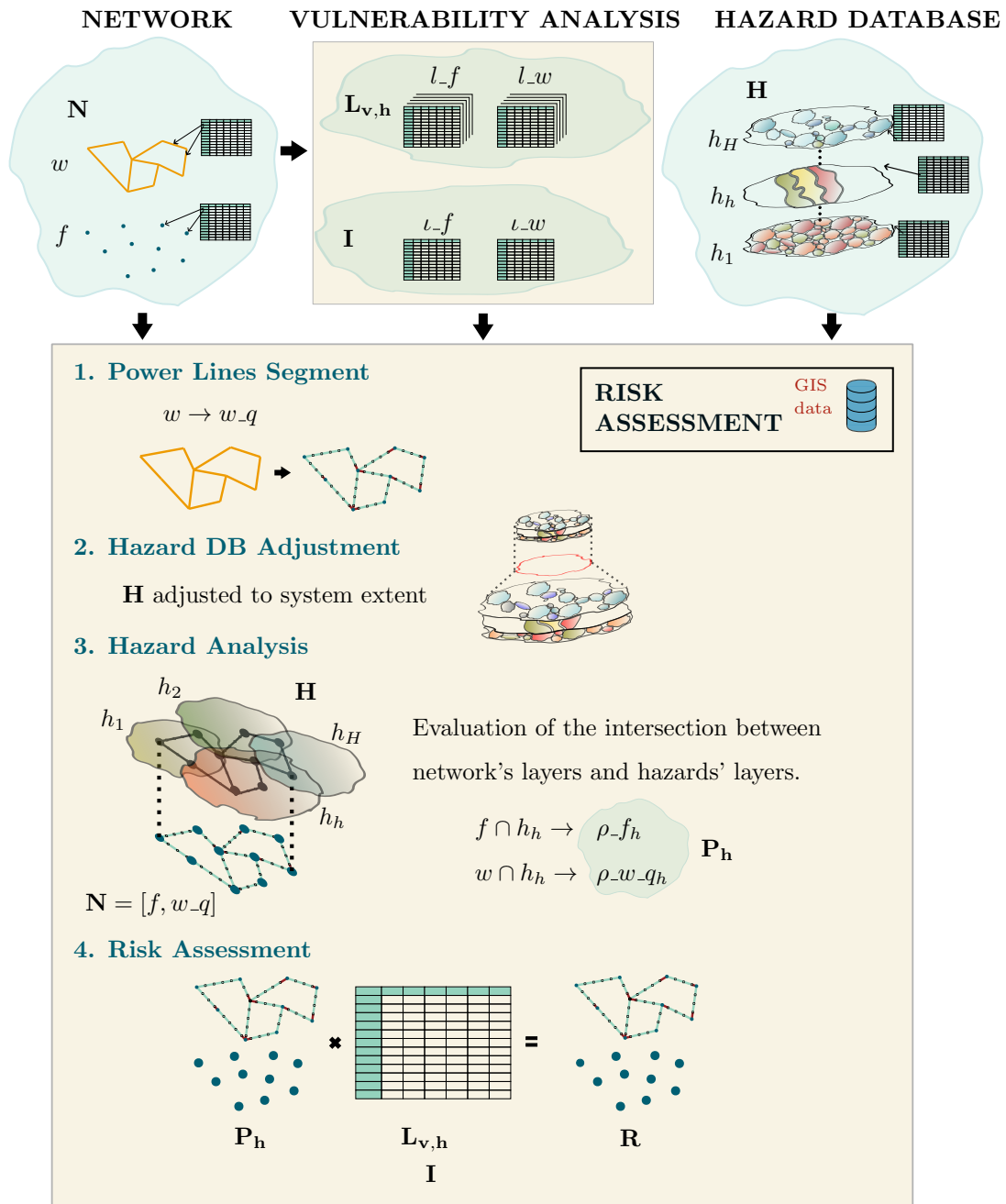


Figure 50: Risk Assessment

4.3 Case Study

This section presents a simplified case study to validate the presented resilience analysis. First, Section 4.3.1 builds a hazard database, **H**, from 3 simple hazards that might damage the system. Second, Section 4.3.2 performs the vulnerability analysis of the considered network, **N**. This simplified case study considers a single vulnerability: the presence of close dense vegetation. Third, Section 4.3.3 evaluates how the three hazards considered and the presence of close defense vegetation might affect the system's resilience.

The case study is in a rural area of Catalonia, Spain’s northeast region. Figure 51 shows the topology, buses with a load connected and the maximum demand registered in each.

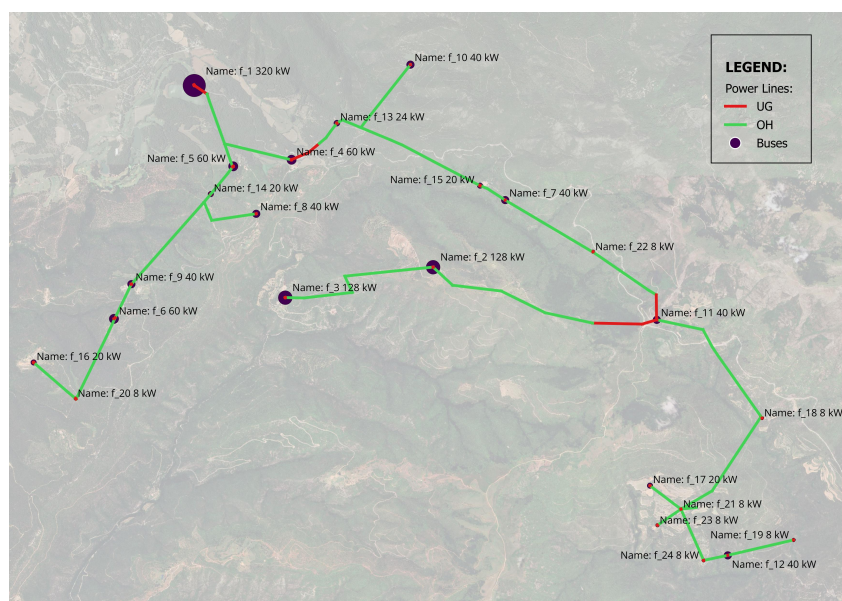


Figure 51: Case Study Definition

Additionally, in bus $i = f_{-1}$, a 100 kW facility is considered. The controllability of the facility is limited and the inverters installed can not operate in islanded mode. In that context, the PV facility should be modeled as a PQ generator in the OPF analysis.

Figure 52 shows the interconnection of the network with the external grid.



Figure 52: Case Study Definition - Zoom external grid

Regarding the power lines, the ones shown in red in Figure 51 are underground while the ones in

green are overhead.

As for the power lines, the network includes 11 different types of lines, its main characteristics are:

Name	r_ohm_per_km	x_ohm_per_km	c_nf_per_km	max_i_ka
std_01	0.0460	0.1000	0	0.630
std_02	0.1610	0.1050	0	0.415
std_03	0.2620	0.1210	0	0.315
std_04	0.2620	0.1160	0	0.315
std_05	0.2620	0.1170	0	0.300
std_06	0.2700	0.1260	0	0.305
std_07	0.4030	0.1200	0	0.250
std_08	0.6140	0.3740	0	0.200
std_09	0.7900	0.3800	0	0.180
std_10	1.0736	0.3850	0	0.140
std_11	1.2150	0.4000	0	0.130

Table 10: Types of power lines

4.3.1 Hazard Database

This case study considers three simple hazards: wildfires, wind and heat waves. Wildfires and wind hazards are obtained from [59] and heat wave hazard from [60].

For wildfire hazard assessment, the geospatial data assigns each region a qualitative value: very high, high, moderate, low, or no risk. From the qualitative data, the probability of having a wildfire in each region in each season has been established as:

Category	SUMMER	WINTER	AUTUMN	SPRING
Very High	20.00 %	2.00 %	5.00 %	5.00 %
High	10.00 %	1.00 %	2.50 %	2.50 %
Moderate	7.00 %	0.70 %	1.75 %	1.75 %
Low	4.00 %	0.40 %	1.00 %	1.00 %
No Hazard	0.00 %	0.00 %	0.00 %	0.00 %

Table 11: Probability of having a wildfire per season

Figure 53 shows the probability of having a wildfire in a day d during summer.

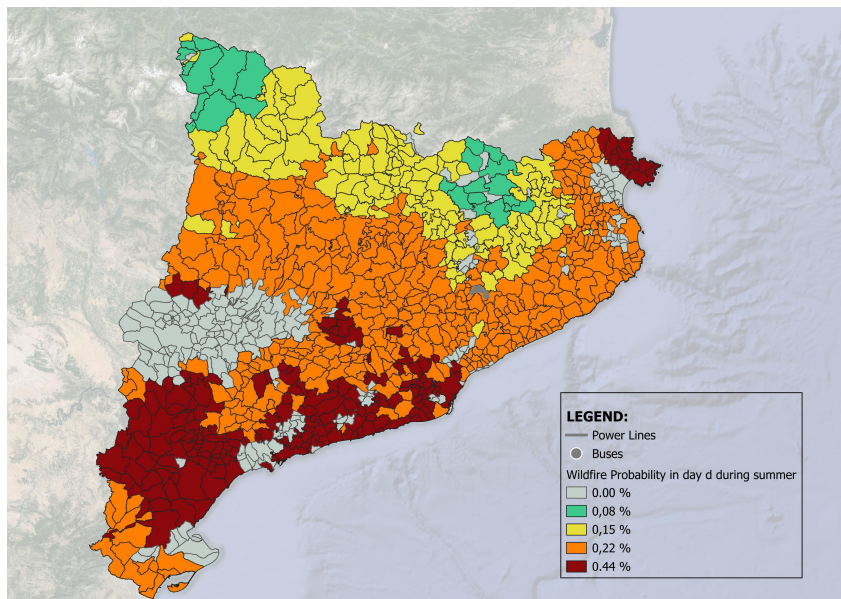


Figure 53: Wildfire Probability in day *d* during summer

The wind geospatial data provides information on the frequency of days with wind gusts exceeding 20 m/s in each region. The distribution of the number of days is uniform across the different seasons of the year. Figure 54 displays the probability of experiencing a wind gust exceeding 20 m/s in a day *d*.

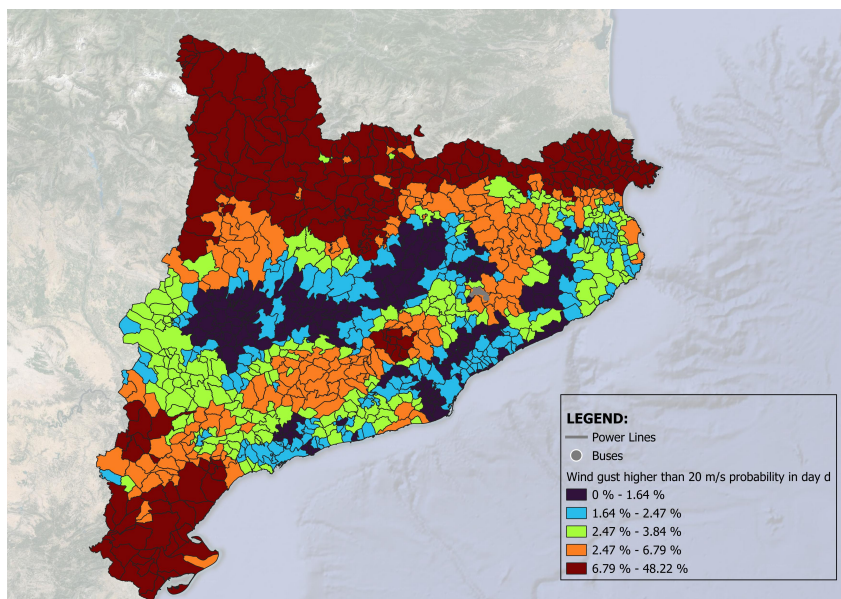


Figure 54: Wind gust probability in day *d* during summer

The heat wave geospatial data considers the RCP 4.5 scenario in the medium future. This data illustrates the frequency of days with a minimum temperature exceeding 20°C. The distribution of the number of days across different seasons is outlined in Table 13.

SEASON	SUMMER
summer	70.00 %
winter	0.00 %
autumn	15.00 %
spring	15.00 %

Table 12: Probability of having a wildfire per season

Figure 55 shows the probability of having a minimum temperature higher than 20°C in a day *d* during summer.

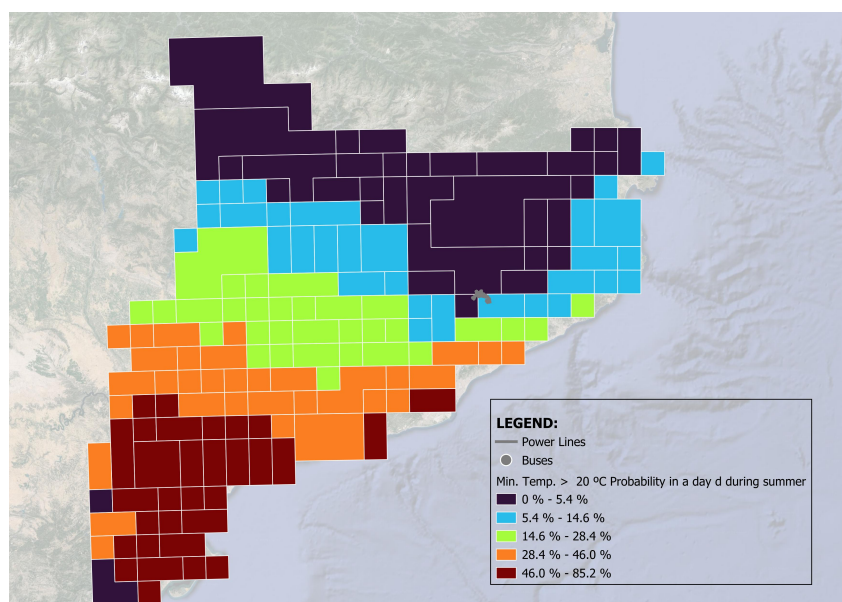


Figure 55: Heatwave probability in day *d* during summer

As previously mentioned, this case study would only consider a single vulnerability: the presence of high-dense vegetation. Thus, the heatwave is not a hazard by itself. However, it might be a significant hazard when combined with others. In that context, the following hazards, simple and combined, have been considered in this case study:

HAZARD	Type	Type of events
Wind [WD]	Simple	
Wildfire [WF]	Simple	
Wildfire + Wind	Combined	Independent
Wildfire + Heatwave [HW]	Combined	Dependent
Wildfire + Heatwave + Wind	Combined	Dependent (WD - HW) & Independent ([WF - HW] - WD)

Table 13: Hazards considered in the analysis

4.3.2 Vulnerability analysis

A single vulnerability, the presence of high-dense vegetation, is considered in this analysis. As mentioned in Section 4.2.2, likelihood and impact define a vulnerability. This section evaluates the likelihood of being affected by the vulnerability given a hazard of the database and determines the consequence of losing each element on the network.

The Green Lead Index (GLI) is used to quantify the vulnerability's likelihood. GLI allows the identification of the vegetation's density. The index measures the vegetation density based on the RGB composition of the aerial images of a region. Compared to other methods, GLI only requires visible bands (Red - Green - Blue). The method compares the reflectance in the green channel to the other visible wavelengths (red and blue), [61]. GLI is defined as:

$$GLI = \frac{2G - R - B}{2G + R + B} \quad (70)$$

The index results in negative values in regions with soil or nonliving objects. Conversely, positive values indicate the presence of vegetation. The likelihood of the vulnerability is established proportionally to the vegetation density, i.e. high-density vegetation areas result in a higher vulnerability likelihood. The vulnerability likelihood has established in a range from 0 % to 65 %.

The vegetation only affects the overhead power lines. Buses and underground power lines are not vulnerable because of high-density vegetation. The likelihood of being damaged because of the vulnerability is assumed equal in the occurrence of each hazard, simple or combined, included in the database. Thus, Figure 56 shows the network's vulnerability likelihood when a hazard occurs.

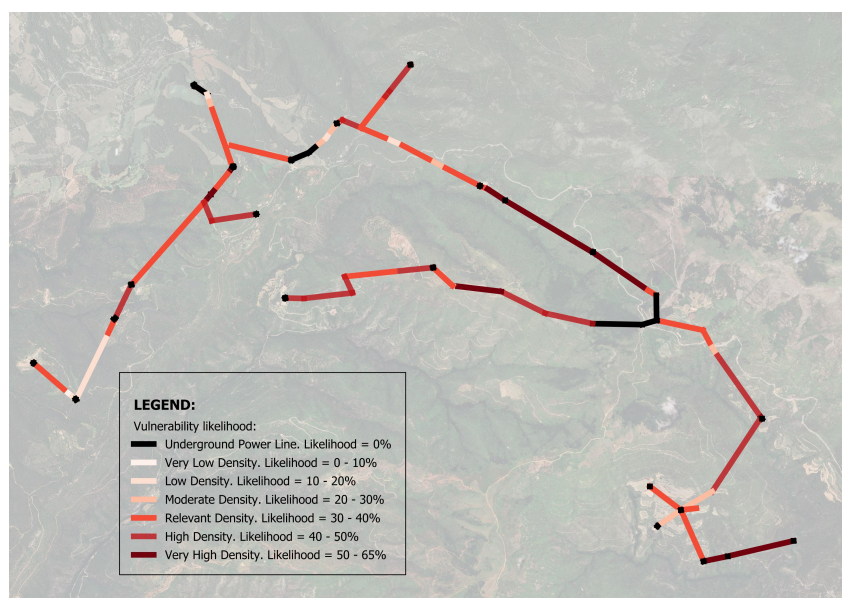


Figure 56: Likelihood of being affected by the vulnerability given a hazard

The OPF methodology described in Section 4.2.2 determines the impact of each element. The impact only considers the active power delivered to the loads, so the impact difference obtained through a DC

or AC OPF is lower than 1 %.

Figure 57 shows the impact of each element. Those elements closer to the external grid are the ones that have more influence on the system in case of failure. As no generator could operate in island mode, in the case of losing the connection with the external grid, all loads remain unsupplied.

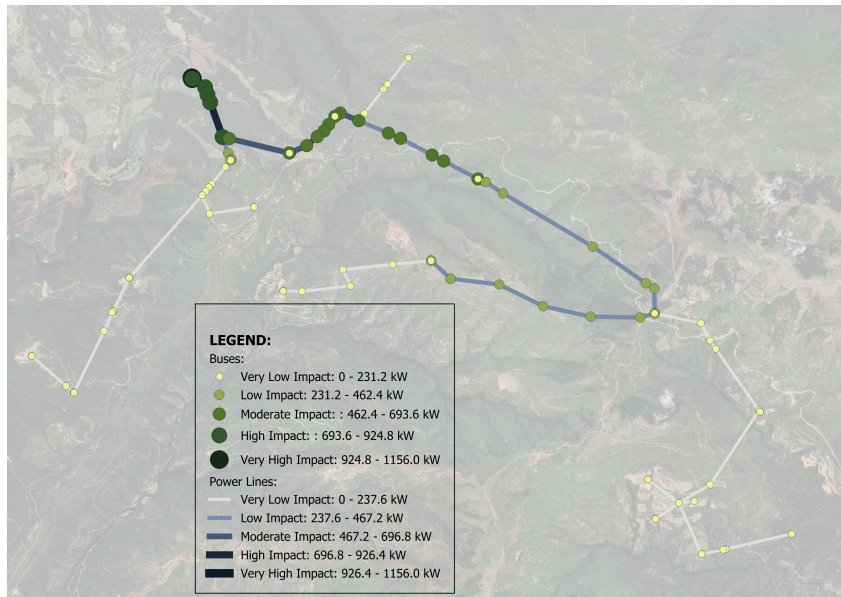


Figure 57: Impact of each element based on maximum loads

Furthermore, the impact of each element can be quantified in terms of energy. This work introduces three distinct demand profiles, as illustrated in Figure 58.

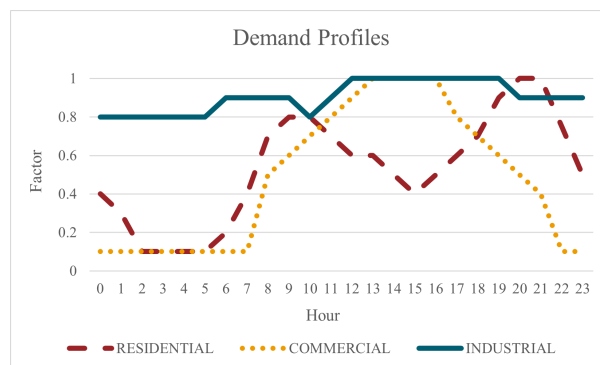


Figure 58: Types of demand profiles

The maximum loads defined in Figure 51 are adjusted hourly based on the following profile assignment:

BUS	PROFILE	BUS	PROFILE
f_1	residential	f_13	industrial
f_2	commercial	f_14	residential
f_3	residential	f_15	commercial
f_4	residential	f_16	commercial
f_5	industrial	f_17	residential
f_6	commercial	f_18	residential
f_7	residential	f_19	residential
f_8	industrial	f_20	residential
f_9	commercial	f_21	commercial
f_10	commercial	f_22	residential
f_11	residential	f_23	commercial
f_12	commercial	f_24	residential

Table 14: 24-hour demand profile assignment

As a result, Figure 59 shows the impact of each element considering the daily profiles.

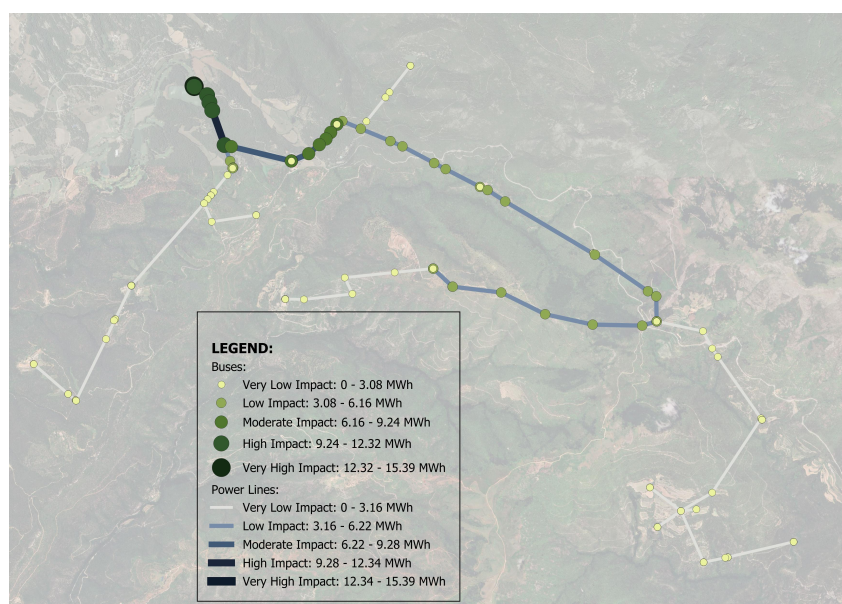


Figure 59: Impact of each element based on demand profiles

As shown in the instantaneous analysis, those buses and power lines closer to the external grid have a higher impact on the system in case of failure.

4.3.3 Risk Assessment and Resilience Analysis

This section considers the database developed on Section 4.3.1 and the vulnerability analysis performed in Section 4.2.2. Regarding the vulnerability analysis, this section considers the results obtained from

the hourly OPF and reported in Figure 59.

The risk assessment and the resilience analysis are performed during the summer.

Figure 60 shows the energy at risk in each element because of close high-density vegetation and hazard exposure. In this simplified case study, buses and underground power lines do not have any energy at risk because the presence of vegetation is not a vulnerability for them. Regarding the overhead power lines, the energy at risk in each element is notably low because, first, the hazards are expressed in the probability of occurrence in day d and, second, the total potential impact of each element is given by the amount of energy consumed by the loads in a single day. Notwithstanding, the energy at risk allows a comparison of the different elements of the system. In this way, the methodology identifies the most critical elements in the system where mitigation actions would be advisable.

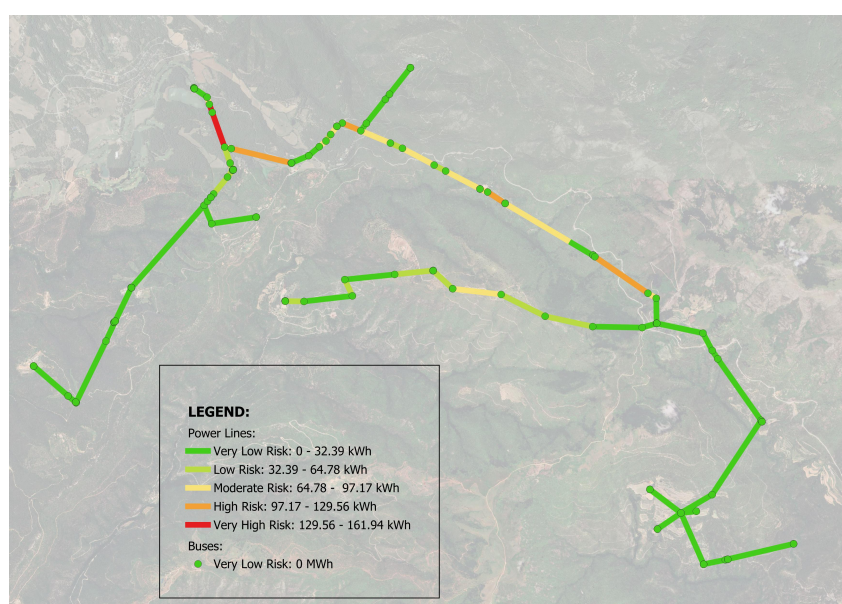


Figure 60: Amount of energy at risk in each element of the system because of the vulnerability and the hazards

Finally, the methodology gives a 99.76 % resilience index in this case. The obtained resilience index does not mean an almost fully resilient system. The value means that the presence of close high-density vegetation, considering five different hazards and hazard combinations, does not have a significant impact on the system's resilience.

4.4 Conclusions

This section presented a GIS-based methodology to address the electrical network's resilience. Resilience has concluded as a very complex topic that requires coordination between the different stakeholders of the system. On one hand, the hazards database needs to be constantly updated and extended. On the other hand, ongoing analysis of the network's vulnerabilities is essential to identify emerging vulnerabilities and address previously mitigated ones. As a result, resilience studies require a large amount of data. In

that context, this work identified the potential of geospatial data to manage the large amount of expected data.

The proposed methodology allows the management of many hazards and the potential combinations between them. The hazards database might encompass information for broader regions than a specific network. Thus, during the risk assessment, the hazard database extension is adjusted to the network evaluated. As a result, the geometries compared are reduced and the computational time required is optimized.

The vulnerability analysis is a complex stage. This work proposes a qualitative method to identify the vulnerabilities of the system and its likelihood of impacting when a specific hazard occurs. In turn, an OPF approach is proposed to estimate the impact of each network's element. This method provides a fast and accurate impact quantification. However, other methods are compatible with the risk assessment and resilience analysis. In that context, the proposed GIS-methodology allows the direct introduction of the vulnerabilities obtained through different approaches.

Finally, the developed methodology allows the identification of the most critical elements or parts of the network. As a result, many mitigation actions can be evaluated. The global resilience index provides information about how the identified vulnerabilities might affect the system considering the hazards included in the database. Additionally, this index is useful to evaluate the global impact of various mitigation actions.

Future work on this project will focus on developing a more realistic case study. First, the hazard database will be expanded. Second, a more detailed analysis will be conducted in collaboration with the DSO.

5 Conclusions

This document provides methodologies to size and locate multiport converters and analyse distribution network resiliency. These outcomes are developed under Work Package 1 of iPlug project, and enable the later application on use cases to evaluate the introduction of multiport converters.

An optimisation-based methodology to size multiport converters is presented. This optimisation can include AC power flow constraints or consider only the energy part. The inputs required are annual load and generation profiles, and elements' characteristics and costs. If grid constraints are considered, the methodology also considers other steps to simplify the problem and example algorithms are provided. A methodology to locate the multiport converter based on a loop of the sizing optimisation with different network configurations is also proposed. All methodologies perform a techno-economical analysis and provide indicators for further evaluation of the multiport converter integration. Two case studies are also presented to validate the methodologies, where the multiport converter is expected to reduce renewable energy curtailment and to avoid undervoltages and reduce losses. Then, the results are discussed comparing the multiport converter with conventional options such as SOPs and switches.

Regarding the resilience methodology, developing an accurate and detailed hazard database for a specific region is essential for utilizing a GIS-based approach to enhance the network's resilience. Moreover, the various system stakeholders must identify vulnerabilities as a crucial stage in resilience analysis. They should characterize vulnerabilities by their likelihood of occurrence during specific hazards and the potential impact on the system.

Following this work, the iPlug project will analyze the resilience of a specific system through the methodology detailed in this document. The actual system comprises a MV distribution network located in a rural area of the Catalonia region in northeastern Spain.

Future work on this project will focus on integrating both methodologies, thereby incorporating a resilience perspective into the multiport sizing and location optimization. The location and size would be constrained to the resilience impact on the system.

After this task, the iPlug project will evaluate the case studies presented in Deliverable 1.1 of the project with the resilience, sizing and location methodologies. This will provide a comprehensive analysis of the advantages of installing a multiport converter compared to alternative options, and the identification of scenarios where multiport converters can be considered as a potential solution.

References

- [1] European Commission, “2050 long-term strategy,” https://climate.ec.europa.eu/eu-action/climate-strategies-targets/2050-long-term-strategy_en, accessed on 2023-06-26.
- [2] —, “Renewable energy targets,” https://energy.ec.europa.eu/topics/renewable-energy/renewable-energy-directive-targets-and-rules/renewable-energy-targets_en, accessed on 2023-06-26.
- [3] —, “Energy storage,” https://energy.ec.europa.eu/topics/research-and-technology/energy-storage_en, accessed on 2023-06-26.
- [4] CIGRE WG C6.24, “Capacity of Distribution Feeders for Hosting Distributed Energy Resources,” Tech. Rep. June, 2014.
- [5] S. Sinha and S. Chandel, “Review of software tools for hybrid renewable energy systems,” *Renewable and Sustainable Energy Reviews*, vol. 32, pp. 192–205, 2014. [Online]. Available: <https://www.sciencedirect.com/science/article/pii/S136403211400046X>
- [6] P. Tozzi and J. H. Jo, “A comparative analysis of renewable energy simulation tools: Performance simulation model vs. system optimization,” *Renewable and Sustainable Energy Reviews*, vol. 80, pp. 390–398, 2017. [Online]. Available: <https://www.sciencedirect.com/science/article/pii/S1364032117307761>
- [7] HOMER, “HOMER Pro documentation,” <https://www.homerenergy.com/products/pro/docs/3.14/index.html>, accessed on 2023-03-06.
- [8] R. D. Zimmerman and C. E. Murillo-Sanchez, “MATPOWER,” <https://matpower.org/>, accessed on 2023-08-03.
- [9] R. D. Zimmerman and C. E. Murillo-Sánchez, “MATPOWER User’s Manual,” <https://matpower.org/docs/MATPOWER-manual.pdf>, accessed on 2023-08-03.
- [10] R. D. Zimmerman, C. E. Murillo-Sánchez, and R. J. Thomas, “MATPOWER: Steady-State Operations, Planning, and Analysis Tools for Power Systems Research and Education,” *IEEE Transactions on Power Systems*, vol. 26, no. 1, pp. 12–19, 2011.
- [11] A. G. Insights, “GridCal,” <https://www.advancedgridinsights.com/gridcal>, accessed on 2023-08-03.
- [12] S. P. Vera, “GridCal,” <https://github.com/SanPen/GridCal>, accessed on 2023-08-03.
- [13] —, “GridCal’s documentation,” <https://gridcal.readthedocs.io/en/latest/index.html>, accessed on 2023-08-03.
- [14] T. Brown, F. Neumann, P. Glaum, M. Parzen, J. Hampf, I. Riepin, F. Hofmann, M. Victoria, J. Hörsch, L. Zeyen, and M. Maria, “PyPSA project,” <https://pypsa.org/>, accessed on 2023-08-03.

- [15] T. Brown, J. Hörsch, F. Hofmann, F. Neumann, L. Zeyen, M. Frysztacki, P. Glaum, M. Parzen, and D. Schlachberger, “PyPSA: Python for Power System Analysis,” <https://pypsa.readthedocs.io/en/latest/>, accessed on 2023-08-03.
- [16] T. Brown, J. Hörsch, and D. Schlachtberger, “PyPSA: Python for Power System Analysis,” *Journal of Open Research Software*, vol. 6, no. 1, p. 4, jan 2018. [Online]. Available: <https://doi.org/10.5334%2Fjors.188>
- [17] A. Bosisio, A. Berizzi, C. Bovo, and E. Amaldi, “Urban distribution network planning with 2-step ladder topology considering joint nodes,” in *2017 IEEE Manchester PowerTech*, pp. 1–6.
- [18] A. Bosisio, A. Berizzi, C. Bovo, E. Amaldi, and S. Fratti, “Gis-based urban distribution networks planning with 2-step ladder topology considering electric power cable joints,” in *2018 AEIT International Annual Conference*, 2018, pp. 1–6.
- [19] T. Antić, A. Hrga, and T. Capuder, “Sens - tool for planning and operation of smart distribution networks,” in *27th International Conference on Electricity Distribution (CIRED 2023)*, vol. 2023, 2023, pp. 691–695.
- [20] J. M. Bloemink and T. C. Green, “Increasing distributed generation penetration using soft normally-open points,” in *IEEE PES General Meeting, PES 2010*. IEEE, 2010, pp. 1–8.
- [21] M. Ehsanbakhsh and M. S. Sepasian, “Optimal allocation of soft open points in active distribution networks considering wind generation uncertainty,” in *2023 27th International Electrical Power Distribution Networks Conference (EPDC)*, 2023, pp. 130–135.
- [22] M. Ehsanbakhsh and M. S. Sepasian, “Simultaneous siting and sizing of soft open points and the allocation of tie switches in active distribution network considering network reconfiguration,” *IET Generation, Transmission & Distribution*, vol. 17, no. 1, pp. 263–280, 2023.
- [23] “IEEE Guide for Using IEEE Std 1547 for Interconnection of Energy Storage Distributed Energy Resources with Electric Power Systems,” *IEEE Std 1547.9-2022*, pp. 1–87, 2022.
- [24] F. Díaz-González, A. Sumper, and O. Gomis-Bellmunt, *Energy Storage in Power Systems*. Wiley, 2016. [Online]. Available: <https://books.google.es/books?id=wfpCgAAQBAJ>
- [25] A. Sumper, *Sistemas Eléctricos de Potencia*. Universitat Politecnica de Catalunya, 2017.
- [26] CIGRE Task Force C6.04, “Benchmark Systems for Network Integration of Renewable and Distributed Energy Resources,” Tech. Rep. April, 2014.
- [27] “Datadis,” <https://datadis.es/home>, accessed on 2021-03-05.
- [28] S. Pfenninger and I. Staffell, “Renewables.ninja,” <https://www.renewables.ninja/>, accessed on 2021-03-05.

- [29] S. H. Dolatabadi, M. Ghorbanian, P. Siano, and N. D. Hatziargyriou, “An enhanced IEEE 33 bus benchmark test system for distribution system studies,” *IEEE Transactions on Power Systems*, vol. 36, no. 3, pp. 2565–2572, 2021.
- [30] C. S. Holling, “Resilience and stability of ecological systems,” *Annual Review of Ecology and Systematics*, vol. 4, pp. 1–23, 1973. [Online]. Available: <http://www.jstor.org/stable/2096802>
- [31] F. H. Jufri, V. Widiputra, and J. Jung, “State-of-the-art review on power grid resilience to extreme weather events: Definitions, frameworks, quantitative assessment methodologies, and enhancement strategies,” *Applied Energy*, vol. 239, pp. 1049–1065, 2019. [Online]. Available: <https://www.sciencedirect.com/science/article/pii/S0306261919303071>
- [32] M. Panteli and P. Mancarella, “The grid: Stronger, bigger, smarter?: Presenting a conceptual framework of power system resilience,” *IEEE Power and Energy Magazine*, vol. 13, no. 3, pp. 58–66, 2015.
- [33] *Managing the Risks of Extreme Events and Disasters to Advance Climate Change Adaptation: Special Report of the Intergovernmental Panel on Climate Change*. Cambridge University Press, 2012.
- [34] M. AR, B. P, and G. E, “Building a scientific narrative towards a more resilient EU society part 1: a conceptual framework,” Luxembourg (Luxembourg), Scientific analysis or review KJ-NA-28548-EN-N, 2017.
- [35] “Opinion of the European Economic and Social Committee communication on ‘from the Commission to the European Parliament and the Council — 2020 Strategic Foresight Report — Strategic Foresight — Charting the Course Towards a More Resilient Europe’ (COM(2020) 493 final),” pp. 67–71, Jun 2021.
- [36] T. E. Parliament and T. C. of the European Union, “Regulation (EU) 2021/241 of the European Parliament and the Council,” Official Journal of the European Union, February 2021.
- [37] —, “Regulation (EU) 2023/435 of the European Parliament and the Council,” Official Journal of the European Union, February 2023.
- [38] S. of Energy, “2021 climate adaptation and resilience plan,” US Department of Energy, Tech. Rep., 2021.
- [39] E. Hotchkiss and A. Dane, “Resilience Roadmap: A Collaborative Approach to Multi-Jurisdictional Resilience Planning,” National Renewable Energy Laboratory, Golden, CO, Tech. Rep. NREL/TP-6A20-73509, 2019. [Online]. Available: <https://www.nrel.gov/docs/fy19osti/73509.pdf>
- [40] K. Anderson, E. Hotchkiss, L. Myers, and S. Stout, “Energy Resilience Assessment Methodology,” National Renewable Energy Laboratory, Golden, CO, Tech. Rep. NREL/TP-7A40-74983, 2019. [Online]. Available: <https://www.nrel.gov/docs/fy20osti/74983.pdf>

- [41] L. Leddy, D. Jenket, D.-M. Thomas, S. Ericson, J. Cox, N. Grue, and E. Hotchkiss, “Measuring and valuing resilience: A literature review for the power sector,” National Renewable Energy Laboratory, Golden, CO, Tech. Rep. NREL/TP-5R00-87053, 2023. [Online]. Available: <https://www.nrel.gov/docs/fy23osti/87053.pdf>
- [42] S. Ericson, N. Grue, E. Hotchkiss, and M. Brown, “Applications of measuring and valuing resilience in energy systems,” National Renewable Energy Laboratory, Golden, CO, Tech. Rep. NREL/TP-5R00-83841, 2023. [Online]. Available: <https://www.nrel.gov/docs/fy23osti/83841.pdf>
- [43] C. Murphy, E. Hotchkiss, K. Anderson, C. Barrows, S. Cohen, S. Dalvi, N. Laws, J. Maguire, G. Stephen, and E. Wilson, “Adapting existing energy planning, simulation, and operational models for resilience analysis,” National Renewable Energy Laboratory, Golden, CO, Tech. Rep. NREL/TP-6A20-74241, 2020. [Online]. Available: <https://www.nrel.gov/docs/fy20osti/74241.pdf>
- [44] —, “Adapting existing energy planning, simulation, and operational models for resilience analysis,” National Renewable Energy Laboratory, Golden, CO, Tech. Rep. NREL/TP-6A20-74241, 2020. [Online]. Available: <https://www.nrel.gov/docs/fy20osti/74241.pdf>
- [45] I. P. I. T. R. T. Force, “The definition and quantification of resilience,” IEEE PES, Tech. Rep., 2018.
- [46] C.-C. Liu, “Distribution systems: Reliable but not resilient? [in my view],” *IEEE Power and Energy Magazine*, vol. 13, no. 3, pp. 93–96, 2015.
- [47] R. J. Campbell and S. Lowry, “Weather-related power outages and electric system resiliency.” Congressional Research Service, Library of Congress Washington, DC, 2012.
- [48] Z. Bie, Y. Lin, G. Li, and F. Li, “Battling the extreme: A study on the power system resilience,” *Proceedings of the IEEE*, vol. 105, no. 7, pp. 1253–1266, 2017.
- [49] G. Liu, T. B. Ollis, Y. Zhang, T. Jiang, and K. Tomsovic, “Robust microgrid scheduling with resiliency considerations,” *IEEE Access*, vol. 8, pp. 153 169–153 182, 2020.
- [50] K. P. Schneider, F. K. Tuffner, M. A. Elizondo, C.-C. Liu, Y. Xu, S. Backhaus, and D. Ton, “Enabling resiliency operations across multiple microgrids with grid friendly appliance controllers,” *IEEE Transactions on Smart Grid*, vol. 9, no. 5, pp. 4755–4764, 2018.
- [51] R. Nourollahi, P. Salyani, K. Zare, and B. Mohammadi-Ivatloo, “Resiliency-oriented optimal scheduling of microgrids in the presence of demand response programs using a hybrid stochastic-robust optimization approach,” *International Journal of Electrical Power & Energy Systems*, vol. 128, p. 106723, 2021. [Online]. Available: <https://www.sciencedirect.com/science/article/pii/S0142061520342678>

- [52] J. Jasiūnas, P. D. Lund, and J. Mikkola, “Energy system resilience – a review,” *Renewable and Sustainable Energy Reviews*, vol. 150, p. 111476, 2021. [Online]. Available: <https://www.sciencedirect.com/science/article/pii/S1364032121007577>
- [53] N. Bhusal, M. Abdelmalak, M. Kamruzzaman, and M. Benidris, “Power system resilience: Current practices, challenges, and future directions,” *IEEE Access*, vol. 8, pp. 18 064–18 086, 2020.
- [54] M. Waseem and S. D. Manshadi, “Electricity grid resilience amid various natural disasters: Challenges and solutions,” *The Electricity Journal*, vol. 33, no. 10, p. 106864, 2020. [Online]. Available: <https://www.sciencedirect.com/science/article/pii/S1040619020301561>
- [55] L. Xu, Q. Guo, Y. Sheng, S. Muyeen, and H. Sun, “On the resilience of modern power systems: A comprehensive review from the cyber-physical perspective,” *Renewable and Sustainable Energy Reviews*, vol. 152, p. 111642, 2021. [Online]. Available: <https://www.sciencedirect.com/science/article/pii/S1364032121009175>
- [56] M. N. Kamel Boulos, G. Peng, and T. VoPham, “An overview of geoi applications in health and healthcare,” *International Journal of Health Geographics*, vol. 18, no. 1, p. 7, 2019. [Online]. Available: <https://doi.org/10.1186/s12942-019-0171-2>
- [57] M. van Maarseveen, J. Martinez, and J. Flacke, Eds., *GIS for Sustainable Urban Planning and Management*. CRC Press, 2019. [Online]. Available: <http://library.oapen.org/handle/20.500.12657/27516>
- [58] V. Proag, “The concept of vulnerability and resilience,” *Procedia Economics and Finance*, vol. 18, pp. 369–376, 2014, 4th International Conference on Building Resilience, Incorporating the 3rd Annual Conference of the ANDROID Disaster Resilience Network, 8th – 11th September 2014, Salford Quays, United Kingdom. [Online]. Available: <https://www.sciencedirect.com/science/article/pii/S2212567114009526>
- [59] “Protecció civil cat,” 2024, accessed: 2024-05-29. [Online]. Available: <https://pcivil.icgc.cat/pcivil/v2/index.html#41.71619,1.73656,3z>
- [60] “Visor de escenarios de cambio climático,” 2024, accessed: 2024-05-29. [Online]. Available: <https://escenarios.adaptecca.es/#&model=EURO-CORDEX-EQM.average&variable=tasminNa20&scenario=rcp45>
- [61] L. S. Eng, R. Ismail, W. Hashim, and A. Baharum, “The use of vari, gli, and vigreen formulas in detecting vegetation in aerial images,” *International Journal of Technology*, vol. 10, no. 7, pp. 1385–1394, 2019.
- [62] Pyomo, “Pyomo Documentation 6.6.1,” <https://pyomo.readthedocs.io/en/stable/index.html>, accessed on 2021-12-13.

- [63] M. L. Bynum, G. A. Hackebeit, W. E. Hart, C. D. Laird, B. L. Nicholson, J. D. Sirola, J.-P. Watson, and D. L. Woodruff, *Pyomo - Optimization Modeling in Python*, 3rd ed. Springer.
- [64] W. E. Hart, J.-P. Watson, and D. L. Woodruff, “Pyomo: modeling and solving mathematical programs in Python,” *Mathematical Programming Computation*, vol. 3, no. 3, pp. 219–260, 2011.
- [65] Coin-or, “Ipopt documentation,” <https://coin-or.github.io/Ipopt/>, accessed on 2023-03-06.

Annex I: QGIS Plugin

As mentioned in Section 4.2, this work developed 3 QGIS Plugin to apply the proposed GIS - based methodology to any electrical network:

1. **Hazard Combination** → This Plugin creates a new layer providing the probability of occurrence of a combined event from simple events. The user should indicate the type of relation between events: dependent or independent.
2. **Impact Evaluation** → This Plugin determines the impact of each element based on an OPF analysis. The user should introduce one layer for buses and one for power lines. The Attribute Table of each layer should include the required parameters to perform the OPF analysis. Besides, the user can select the type of OPF (AC or DC) and the simulation (24-hour profile or instantaneous). As a result, the Plugin created two new layers, one for buses and one for power lines. Each new layer includes, in the attribute table, the impact of each element in power or energy, depending on the simulation type selected. Finally, the Plugin provides a spreadsheet with the same information.
3. **Risk Assessment and Resilience Index** → This Plugin evaluates power/energy at risk in each element based on the hazards that might affect a system and its vulnerabilities. First, the user should indicate the year's season to perform the analysis. Then, the maximum power line's segment length. Finally, the user should upload a spreadsheet with the system's vulnerabilities.

This Annex describes the features of each Plugin.

A.1 Installation

A.1.1 Permission access

The Plugins are available in a GitHub private repository. We ask new users to request permission access from the iPlug administration to continue.

You can obtain permission by emailing montserrat.montala@upc.edu indicating an Affiliation Link and the purpose of the request.

A.1.2 General Requirements

- **QGIS ≥ 3.0:** Download from [QGIS OfficialSite](#).

A.1.3 Recommended additional Plugins

- **Plugin Reloader:** Download from [Plugin Reloader OfficialSite](#).

A.1.4 Specific requirement for → Impact Evaluation

- **Pandapower ≥ 6.4:**

- Open OSGeo4W shell (packed with QGIS in the start menu)
- Install the library using "pip", following the instructions at the [Pandapower OfficialSite](#).

A.1.5 Plugin Installation steps

- Download from the repository the required Plugin.
- Unzip the folder.
- Save the folder in the QGIS' Active User Profile.
 - Linux:


```
C:\Users\USER\AppData\Roaming\QGIS\QGIS3\profiles\default\python\Plugins\ORStools
```
 - Windows:


```
C:\Users\USER\AppData\Roaming\QGIS\QGIS3\profiles\default\python\Plugins\ORStools
```
 - Mac OS:


```
Library/Application Support/QGIS/QGIS3/profiles/default/python/Plugins/ORStools
```

If not found, the QGIS' Active User Profile Folder can be accessed through "QGIS" ► "Settings" ► "User Profile" ► "Open Active Profile Folder"

A.2 Usage

- Before using a Plugin, using the Reload Plugin through "Plugin Reloader" is recommended.
- Follow the instructions detailed in Sections A.3 to A.5 for each Plugin.

A.3 Hazards Combination

As mentioned in Section 4.2.1, resilience analysis should consider all potential hazards that might affect the system. Different institutions and organizations provide geolocated information about simple hazards. The user should store all simple hazards in a **QgsTreeLayer** called *Hazards*, otherwise the Plugin will not consider them. The Layers included in the QgsTreeLayer should contain at least the following information in its Attribute Table:

1. Field *SUMMER* → probability of occurrence during summer.
2. Field *WINTER* → probability of occurrence during winter.
3. Field *AUTUMN* → probability of occurrence during autumn.
4. Field *SPRING* → probability of occurrence during spring.

Simple hazards can simultaneously occur, increasing the vulnerabilities of the system. In that context, the Hazard Combination Plugin results in a new layer that includes the probability of having the combined events in each season of the year.

Figure 61 shows the Dialog Box of this Plugin. First, the user should select the type of combination between events: dependent or independent. Second, the user should choose *Event A* and *Event B* among all layers included in the QgsTreeLayer called *Hazards*.

The Plugin will unlock the $P(A|B)$ boxes when the user chooses dependent events. The user should introduce how the probability of having *Event A* varies once *Event B* occurs. Introduce this variation using per unit (p.u.) notation: 1 signifies no variation, 0.5 represents half the probability, and 2 indicates double the probability.

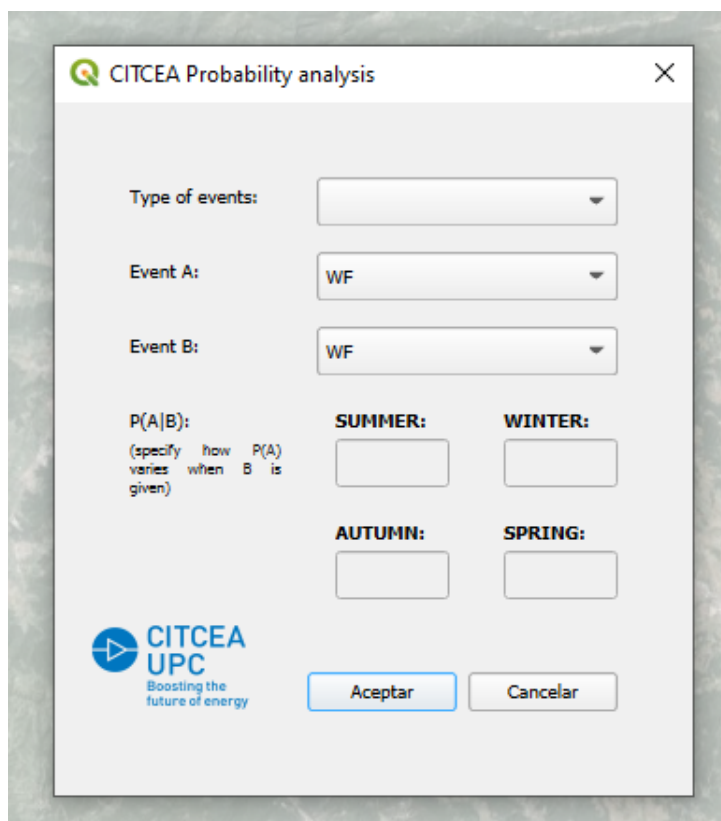


Figure 61: Dialog Box of CITCEA Probability Analysis Plugin

The Plugin adds a new layer to the hazard database, including the combined probability. The layer should be moved to the QgsTreeLayer *Hazards* after being validated. Once included, the user can select the layer in subsequent event combinations.

A.4 Impact Evaluation

As mentioned in Section 4.2.2, an OPF analysis of the system can provide the impact of each element on the network. The Impact Evaluation Plugin generates a new layer that includes the element's impact.

A QgsTreeLayer called *System_TBA* should include the layers of the network. At least two layers are requested: one for buses and one for power lines. The Layers included in the QgsTreeLayer should contain at least the following information in the Attribute Table:

1. Buses Layer:

- (a) Field *Voltage.kV* → voltage level in kV.
- (b) Field *P_GEN* → power injected from a generator to the bus in MW.
- (c) Field *Type_GEN* → the generators can be modeled as a PQ or PV. A PQ generator provides constant active and reactive power while a PV provides constant active power while fixing the voltage in a given setpoint.
- (d) Field *P_LOAD* → power demanded to the bus in MW.
- (e) Field *GRID* → 1 in case of being the 0 connected to the external grid, 0 otherwise.
- (f) Field *DEM_PROF* → this item is only necessary if an hourly OPF is expected. The user should indicate the type of daily profile from: *COMMERCIAL*, *RESIDENTIAL* or *INDUSTRIAL*. The power specified in *P_GEN* is assumed as the maximum power and scaled according to Figure 62.

2. Power Lines Layer:

- (a) Field *STD_Line* → Type of standard type among the types included in Table 15
- (b) Field *PARALLEL* → number of parallel line systems

The *From* and *To* buses, as well as the *Length*, are automatically determined through the geolocated data.

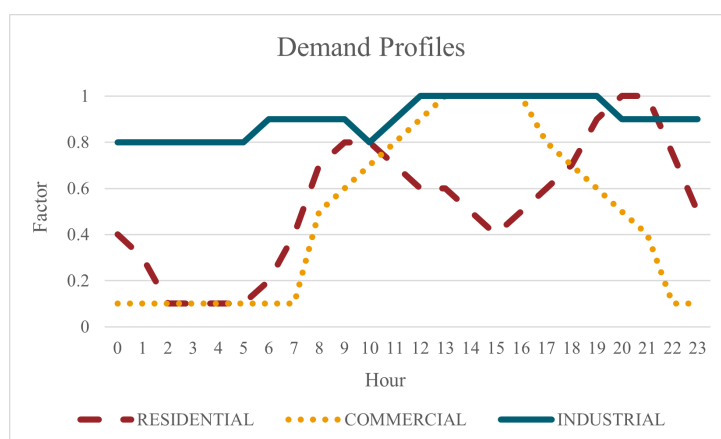


Figure 62: Demand Profiles hourly adjusting factor

STD_Line	r_ohm_per_km	x_ohm_per_km	c_nf_per_km	max_i_ka
ES.01	0.0460	0.1000	0	0.630
ES.02	0.1610	0.1050	0	0.415
ES.03	0.2620	0.1210	0	0.315
ES.04	0.2620	0.1160	0	0.315
ES.05	0.2620	0.1170	0	0.300
ES.06	0.2700	0.1260	0	0.305
ES.07	0.4030	0.1200	0	0.250
ES.08	0.6140	0.3740	0	0.200
ES.09	0.7900	0.3800	0	0.180
ES.10	1.0736	0.3850	0	0.140
ES.11	1.2150	0.4000	0	0.130

Table 15: Standard Lines. Additionally, the standard lines from pandapower can be specified by the user: `pandapower_standard_lines`

The Dialog Box of the Plugin is represented as Figure 63.

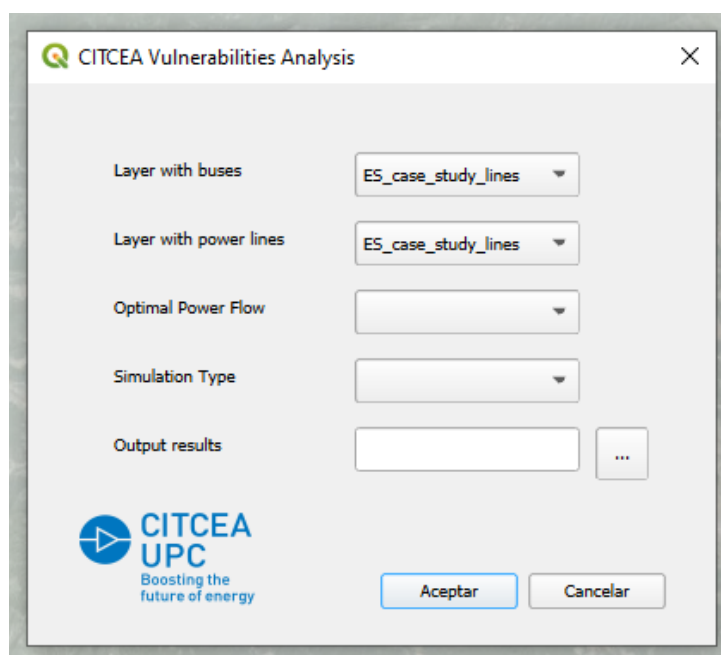


Figure 63: Dialog Box of CITCEA Probability Analysis Plugin

First, the user should select the layers with buses and power lines in the first and second dropdown lists, respectively. The list shows all layers included in the `QgsTreeLayer System.TBA`. Second, the user can select between a DC and AC OPF depending on the system characteristics and the expected accuracy. Third, the user should choose between instantaneous or hourly OPF. Finally, the user should name a `.csv` file to save the element's impact obtained.

As a result, the Plugin generates two new layers, one for buses and one for power lines. The layers contain the same data in the Attribute Table as the input layers and a new Field called *Impact*. The Field *Impact* includes the amount of energy or power that would be unsupplied in case of losing the element.

Impact is quantified in terms of power if the user selects an instantaneous analysis. Additionally, the .csv includes a list of elements and their impact.

A.5 Risk Assessment and Resilience Index

As mentioned in Section 4.2.3, the resilience analysis considers all hazards that might affect a system and its vulnerabilities. The Resilience Analysis Plugin enables risk assessment and the calculation of the system's resilience index. Figure 64 shows the Plugin Dialog Box.

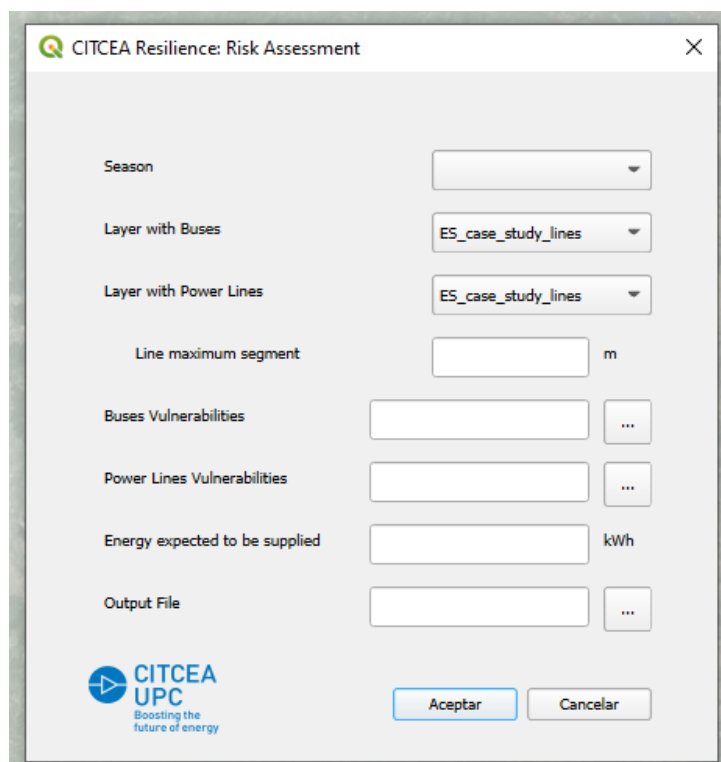


Figure 64: Dialog Box of CITCEA Resilience Index Plugin

First, the user should select the year's season to analyze. Second, the user should choose the layer with buses and power lines in the dropdown lists. The dropdown lists include all layers saved in the `QgsTreeLayer System.TBA`. Third, the user can specify the maximum length of each segment of the power lines. In case of not expecting a segmentation in power lines, introduce a value a high value. Fourth, the user should introduce a .csv file with the vulnerabilities of the buses and power lines, respectively. Fifth, the user should manually introduce the sum of total impacts. Finally, the user should specify the .csv file to save the risk assessment results.

Regarding the .csv of the vulnerabilities, the minimum content should be:

1. Column name: *Name* → The name of each bus / power line. The elements should have the same name used in the layers included in `QgsTreeLayer System.TBA`. The name of each element should be repeated for each vulnerability, i.e. if an element has 10 vulnerabilities, the .csv should include

10 rows and each row should include the element's name.

2. Column name: *VULNERABILITY* → Vulnerability's name. The user should specify each vulnerability in a different row.
3. Column name: *hazard-name_likelihood* → As many columns as hazards included in the QgsTreeLayer *Hazards* need to be included replacing *hazard-name* by the layer's name. In each row, the user should specify the likelihood of the vulnerability affecting the system once the hazard occurs.
4. Column name: *hazard-name_damage* → As many columns as hazards included in the QgsTreeLayer *Hazards* need to be included replacing *hazard-name* by the layer's name. In each row, the user should specify the element's impact on the system. Those impacts can be estimated through an OPF analysis using the methodology described in Section 4.2.2 implemented in the Plugin detailed in Section A.4.

This Plugin adds two more layers to the QGIS project for buses and power lines. The Attribute Table of each layer includes the name of the element and the total power or energy risked in it. In the case of power lines, each segment is an independent feature in the resulting layer.

Finally, the .csv file includes more detailed information. The user can check the amount of power or energy risked in each element because of each vulnerability. This information might be helpful to assess the introduction of mitigation action in the system.

Annex II: Sizing and location optimisation tool

This Annex explains how to access the scripts developed with the sizing and location methodologies and presents specifically the grid-based optimisation tool. The other tools follow the same structure as shown in Section B.2.

B.1 Access to scripts

The optimisation methodologies presented in Section 3.3 have been implemented in Python. All those scripts are available in a GitHub private repository. New users can request permission access from the iPlug administration by emailing paula.munoz.pena@upc.edu indicating an Affiliation Link and the purpose of the request.

B.2 Grid-based multiport converter sizing tool

In the development of the methodology presented in Section 3.3.4, different software tools have been used. Representative days selection has been done quite manually in Excel, whereas storage sizing and results visualisation and analysis were first implemented in Matlab. On the other hand, multiport converter sizing optimisation has been performed in Python. Specifically, Pyomo library has been used to model the optimisation problem.

Pyomo is a Python-based, open-source optimisation modelling language [62–64]. Pyomo supports an object-oriented design for the definition of optimisation models. The main steps of the modelling process are: create the model and declare components, instantiate the model, apply solver, and analyse results. A Pyomo model consists of a group of modelling components, including index sets, symbolic parameters, decision variables, constraints, and objectives (to maximise or minimise). Pyomo supports a wide range of problem types, including LP and mixed-integer non-linear programming (MINLP). Solving these problems requires using commercial or open-source solvers (not all distributed with Pyomo) [62]. The multiport converter sizing optimisation is a NLP problem. Therefore, IPOPT solver [65] is used, which is an open-source software package that can deal with large-scale NLP problems. IPOPT implements an interior point line search filter method [65], and it is designed to exploit 1st derivative (gradient) and 2nd derivative (Hessian) information.

The Python program developed in this thesis has the structure shown in Figure 65 and 66. Where *Data.xlsx* contains all the inputs, the models are inside the *blocks* folder, and all files are called from the *main.py* script.

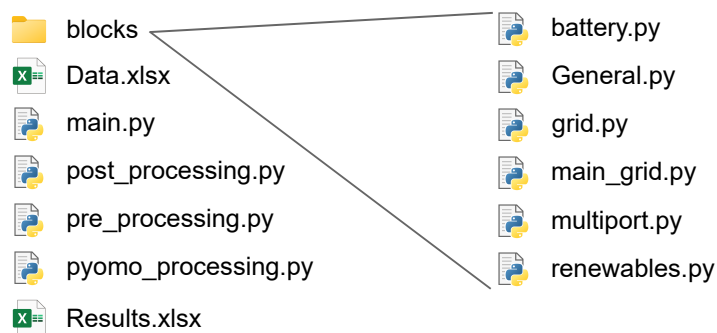


Figure 65: Optimisation program structure

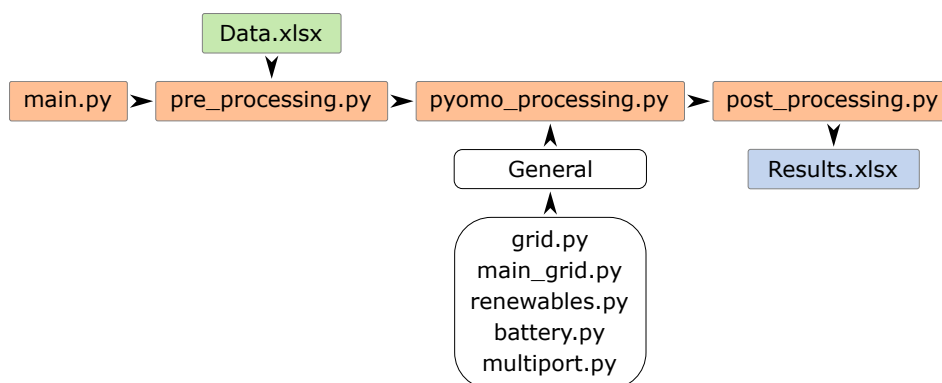


Figure 66: Flowchart of the scripts

The inputs correspond to the case study definition and have to be introduced through Excel. *Data.xlsx* includes several sheets for each system component, as shown in Figure 67. Also, inputs in the form of time series are introduced in different sheets. The datasheets (Figure 67) include the following information:

- *General* sheet indicates the number of multiport converters considered and its lifetime, how time data are structured, and base power and impedance.
- *Bus* sheet includes the voltages and type of bus.
- *Lines* sheet indicates the buses that connect, its impedance and capacity.
- *Trafos* sheet indicates the buses that connect, its impedance and rated apparent power.
- *Loads* and *Renewables* sheets indicate the type of load, to which bus is connected, and how to calculate active and reactive power.
- *Load P TS*, *Load Q TS* and *Renewables TS* sheets include the time series of active load, reactive load, and active generation respectively.
- *Battery* sheet indicates to which bus is connected, rated power and storage, SOC limits, efficiencies and cost.
- *Main grid* sheet indicates the buses that are connected to the external grid.

- *MPC* sheet indicates the buses that correspond to the multiport converter terminals, which terminals correspond to the each MPC, and the cost of each terminal.
- *Weights* sheet indicates the weight of each day.

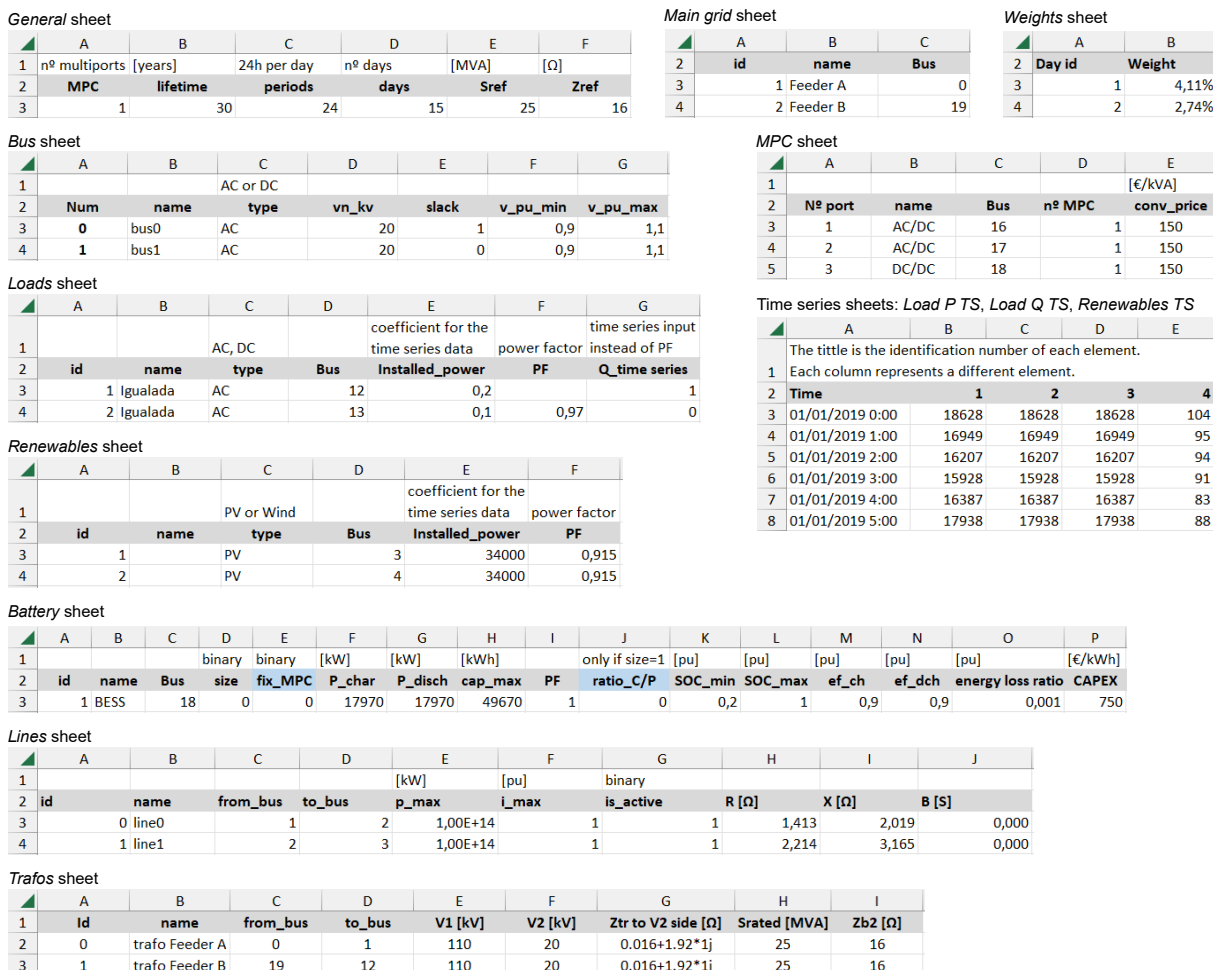


Figure 67: Inputs structure of *Data.xlsx*

After writing all the inputs, *main.py* has to be run. This file includes the main loop and starts calling *pre_processing.py*, then *pyomo_processing.py*, solves the optimisation, and finally it calls *post_processing.py*. *pre_processing.py* imports the inputs from *Data.xlsx* and stores them in a single data class, it also puts the time data in the format required by Pyomo. *pyomo_processing.py* defines the optimisation model with the sets, the main decision variables and the objective function. It also includes the optimisation of all the selected days by calling to *General.py* and using the *Block()* attribute of Pyomo. *post_processing.py* takes the optimisation results and saves them by writing *Results.xlsx*.

The detailed optimisation model is inside the *blocks* folder. Each system component is defined in a separate script with its corresponding variables, parameters and constraints for a certain time horizon. *General.py* has the optimisation model for a single day. This script calls the model of all system components, but also adds the relationship between the elements and defines general system

parameters and constraints.

Glossary

Acronyms

AC	Alternating current
BESS	Battery Energy Storage System
DC	Direct current
DER	Distributed energy resources
ESS	Energy storage systems
EV	Electric vehicle
LV	Low voltage
MINLP	Mixed-integer non-linear programming
MIP	Mixed-integer programming
MPC	Multiport Converter
MV	Medium voltage
NLP	Nonlinear programming
OPF	Optimal power flow
PF	Power flow
PV	Photovoltaic
RES	Renewable energy sources
SOC	State of Charge of the battery
SOP	Soft Open Point
VSC	Voltage Source Converters

Parameters

ΔC_{cap} Variation of the battery cost in [%]

ΔC_{conv} Variation of the converter cost in [%]

- ΔPBT Variation of the payback time respect to Ref in [%]
- Δt Time-step of the model in [h]
- $\delta_{y_{i,k}}$ Admittance phase of the line between nodes i, k in [$^{\circ}$]
- $\delta_{z_{i,k}}$ Impedance phase of the line between nodes i, k in [$^{\circ}$]
- η_{char} Charging efficiency of the battery in [p.u.]
- η_{disch} Discharging efficiency of the battery in [p.u.]
- τ_{bat} Energy loss ratio of the battery in [p.u.]
- $B_{i,k}$ Imaginary part of the Y_{bus} matrix at nodes i, k in [p.u.]
- $c_{buy-MG,i,t,d}$ Price of buying energy to the main grid MG connected to the node i at hour t of the day d in [€/kWh]
- $C_{capexBESS-b}$ Price of the energy storage of the battery b in [€/kWh]
- C_{conv-k} Unitary cost of the multiport converter terminal k in [€/kW] or [€/kVA]
- C_{conv} Price of converter associated to the battery b in [€/kW]
- C_{en} Average annual energy price in [€/kWh]
- $c_{sell-MG,i,t,d}$ Price of selling energy to the main grid MG connected to the node i at hour t of the day d in [€/kWh]
- $E_{cap-b,i}$ Energy storage capacity of the battery b connected to the node i in [kWh]
- E_{ren-bc} Annual renewable generation in the base configuration in [kWh]
- $E_{ren-max}$ Annual renewable energy available in [kWh]
- $G_{i,k}$ Real part of the Y_{bus} matrix at nodes i, k in [p.u.]
- $i_{max,MPC-k,i}$ Maximum current of the multiport converter terminal k connected to the node i in [p.u.]
- $i_{max-b,i}$ Maximum current of the battery b connected to the node i in [p.u.]
- $i_{max-g,i}$ Maximum current of the generator g connected to the node i in [p.u.]
- $i_{max-i,k}$ Maximum current magnitude of the line between nodes i, k in [p.u.]
- $p_{load-i,t,d}$ Active power load in [p.u.]
- $p_{max-buy-MG,i,t,d}$ Maximum power bought to the main grid MG connected to the node i at hour t of the day d in [p.u.]

$p_{max-g,i,t,d}$ Maximum available power from the generator g connected to the node i at hour t of the day d in [p.u.]

$p_{max-sell-MG,i,t,d}$ Maximum power sold to the main grid MG connected to the node i at hour t of the day d in [p.u.]

$p_{n-b,i}$ Nominal active power of the battery b connected to the node i in [p.u.]

$p_{n-g,i}$ Nominal active power of the generator g connected to the node i in [p.u.]

$PF_{b,i}$ Power factor of the battery b connected to the node i in [p.u.]

$PF_{g,i}$ Power factor of the generator g connected to the node i in [p.u.]

$q_{load-i,t,d}$ Reactive power load in [p.u.]

S_b Base power of the system in [kW]

$s_{max-b,m}$ Maximum apparent power of the battery b connected to the node i in [p.u.]

$s_{max-g,m}$ Maximum apparent power of the generator g connected to the node i in [p.u.]

$SOC_{max-b,i}$ Maximum state of charge of the battery b connected to the node i in [p.u.]

$SOC_{min-b,i}$ Minimum state of charge of the battery b connected to the node i in [p.u.]

T Amount of time steps in each day d

$v_{max,i}$ Maximum voltage magnitude value of node i , supposed as 1.1 p.u.

$v_{min,i}$ Minimum voltage magnitude value of node i , supposed as 0.9 p.u.

v_{n-i} Nominal voltage magnitude of the node i in [p.u.]

w_d Weight of the representative day d in the year

$y_{i,k}$ Admittance magnitude of the line between nodes i, k in [p.u.]

$z_{i,k}$ Impedance magnitude of the line between nodes i, k in [p.u.]

Variables

$\delta_{V,i,t,d}$ Voltage angle of node i at hour t of the day d in [°]

C_{BESS-b} Cost of the battery storage b in [€]

$C_{buy-MG,i,t,d}$ Cost of buying energy to the main grid MG connected to the node i at hour t of the day d in [€/kWh]

C_{MPC} Total cost of the multiport converter in [€]

- C_{oth} Cost of other additional equipment in [€]
- $C_{sell-MG,i,t,d}$ Cost of selling energy to the main grid MG connected to the node i at hour t of the day d in [€/kWh]
- C_T Total investment cost in [€]
- E_{curt} Annual renewable generation curtailment in [%]
- E_{ren} Annual renewable generation in [kWh]
- $i_{i,k,t,d}$ Current of the line between nodes i, k at hour t of the day d in [p.u.]
- I_{ren} Annual income from renewable generation in [kWh]
- k_{bat} Slope of the regression that relates variations of the payback time and battery cost in [p.u.]
- k_{conv} Slope of the regression that relates variations of the payback time and converter cost in [p.u.]
- $p_{buy-MG,i,t,d}$ Active power bought from the main grid in [p.u.]
- $p_{char-b,i,t,d}$ Active charging power of the battery b connected to the node i at hour t of the day d in [p.u.]
- $p_{disch-b,i,t,d}$ Active discharging power of the battery b connected to the node i at hour t of the day d in [p.u.]
- $p_{g,i,t,d}$ Active power provided by the generator g connected to the node i at hour t of the day d in [p.u.]
- $p_{i,t,d}$ Total active power injected at node i at hour t of the day d in [p.u.]
- $p_{MPC-k,i,t,d}$ Active power exchanged by the multiport converter terminal k connected to the node i at hour t of the day d in [p.u.]
- $p_{sell-MG,i,t,d}$ Active power sold to the main grid in [p.u.]
- PBT Payback time respect an initial base configuration in [years]
- $q_{b,i,t,d}$ Reactive power provided by the battery b connected to the node i at hour t of the day d in [p.u.]
- $q_{g,i,t,d}$ Reactive power provided by the generator g connected to the node i at hour t of the day d in [p.u.]
- $q_{i,t,d}$ Total reactive power injected at node i at hour t of the day d in [p.u.]
- $q_{MG,i,t,d}$ Reactive power exchanged with the main grid in [p.u.]
- $q_{MPC-k,i,t,d}$ Reactive power exchanged by the multiport converter terminal k connected to the node i at hour t of the day d in [p.u.]

$s_{n,MPC-k,i}$ Maximum apparent power of the multiport converter terminal k connected to the node i in [p.u.]

$SOC_{b,i,t,d}$ State of charge of the battery b connected to the node i at hour t of the day d in [p.u.]

$v_{i,t,d}$ Voltage magnitude of node i at hour t of the day d in [p.u.]



**Funded by
the European Union**

This project has received funding from the European Union's Horizon Europe research and innovation programme under grant agreement No. 101069770